CHARACTERIZATION OF THE EFFECTS OF HYGROTHERMAL-AGING ON MECHANICAL PERFORMANCE AND DAMAGE PROGRESSION OF FIBERGLASS EPOXY COMPOSITE

by

Michael Mark Voth

A thesis/dissertation submitted in partial fulfillment
of the requirements for the degree

of

Master of Science

in

Mechanical Engineering

MONTANA STATE UNIVERSITY
Bozeman, Montana

April 2018

ACKNOWLEDGMENTS

I would like to express my gratitude to my advisor Dr. David Miller for sparking my interest in composite research and his mentorship through my research at Montana State University. Thank you to Dr. Douglas Cairns, Dr. Cecily Ryan and Daniel Samborsky for their expertise which was instrumental to my success as a graduate student. I am also grateful for the great people that are a part of the MSU Composites Group, it was a pleasure to work with them. Finally, I would like to thank my parents Mark and Lynn Voth for their unwavering support and throughout my life on all endeavors I pursue.

TABLE OF CONTENTS

TABLE OF CONTENTS – CONTINUED

LIST OF TABLES

LIST OF FIGURES

Figure Page

LIST OF FIGURES – CONTINUED

Figure Page

LIST OF FIGURES – CONTINUED

Figure Page

LIST OF FIGURES – CONTINUED

Figure Page

ABSTRACT

Marine Hydro-Kinetic Devices (MHK) are a developing renewable energy technology that allows energy to be harvested from the natural flow of water due to tides, currents, and waves. Fiber Reinforced Polymers (FRP), which have been extensively used in wind energy applications, offer favorable mechanical properties as well as low costs and manufacturability making them a viable option for construction of MHK devices. However, exposure to a harsh marine environment results in moisture uptake into the FRP, often degrading mechanical properties. A study of a fiberglass-epoxy FRP was conducted to characterize the effects of moisture on mechanical properties and damage behavior of the material as well as classify the degradation mechanisms responsible for changes in performance. Environmental exposure was simulated through hygrothermal aging, exposing the FRP samples to distilled water and elevated temperature (50 °C) to accelerate the environmental effects. Quasi-static tension tests of both unidirectional and cross-ply laminates were conducted to classify the effects of moisture on mechanical properties of constituent and multi-angle laminates. Cross-ply laminates experienced 54% reduction in strengths due to moisture absorption, while unidirectional laminates strengths were reduced by 40%. Constitutive stress-strain response in conjunction with Acoustic Emission (AE) monitoring describe changes in damage behavior due to hygrothermal aging. This work also characterizes hygrothermal effects on pure/neat epoxy material to aid in interpreting hygrothermal degradation mechanisms in the composite as well as guided ultrasonic evaluation of composite specimens to characterize effects of moisture on AE signals.

INTRODUCTION

In an era of increasing energy demands and increasing environmental concern, there is a need for more diverse and eco-friendly energy sources. Since Benjamin Franklin's legendary encounter with electricity during his kite flight in 1852, innovation in electrical power ensued; Thomas Edison invented the lightbulb and raced Nikola Tesla to deliver power to the populace. Now, electricity provides much more than just light and plays a pivotal role in modern life. Consequently, current electric energy demands in the US exceed 4 trillion kilo-watthours annually [1].

Energy sources, although modernized and scaled to meet demands, have remained remarkably unchanged through the last century. Early power plants utilized coal as an energy source, using steam engines to turn generators, a method still implemented in many power plants today. Fossil fuels including coal and natural gas make up 64% of electrical power generation in the US today. Environmental impacts of combustion-type power generation coupled with a limited supply of fossil fuels have driven the development of renewable energy sources. Specifically, the cultivation of wind energy and Marine Hydro-Kinetic (MHK) devices, which serves as the motivation for this research.

Wind turbines are growing in both size and number with large farms being constructed inland, and more recently, off-shore. Off-shore turbines offer benefits over their land-based counterparts with consistently strong winds and the ability to build turbines on a larger scale. The Vesta V164 is currently the world's largest turbine with 80-meter blades and the ability to generate 9 Megawatts of power. High coastal population

densities make off-shore wind power easily accessible and reduce transmission losses. Combined, these reasons increase the viability of wind energy production.

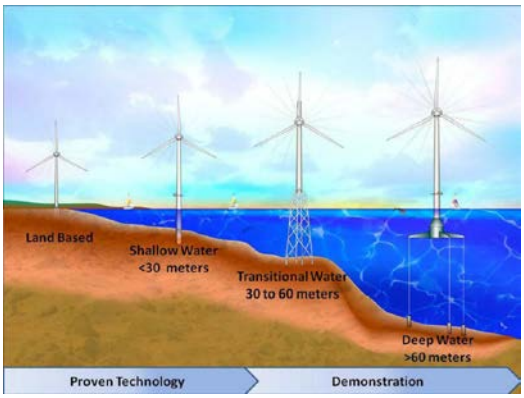

Figure 1: Progression from land-based to off-shore wind turbines

MHK devices, rather than capturing energy from naturally flowing wind, harness the power of natural flowing water. Unlike wind energy, the sources available for MHK devices are diverse, as energy can be captured from currents, tides, waves, and thermal gradients [2]. MHK design still resides in its early stages, thus these devices take many forms.

Figure 2 shows some the unique configurations available for capturing open water currents. Proximity to population centers make the implementation of MHK more feasible. A mapping assessment by the Power Research Institute estimates that along US coastlines, there is a potential to generate 898-1229 TWh/year from wave sources and 222-234 TWh/year for ocean currents [2]. This largely untapped energy source will fuel design and innovation of MHK devices.

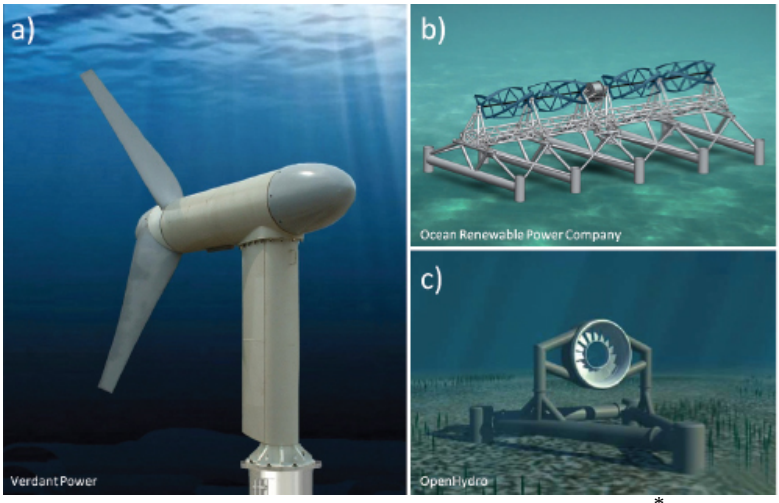

Figure 2: Several emerging MHK designs*

Composite materials have been the premier choice in the construction of wind turbines. Composites feature high specific strengths and specific stiffnesses which allow the mass to be minimized, enabling larger more efficient turbines ("specific" is the mass-normalized property). High fatigue performance of composite materials provides longer design lives under the oscillatory loads encountered in a rotating wind turbine. In terms of manufacturability, composite materials allow the creation of complex 3D surfaces necessary for efficient blades. Composites, specifically fiber-glass reinforced epoxy, have been well studied and qualified for wind energy applications [3, 4]. Shared design criteria for wind turbines and MHK devices, make these well-qualified wind-energy materials a logical choice for implementation in emerging MHK technologies.

* www.nap.edu

Design of wind-turbines and, MHK devices must also consider environmental effects on the integrity of the structure. Exposure to high humidity or complete submersion often causes detrimental effects on materials. Fortunately, composites don't corrode like metallic materials, but the absorption of moisture has been shown to reduce durability and mechanical performance of composite materials. The effect of water on composite materials presents a complex problem and affects the composite through a variety of different mechanisms. This work aims to determine the effects of a moisture on the mechanical performance of a fiberglass epoxy system and determine that nature of degradation mechanisms. Findings will aid engineers to account for environmental effects in subsequent tiers of the design process, ultimately improving the performance and longevity of MHK devices and wind turbines.

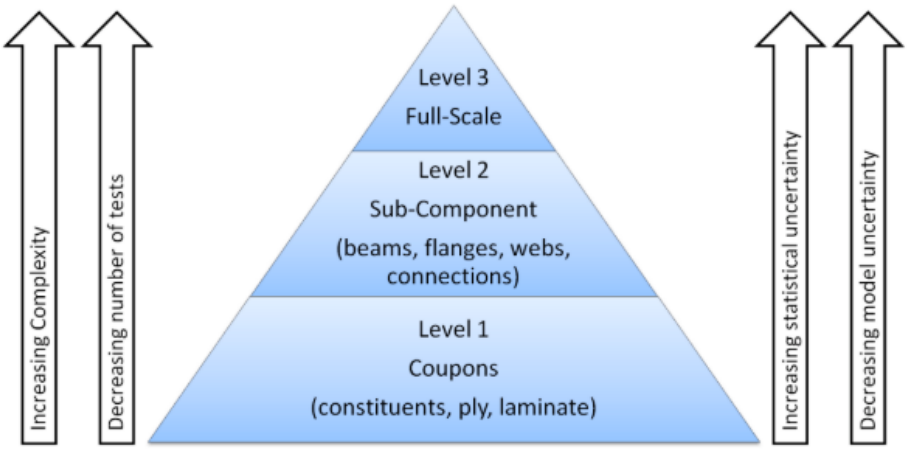

Figure 3: Design process for composite structures [3]

THEORETICAL BACKGROUND

Composite Materials

As shown in Figure 3, materials are the foundation of structural design. Material selection is a critical aspect of creating an effective design in any engineering application. In general, engineering materials fall into 3 categories: metals, ceramics, and polymers. Each of these types of materials offers various benefits exploited in design. Metals offer high conductivity, strength, and formability; ceramics offer high stiffness and corrosion resistance; and polymers offer low density, low cost, and ease-of-manufacturability. A composite material is formed by the combination of two or more of these engineering materials to form a new material with enhanced properties. Composite materials are a combination of some type of reinforcement such as a fiber or particles held together by a supporting material referred to as the matrix. Wood and concrete are prime examples of composite materials; wood combines strength and stiffness of a cellulose fiber in a lignin matrix, while concrete uses cement matrix to bond aggregate rocks to form a rock-like material. Composite materials are classified by both the type of reinforcement and the matrix. Fiber-Reinforced-Polymers (FRP's) are the focus of this work, specifically, fiberglass reinforced epoxy.

When combined, fiber reinforcements and polymer matrices offer superior mechanical properties over constituent materials. Typically, in fiber form, a material is significantly stronger than the material in its bulk form [5]. In fiber-form, the material can have fewer defects compared to the bulk form, such as in glass. A reduction in the defect density increases the strength of the material. Polymer fibers such as aramid, as well as

carbon fibers experience micro-structural alignment in the fiber form which increases the fiber strength over that of the bulk material. Fibers are not particularly useful on their own, as they can only sustain tensile load along their length, and difficulties with load introduction. The polymer matrix material allows these downfalls to be overcome.

The polymer matrix holds reinforcement fibers together to create a functional material. The polymer acts as a support, aligning, and holding fibers together such that the strength and stiffness properties of the fibers can be utilized. The polymer adds little strength and stiffness to the material, but the resulting composite still features strength to weight and stiffness to weight ratios far better than the materials in their bulk form.

The amount of reinforcement in the composite is represented the fiber volume fraction, $v_{f,}$ given in Equation 1.

$$v_f = \frac{Volume\ of\ fiber}{Total\ Volume} \tag{1}$$

Typically, the higher the volume fraction, the higher the mechanical properties. Additionally, the matrix allows for load sharing between fibers, through shear lag. This quality increases the toughness and damage tolerance of FRP materials, allowing strength and stiffness properties to remain largely intact even with the presence of damage or defects. FRP's also possess excellent fatigue properties, making them an optimal choice for large dynamic structures.

The polymers that make up the matrix can be categorized into two general types: thermoset and thermoplastic. Thermoplastic polymers feature only secondary bonding between polymer chains and can be melted and reformed. However, due to high viscosity

and weak bonds to reinforcement fibers, thermoplastics are used far less frequently than their thermoset counterparts. Thermoset polymers such as the epoxy, feature a non-reversible curing process in which polymer chains are crosslinked with primary bonds. The crosslinking results high stiffness and strength, and a strong fiber-matrix interface.

Although not considered a constituent component of the composite, the fiber matrix interface ensures an adequate bond between the fiber and the matrix. Fiberglass on its own will not bond with a polymer, thus a coating is necessary to facilitate this bond. The coating is referred to as the sizing and is applied to the fibers during manufacturing. This sizing is a silane compound that bridges the dissimilar bonding characteristics hydrophilic fiber to the hydrophobic polymeric material. The silane has a silicon component that bonds well to glass as well as an organic end that bonds well to polymers. In addition to bonding, the sizing adds lubrication to prevent fibers from being destroyed from handling during the manufacturing process. The performance of the sizing is paramount to the composite performance and its exact formulation remains is proprietary to fiber manufactures. Although not considered a constituent of the composite, the interphase of the fiber and matrix is critical for creating a mechanically functional composite.

Fiber reinforcements can be added in several forms, including chopped and continuous fibers. Chopped fibers are discontinuous fibers usually combined in a random orientation resulting in near-isotropic properties. Chopped fiber composites are highly formable, but do not maximize the mechanical properties. Continuous aligned fibers, as the name implies, allows fibers to be positioned in the same direction. The aligned fibers

result in anisotropic behavior with high mechanical properties along the fiber direction, and poor mechanical properties transverse to the fibers. These anisotropic properties of composites can be altered by changing the layup or directionality of the aligned fibers to create a material optimized for its loading condition. These individual layers or plies of the composite are referred to a lamina, or laminae (plural), and when stacked together, form the laminate (Figure 4)

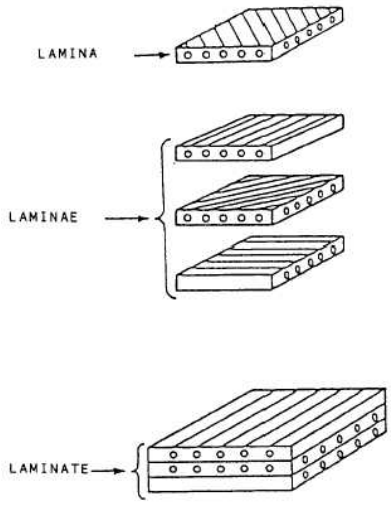

Figure 4: Schematic of composite layup: lamina to laminate.

Manufacturing of Composites

A multitude of techniques exist for manufacturing FRP's, including pultrusion, filament winding, prepreg layup, wet hand layup, and resin transfer molding (RTM). These techniques vary significantly in terms of materials used, equipment, consumable resources, and the intended use/shape of the final design. Specific manufacturing

techniques for MHK devices are not yet well established, but presumably, these processes will closely follow RTM techniques already implemented in the wind turbine industry.

The vacuum-assisted RTM (VARTM) methods utilizes textile type reinforcements. Bundles of fibers, known as tows, are either woven or stitched together to create a reinforcement fabric. These fabrics layers known as plies (analogous to lamina) can be stacked and layered to create a laminate with the desired properties. Various fabric architectures can be created including unidirectional, biaxial, triaxial, and random matt. Unidirectional fabrics, feature tows aligned in the same direction. Pure unidirectional textiles are rare, as the tows must be stitched to either transverse backing strands or random matt to hold the tows aligned (Figure 6). Biaxial and triaxial fabrics feature tows aligned in two and three different directions, respectively, that are stitched together; and as the name implies, Radom matt fabrics consist of nonaligned, randomly-oriented fibers/tows.

The VARTM process is depicted in Figure 5. The layers of fabric are stacked on a one-sided mold and covered with an impermeable plastic film known as a vacuum bag. A vacuum is pulled on the outlet port which causes the vacuum bag to press the layers of fabric into the mold. Once a vacuum is achieved, a low-viscosity resin, introduced at the inlet port, can be pulled through the layers of fabric. This process infuses the resin into the fabric and results in high and consistent volume fractions (~50%). Peel plies and flow media are sacrificial layers that allow laminate separation from the mold and promote resin flow through the laminate during the infusion process.

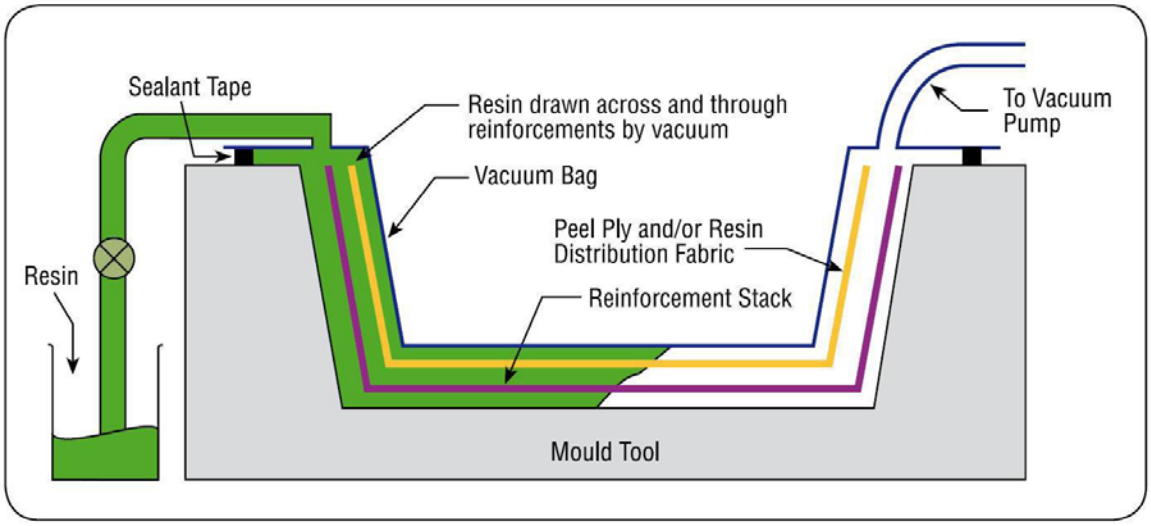

Figure 5: VARTM manufacturing process

The RTM processes can result in several types of defects in the manufactured laminates. Defects such as porosity and inadequately wet-out tows are intrinsic to the manufacturing process itself. Defects from constituent fabrics such as tow waviness and heterogeneity due to spacing tows and the resin-rich areas between tows may also be present. Some of these defects can be seen in Figure 6.

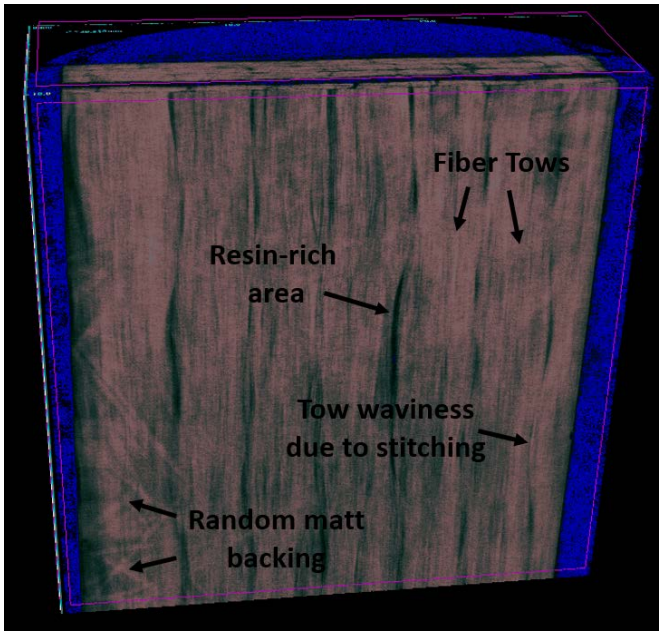

Figure 6: Micro-CT (3D) of unidirectional textile type composite manufactured using VARTM.

Damage Behavior of FRPs

Composite materials possess complex damage modes due to the different damage behavior of the constituents and the interaction between them. Anisotropy and the direction of applied load further complicate the damage mechanisms present in a composite laminate. The load-sharing relationship between the fiber and the matrix leads to interesting micro-mechanical damage mechanisms and that would not be present in a homogeneous isotropic material. Further, this load sharing capability of FRP's allows for the material withstand a sizable amount of damage prior to failure, making composites damage tolerant. The ultimate failure of the FRP depends on the coalescence and growth of these micromechanical damage into the global failure of the material. Understanding of this progressive damage behavior is essential to both development better composite

materials as well as better implementation composite design, particularly when fatigue is present. In terms of wind turbines and MHK devices, this includes incorporating environmental effects damge mechanisms and progression.

Matrix cracking typically resides as the first damage mechanism to occur. The polymer matrix is significantly weaker than the fiber and thus will fail at low-stress levels. Thermoset resins such as epoxy, possess very brittle behavior, making the matrix more sensitive to fracture. The fracture can initiate from either a defect in the material or micromechanical stress concentrations. Defects such as voids or contaminants are prime initiation points for cracks. Stress concentration around fibers, stitching, or other damage sites also initiates cracks. In a homogenous polymer material, a single crack propagates to final failure, however, the fibers in the composite act as crack-blunters, increasing the tortuosity of a crack path and stopping its growth. This behavior can be seen below in

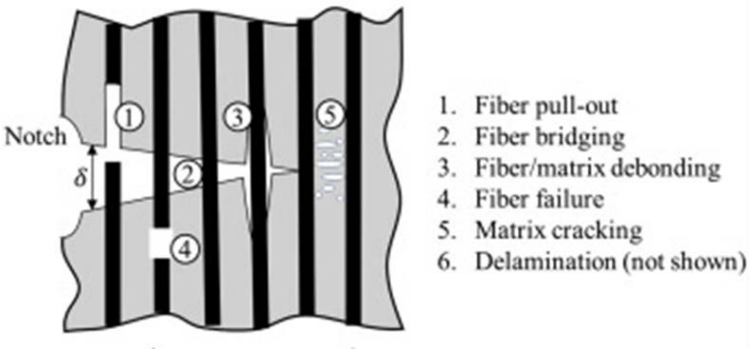

Figure 7.

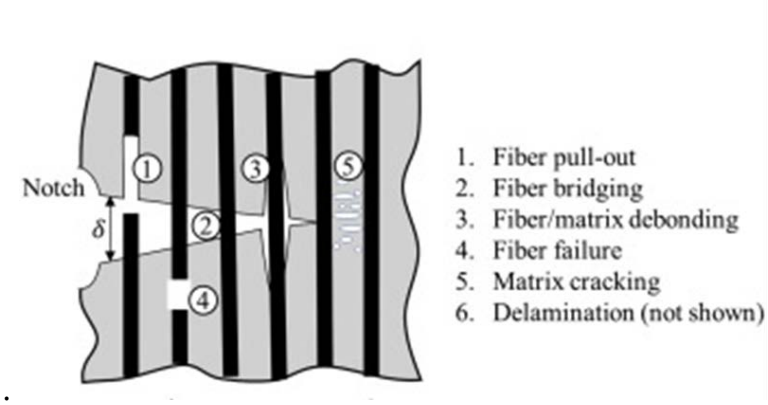

Figure 7: Crack growth in unidirectional laminates [6]

Fibers can only stop cracks from growing in one direction, leading to crack paths following resin rich areas between fibers. This behavior makes cracks in angle plies susceptible to growth along the fiber direction. Stiffness from adjacent plies of different angles can help mitigate this growth. Matrix cracks vary significantly in size ranging from micro-size to full lamina thickness.

Damage mechanisms that occur at the interface are known as fiber pullout and fiber debond. These failures occur when the stress exceeds the adhesiveness of the bond between the fiber and matrix. Fiber pullout occurs when the shear stress at the interface exceeds the shear strength of the fiber- matrix bond, causing separation along the axis of the fiber. Fiber debond occurs when the normal stress at the interface exceeds the fiber-matrix bond strength, causing a separation radially outward from the fiber. Research has shown that theses interface type failures feature lower fracture energies than fiber and matrix failures [7]. Differentiating these mechanisms can be difficult, thus there are often grouped together as an interface/interphase failure. Figure 8 shows images of interface failure types surfaces from a scanning electron microscope (SEM).

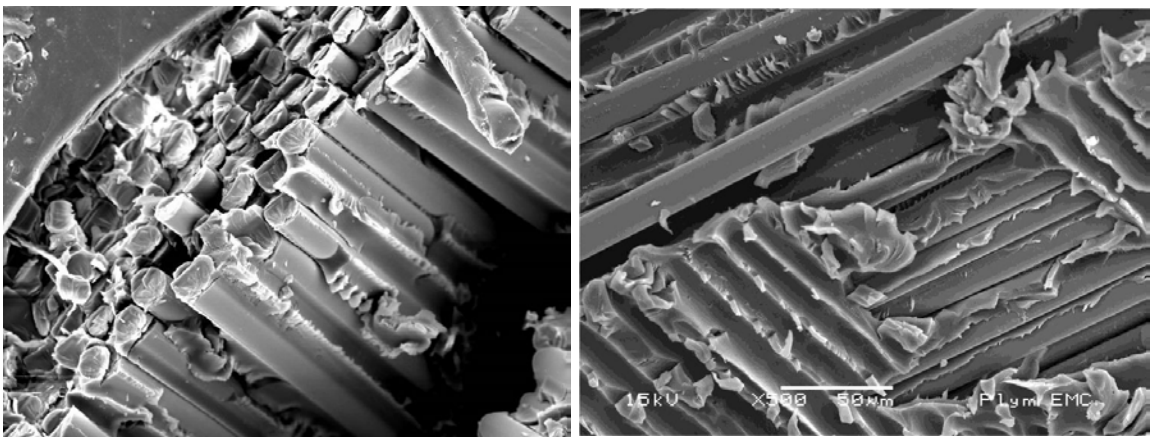

Figure 8: Fiber pullout failure [†](left). Debond failure (right).

In laminates with fibers oriented in the loading direction, fiber failure marks the onset of global failure. Fibers fail when the in-situ stress from the load sharing between fibers exceeds the ultimate stress of the fiber. The fibers provide the stiffness for the material, thus when fibers fail, large amounts of strain energy are released, and the global stiffness is significantly reduced. This results in cascading fiber failure ultimately causing complete failure of the material.

Interactions between the failure mechanisms determine the damage progression of the material. Reifsnider described this progression as can be seen in Figure 9 [8]. The chart shows how damage initiates as matrix cracks and progresses as interface and fiber failures. Damage coalesces to form delaminations, or separations between plies, and localized fiber failures resulting in a final fracture. The amount of damage and types of damage vary depending on the material system utilized. Commonly, the term damage tolerance is used to describe the amount of damage a material can withstand before ultimate failure. Materials with low damage tolerance withstand few damage

[†] John Summerscale

events/occurrences before damage coalesces to final failure, while materials with high damage tolerance will be saturated with damage before the onset of final failure. Typically, engineers seek composite systems with high damage tolerance as they usually provide better fatigue performance and because damage can be detected before catastrophic failure occurs.

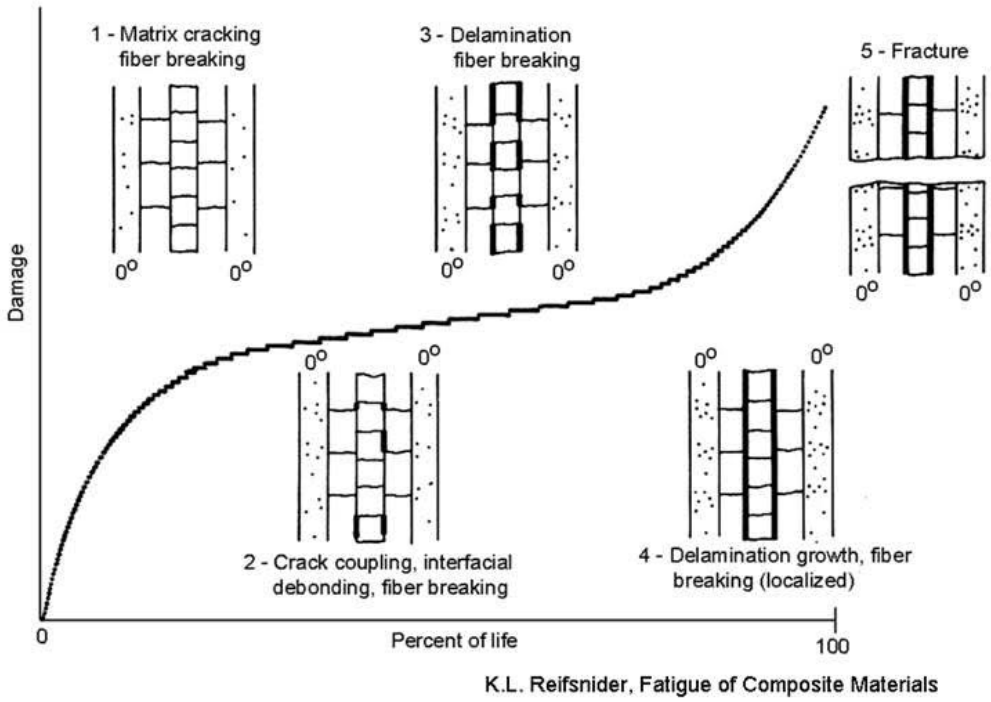

Figure 9: Damage progression in composite materials[8]. Damage initiates as matrix cracks and progresses as interface and fiber failures.

Hygrothermally-Aged Composites

Enhanced mechanical properties compared to conventional engineering materials make FRP's a prominent choice for wind turbine and MHK devices, but environmental effects on these properties must be considered. The exposure of a material to a warm

moist environment of materials is known as hygrothermal aging. Application of FRP materials exposed to hygrothermal environments is not a novel concept and has been a subject of study industries such as boating and marine, aerospace, and civil structures. However, many types of FRP's exist and hygrothermal effects can vary significantly between systems, making the characterization of the effects still a relevant materials and engineering problem

The study hygrothermal effects on a composite are three-fold: 1) understanding of how moisture diffuses into the composite, 2) the resultant change in the mechanical properties due to moisture, 3) determining the mechanisms responsible for the change in mechanical properties. Fortunately, diffusion of moisture into FRP's is well understood and predictable. Property degradation is correlated to moisture uptake, but the exact mechanisms for the degradation are not well understood. Degradation due to hygrothermal aging presents a complex multifaceted problem and can be attributed to a variety of chemical and physical factors singularly or in combination, including hygro-strains, hydrolysis, interface degradation, matrix plasticization, amongst others. The extent of hygrothermal degradation and the mechanisms of degradation will vary significantly with different material systems.

Moisture Diffusion

Moisture diffusion into composite materials exists as a matrix dominated phenomenon, with inorganic fibers absorbing a negligible amount of moisture. Absorption tests are conducted by soaking the composite in either seawater or distilled water, typically at an elevated temperature. The moisture content in the material given by

M in Equation 2, is measured on a bulk basis using the samples initial mass, m_i, and its measured mass, m_t, after some time of exposure, *t*.

$$M(t) = \frac{m_t - m_i}{m_i} \tag{2}$$

This moisture content is tracked through time to determine the diffusion characteristics of the composite.

Fickian Diffusion: The diffusion of moisture into a polymer or composite material can typically be described by Fick's law of diffusion, a partial differential equation which is first order in time, t, and second order in space, *x* (Equation 3).

$$\frac{\partial C}{\partial t} = D_{ij} \frac{\partial C^2}{\partial x_i^2} \tag{3}$$

C is the concentration and the coefficient, *D*, is the diffusivity of the material. For composite materials, the diffusivity coefficient can vary based off the material orientation, as diffusion rates along fibers and across fiber can vary. Previous work at MSU conducted by Mark Stoffels investigated this subject, along with the effect of applied stress on diffusion rates [9]. Fick's law also describes heat diffusion, allowing well-established heat diffusion models to be implemented for modeling moisture diffusion. In most cases, the multidimensional problem can be simplified to a 1-dimensional one. In structures such as turbine blades of wind turbines and MHK devices, water is exposed external surfaces of the structure and then diffuses through the thickness into the laminate. In the laboratory, the thickness of the sample is significantly small

enough that edge diffusion can be considered negligible, permitting the use of 1-D fickian models. A theoretical moisture uptake curve for this Fickian behavior is shown below in Figure 10.

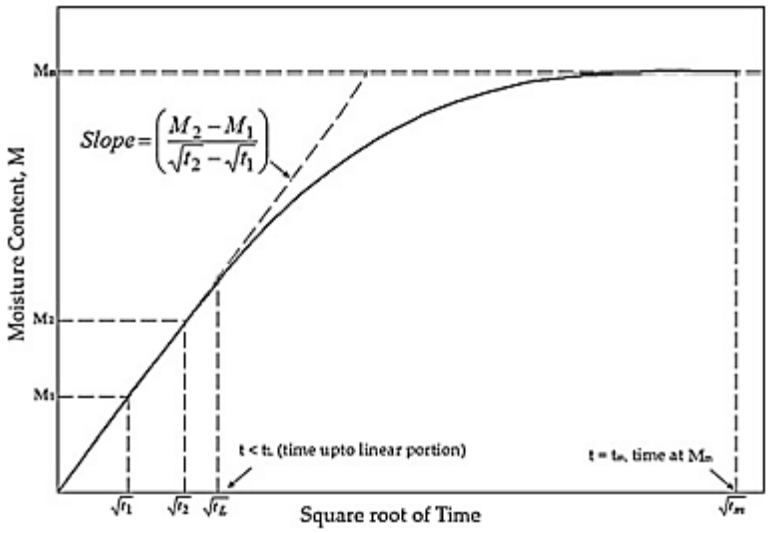

Figure 10: Moisture uptake curve for theoretical 1-D Fickian Diffusion [10]

Diffusion is often plotted versus the square root of time to show the diffusion as linear behavior as given in Equation 4 where M_∞ is the maximum moisture level for Fickian diffusion, *h* is the laminate thickness, and D is the diffusivity constant.

$$M = \frac{4M_\infty\sqrt{tD}}{h\sqrt{\pi}} \tag{4}$$

Most FRP and polymers will display this Fickian- type behavior for the initial adsorption and many over longer times as well.

Temperature Effect on Diffusion At ambient temperatures, diffusion in polymeric materials occurs slowly, resulting in diffusion times on the order of years or decades.

These diffusion rates are pertinent when considering the design of a marine structure, but not practical to implement in the laboratory. Typically, diffusion experiments are conducted at elevated temperatures which increases the diffusivity and decrease the diffusion time. The relationship between diffusivity typically follows the Arrhenius rate law given in Equation 5 where D_0 is the initial diffusion rate at some arbitrary temperature, T is absolute temperature, and C is a quantity related to the activation energy of moisture diffusion in the material [11-15]. The Arrhenius law increases the diffusion rate by a factor of 2 for every 10 °C increase in temperature, allowing much faster diffusion times to be achieved and allowing researchers to simulate moisture uptake levels like those anticipated for a wind blade/ MHK design life at ambient temperatures.

$$D = D_0 e^{(-\frac{C}{T})} \tag{5}$$

Previous research has used temperatures ranging from room temperature to 90 °C. Polymers are sensitive to high temperatures and temperature history, thus aging temperature must be selected so as to not alter the structure of the polymer. Typically, aging 30-40 ° C below the glass transition temperature is adequate. However, aging below the transition temperature may still be problematic; Grammatikops *et al.* reported for a thermoset polyester system, aging 80 °C (40 °C below the cure temperature) resulting in matrix degradation and consequently, non-Fickian diffusion after extended aging [15, 16]. Thus experimentally isolating and preventing temperature effects of the accelerated aging process is an ongoing challenge of hygrothermal investigation of

polymeric materials. The dataset collected for this work was designed to address this concern.

Damage/Defect Effects on Diffusion Diffusion behavior can be affected by other attributes of the FRP. Intuitively, voids and cracks in the laminate offer pathways for water to penetrate the composite. However, diffusion may also cause damage. Sun *et al.* suggested the fiber-matrix interface can serve as diffusion pathway when the bond is weak initially or weakened due to aging [17]. A microstructural model was proposed treating the interface as a diffusion channel and results were compared between the well-bonded interface and one where the fibers were clean (no sizing). Clean fiber specimens showed little change between diffusion cyclic while the diffusivity of the "well-bonded" sample increase with each diffusion cycle suggesting interface degradation. Sun *et al.* also conducted repeated absorption cycles, and which yielded increasing diffusivity rates. SEM images of specimens after subsequent aging cycles showed that damage formed, connecting voids, thus providing diffusion highways. Perroux *et al.* presented a coupled diffusion damage model, showing that damage in the composite could be correlated to increases in diffusivity [18]. These works suggest that diffusion of water into FRP's can cause irreversible damage and is evidence by changing diffusion rates.

Hygrothermal Aging Effects on Mechanical Properties

A variety of test methods may be employed to examine the effects of moisture on the mechanical properties of the FRP. A multitude of mechanical tests have been used to characterize hygrothermal effects on mechanical properties, including uniaxial tension in both static and fatigue [4, 15, 16, 19-24], flexure [23, 25], shear [7, 11], and delamination

[26-28]. The resultant changes mechanical properties are scattered amongst researchers. In general, moisture absorption typically results in a moderate reduction in strength and minor changes in modulus. Results can vary significantly depending on the material system and aging conditions. Previous work at MSU has compared the hygrothermal degradation of two material systems, a glass-vinyl ester and a glass epoxy which showed degradation in static performance of the epoxy system to be much higher than that of the vinyl ester system (Figure 11).

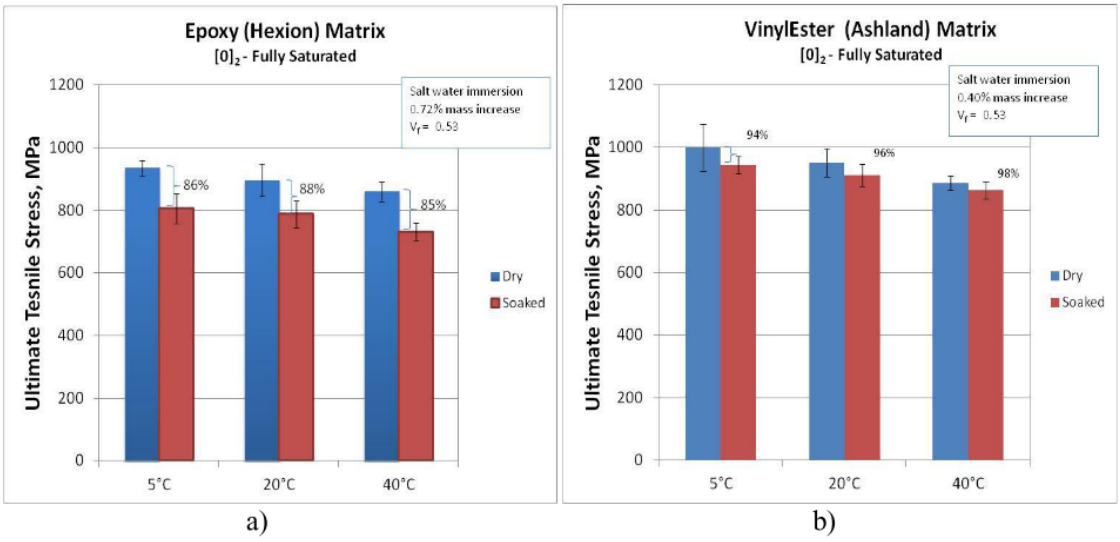

Figure 11: Degradation of static tensile strength for an epoxy system (a) and vinyl-ester system (b) [20]

Even results between similar types of material systems show different varying hygrothermal effects. Mourad *et al.* showed found there to be no changes in mechanical properties for a hygrothermally aged glass-epoxy system [19], while research on another glass-epoxy system conducted by Garg *et al.* observed strength reductions of nearly 65% [16]. The variation between these different studies of comparable material systems

emphasizes the need to address the hygrothermal aging for each FRP system as the specific chemical composition of the matrix, reinforcement and architecture, conditioning parameters, and manufacturing techniques may all have influence hygrothermal response.

Previous research has typically been confined to conducting tests on unidirectional test specimens in both the longitudinal and transverse directions. These conventional tests are among the most important for characterization of composite materials, but little work has been done to expand the lamina-based tests to more complex laminates that may be implemented in the composite design. This was the focus of work done by Nunemaker *et al.* at MSU, which examined the effect of hygrothermal aging on angled laminates as well as cross-ply laminates [21, 22]. This work expands the work done by Nunemaker to include an extensive study of the cross-ply behavior with the addition of the constituent unidirectional lamina behavior.

Hygrothermal Degradation Mechanisms As mentioned previously, moisture uptake occurs predominantly in the matrix material or in the fiber matrix interface regions. Consequentially, degradation in bulk mechanical properties due to aging is largely attributed to degradation of these two phases.

As moisture is absorbed into a composite swelling can cause physical damage in the microstructure. Swelling behavior of aligned fiber composites has been explored previously and can be modeled similarly to thermal expansion with varying expansion coefficients in-line and transverse to the fibers [29]. Consequently, internal stress-levels may change with moisture absorption and induce damage or stress concentrations which alter the mechanical performance of the material. This damage may occur in the matrix,

the interface or in both simultaneously. As previously discussed in the diffusion section, the damage induced from the hygrothermal aging process itself is prevalent.

Additionally, moisture ingress into the composite can alter the molecular structure of the matrix and interface. Water is a known plasticizer in polymeric materials. Plasticization occurs when water occupies free volume between polymer chains and interrupts the secondary bonds between polymer chains and increases chain mobility. In some polymers , water in the free volume of the polymer does not bond or react, making its presence physical rather than chemical. Increasing chain mobility will alter the mechanical properties of the polymer, typically reducing stiffness and strength. In other polymers chemical changes can occur; absorbed water molecules can react with polymer chains, breaking covalent bonds, in a process known as hydrolysis. Further, a comprehensive study of several epoxy systems by Zhou *et al.* found that there is also the possibility for water molecules to form secondary crosslinks between chains when water molecules bridge between chains with a strong secondary bond on each end [12, 13]. The nature of water in the polymer with varies depending on the material system.

Determining mechanical properties of thermoset polymers like epoxy can be difficult due to a brittle mechanical behavior. Mechanical test coupons are sensitive to fracture from defects induced during manufacturing such as porosity or stress concentrations on the specimen edges from post-processing operations. Due to the difficulty of testing thermosets such as epoxy, previous research characterizing the of hygrothermal effects on mechanical properties is sparse. Studies conducted by Papanicolaou *et al.* and Noguiera *et al.* on neat epoxy found that both modulus and

strength of the system was degraded with moisture [14, 30]. Since the polymer serves as the support material for the composite, degradation of its mechanical properties is often attributed to degradation of the composite properties. Many studies have attributed reductions in of the composite to plasticization of the matrix material and its inability to effectively transfer loads in a softened state [11, 16, 19].

Although difficult to measure mechanically, the presence of plasticization and chemical interactions of water with the polymer may be observed by monitoring changes in the glass transition temperature of a polymer with aging. The glass transition temperature (T_g) indicates a physical change of a polymer and is an important attribute when defining the service conditions of a material. T_g differentiates and changes in the microstructure of the polymer. Specifically, T_g marks the transition between two solid phases that have vastly different mechanical properties: the polymer changes from the hard, brittle, “glassy” phase to a soft, viscous, “rubbery” phase. T_g is a value that is often monitored to classify the effects of moisture, and the nature of water in the material for both pure matrix material [12, 13, 30, 31] and the composite [11, 15, 18].

The integrity of the fiber-matrix interface presents another aspect of concern for durability of hygrothermally aged composites. Changes in interfacial properties between commonly attributed to change in mechanical behavior due to hygrothermal aging [11, 15-17, 19, 25, 27, 32, 33]. However, testing and verifying changes interface integrity and its broader impacts on the bulk composite performance is difficult to accomplish experimentally. The interface may be attacked both chemically or physically due to swelling. Most commonly, SEM images of fracture surfaces are used to provide evidence

of the the quality of the interface bond based off the amount of fiber debonding and the smoothness of the fiber surfaces [16, 19, 23, 27, 34]. Figure 12 shows an example of fracture morphology of a degraded fiber-matrix interface due to hygrothermal aging.

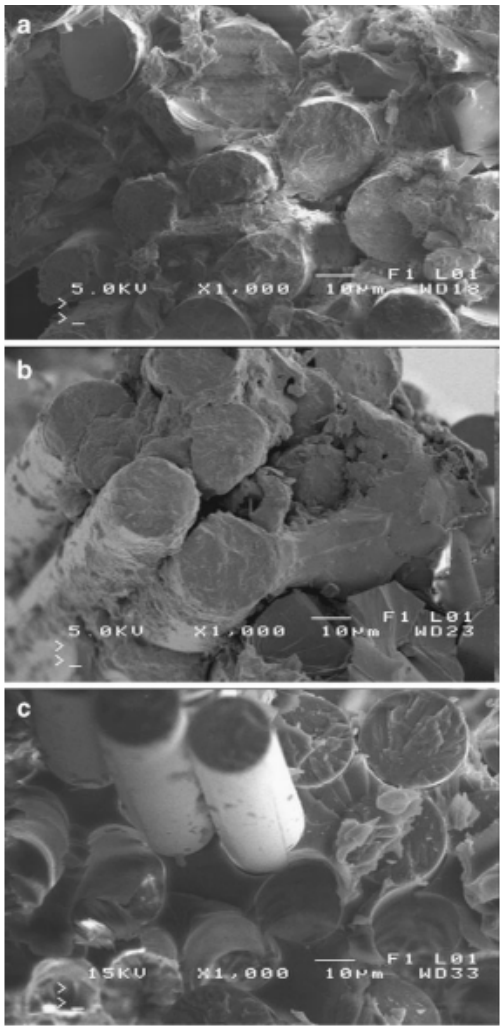

Figure 12: SEM of fracture morphology of glass/polyurethane system a) control b) One-year at room temperature c) One-year of 65 °C [19]

Mechanical tests may also be implemented to better understand the interface behavior. Transverse tension, interlaminar delamination, and interlaminar shear strength

(ILSS by short beam shear) tests can provide insight into interface strength fiber-matrix interface [23, 27, 34]. Liao *et al.* observed a reduced crack density in transverse samples which were attributed to a reduced interface strength causing failure and premature stress redistribution compared to unconditioned samples [23]. Garg *et al.* observed similar failure morphology of delamination samples in both aged conditioned and unconditioned samples which suggests that changes in interlaminar properties were not due to interface degradation [27]. Ray *et al.* showed moisture reduced ILSS in several material systems and used SEM to identify the interface as the degraded phase. These types of test do not isolate interface strengths exclusively, and even with validation from SEM can only provide a qualitative assessment of the interface strength. Micro-mechanical tests such microdroplet [35] and fiber pushout by nanoindentation tests [36] have directly correlated the hygrothermal degradation of the fiber/matrix interface by direct measurement of the interface strength. Interestingly, Bradley *et al.* conducted transverse tension test in addition to fiber pushout tests and found a good correlation between reduced transverse strengths and reduced interface strengths. However, due to competing mechanisms, it is difficult to verify that reduced interface strength was responsible for reduced transverse strengths. The nature of interface degradation is not well understood and could be symptomatic of both physical degradation due to a changing internal stress state in the composite and/or chemical degradation due to the interaction of water with the sizing. The effects of moisture on the interface will not be explored directly in this study but must be considered when interpreting results.

Acoustic Emission

Since FRP's tend to be damage tolerant materials, monitoring the damage state of the material is important to the evaluation of the integrity and residual life of the material. Non-destructive testing (NDT) and non-destructive evaluation (NDE) methods provide means to monitor this damage without alteration of the material itself. These techniques are a subject of great interest for both structural health monitoring (SHM) applications and material characterization. Acoustic Emission (AE) monitoring, an NDE technique was implemented during the mechanical tests conducted in this work both to aid in describing the damage progression of hygrothermally exposed composites, as well as to evaluatethe effectiveness of AE as an SHM method in MHK devices.

AE Theory

Acoustic emission monitors damage indirectly through damage-induced elastic waves that propagate through the material. When damage occurs, strain energy is released in the form of an elastic stress wave. In a plate, theses stress waves, known as lamb waves, cause deflections on the plate surface. Piezoelectric sensors installed on the surface of the plate measure and record these surface deflections.

Lamb waves can propagate as various wave modes at different speeds, governed by the elastic properties and geometry of of the material. The dominant wave modes are the zero-order extensional (symmetric) S_0 and the flexural (anti-symmetric) A_0 wave. Figure 13 shows the mode shapes of these two waves; the extensional wave being in-plane, and the flexural mode being out of the plane.

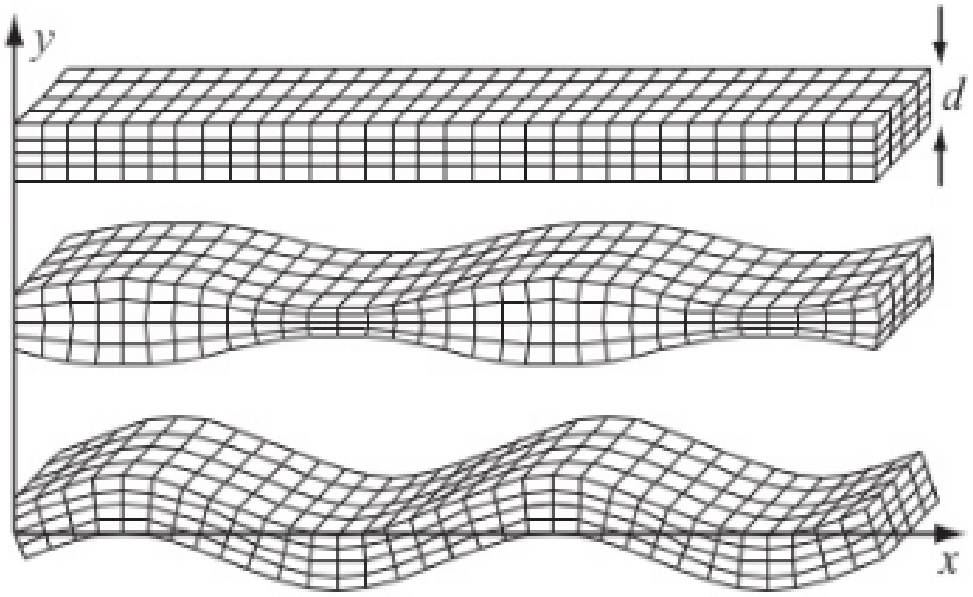

Figure 13: top) undeformed; middle) extensional mode; bottom) flexural mode

Aside from different mode shapes, the extensional and flexural waves travel at different speeds shown in Eqn. 6a and 6b, respectively, where A_{11} and D_{11} are the in-plane and bending stiffens of the laminates, ρ is density, and d is thickness [37]. For the flexural wave, the wave speed is dependent on the frequency, ω making the wave frequency dispersive.

$$c_e = \sqrt{\frac{A_{11}}{\rho d}} \tag{6a}$$

$$c_f = \sqrt[4]{\frac{D_{11}}{\rho d}} * \sqrt{\omega} \tag{6b}$$

The extensional wave resides as the faster of the two waves, but both extensional and flexural waves modes, along with reflections from plate boundaries may be present in recorded AE waveforms, complicating the waveforms and subsequent analysis processes.

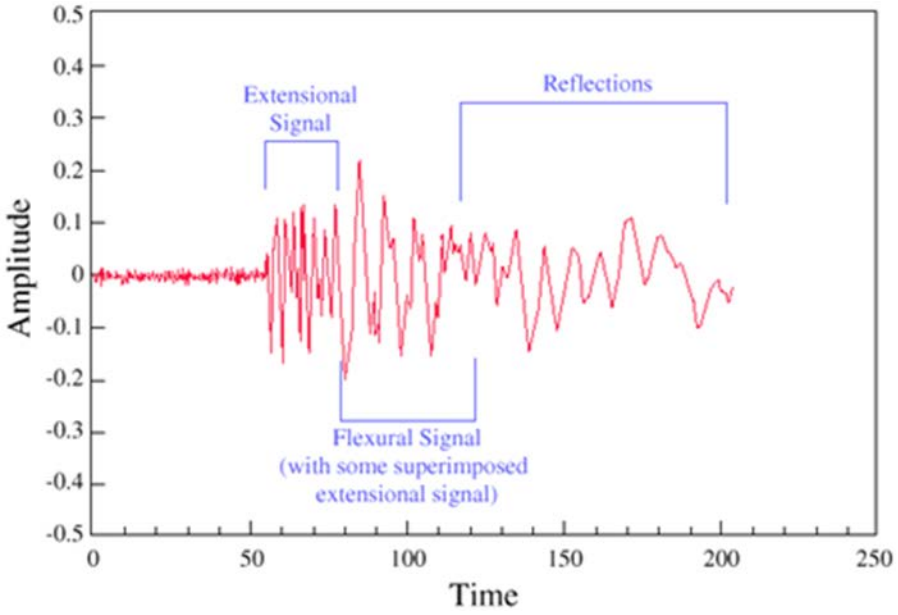

Figure 14: Example AE waveform with wave modes[‡]

AE Analysis Techniques

For material characterization, the goal of acoustic emission monitoring is to identify the damage state of the material. Ideally, this includes identifying what type of damage has occurred and determining its severity. Due to the complexity of the AE waveforms, damage trends and behaviors must be correlated to waveform features and parameters. These parameters are attributes of recorded waveforms and include amplitude, energy, peak frequency by fast Fourier transform (FFT), counts, rise time, and

[‡] Gregory N. Morscher, NASA Lewis Research Centre

duration. Figure 15 depicts some of these waveform features. A detailed explanation of these features can be found in previous work at MSU conducted by Michael Schuster [38].

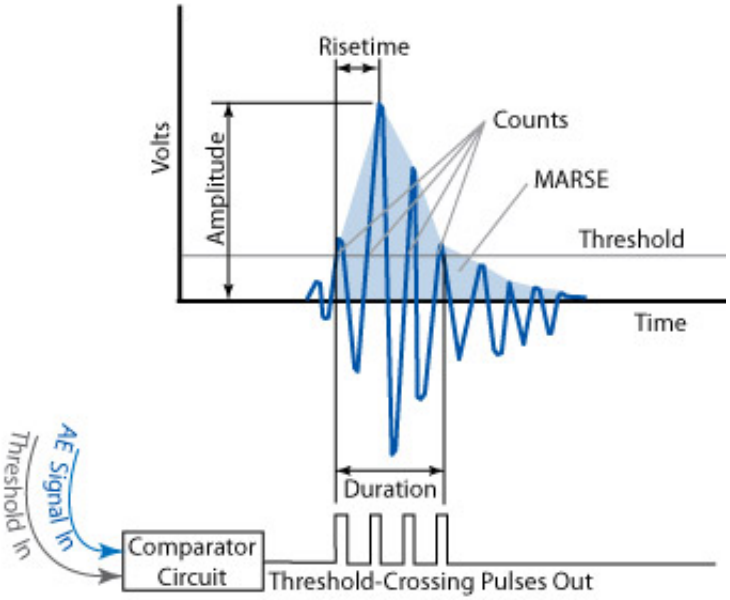

Figure 15: Typical AE waveform features.

A multitude of analysis techniques exist to interpret the AE results including single parameter methods, multiparameter methods, and waveform analysis. Figure 16 summarizes AE data collection and analysis techniques.

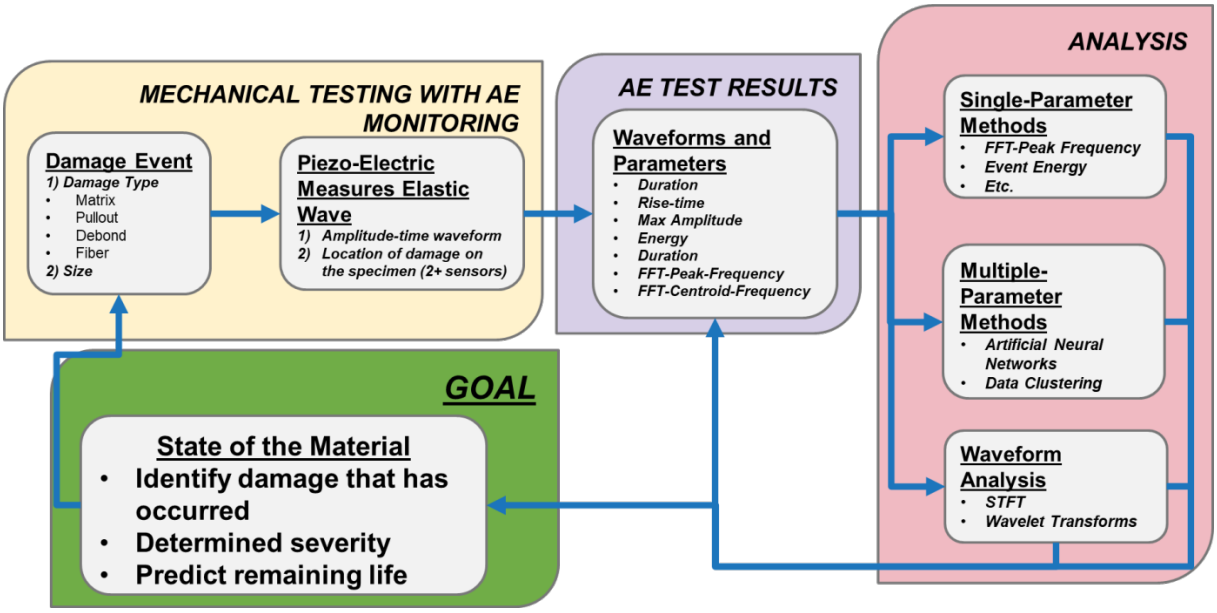

Figure 16: AE Data collection and processing flow chart

Single parameter methods were implemented to categorize and quantify the damage in a composite. As the name suggests, this method categorizes damage events based off one sole parameter. FFT-peak-frequency and energy have been the dominant parameters for differentiating damage, either by size or mechanism. FFT-peak-frequency has made a consistent appearance in literature as a way to distinguish damage mechanisms [39-43]. Damage mechanisms of matrix cracking, fiber matrix debonding, fiber pullout, and fiber fracture were correlated to different ranges of frequencies. Often, debond and pullout events are combined to be described as interphase events. Schuster explored this technique for an assortment of fabric architectures, specifying the frequency bins for glass-epoxy material to be 50-120kHz for matrix cracking, 120-180 kHz for debonding, 180-300 kHz for fiber/matrix debonding, and fiber breakage for events greater than 300 kHz [38].

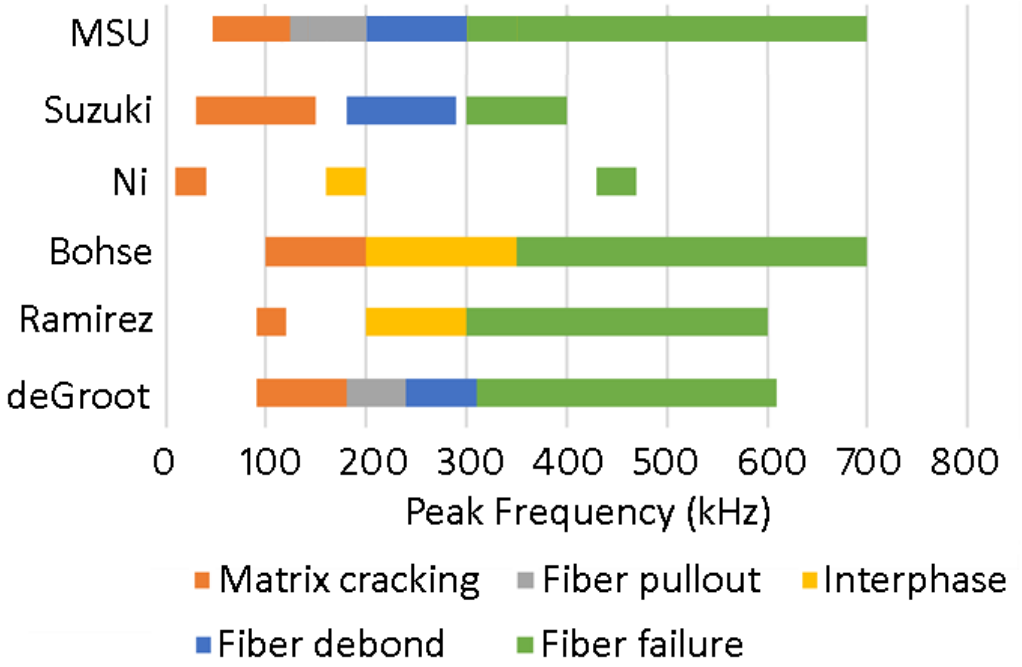

Figure 17: FFT-Peak-frequency bins from literature review and previous work at MSU.

Another single parameter often used to interpret AE data is energy. The energy of the elastic wave, derived from the integration of the time-amplitude plot of each waveform, can be correlated to the dissipated energy of the material. Schuster explored this parameter with load-unload-reload tests and found that AE energy does correlate to dissipated energy and can be useful in predicting the amount of damage, and thus the residual life of the material [38]. This trend between AE energy and damage accumulation has been observed in several other studies [44, 45].

Single parameter techniques, although often showing decent correlation, do not utilize all the available parameters to classify waveforms. Consequently, multi-parameter analysis techniques such as data clustering and artificial neural networks (ANN) have been a subject of current work in acoustic emission. The techniques allow data to be correlated based in multiple dimensions, incorporating more AE waveform features.

Interestingly, clustering studies revealed that peak frequency prevails as the only AE parameter with enough variance to isolate the data into clusters, which presumably represent damage mechanisms [46, 47]. Detailed waveform analysis has also been a been a subject of AE analysis. Waveform analysis examines each waveform in detail in an attempt to isolate wave modes and ultimately lead to new waveform features that are more descriptive of the damage event [48, 49]. Surgeon *et al.* proposed that isolating the features of both the extensional and flexural wave simultaneously could provide more information indicative of source behavior and orientation, but robust techniques to determine these parameters were not well established [48]. Waveform analysis conducted by the author implemented a short-term four transform (STFT) to gather frequency components of just the extensional wave resulting in notable variation from classic FFT-peak-frequency results. However, concrete validation of damage mechanisms and their relation to received AE waveforms remains the ongoing challenge with AE monitoring. Though these advanced techniques possess merit, single parameter analysis of frequency and energy will be the primary techniques employed in this work.

AE and Hygrothermal Aging

AE provides a useful method for interpreting damage progression in composite materials, making AE a logical choice for studying effects of hygrothermal aging on damage behavior of FRPs. Since AE is an indirect method of measuring damage, the measured response is a convolution of the damage behavior itself and the elastic wave propagation/attenuation behavior. Hygrothermal aging may affect both the damage

behavior of the material as well as its wave propagation behavior; thus, part of this research focuses on attempting to isolate these effects.

Previous work including AE monitoring with hygrothermal aging has shown significant changes in AE response due to hygrothermal aging. Hygrothermal aging in conjunction with AE was first demonstrated by Hamstad *et. al.* where the root-mean-square (RMS) energy emitted from a glass-epoxy system decreased after hygrothermal aging [50]. Later, Garg et. al investigated damage initiation in hygrothermal aging of a graphite epoxy system [26, 27]. This work examined both interlaminar and intralaminar damage initiation by means of delamination and transverse-tension tests. Both tests experienced a reduction in cumulative AE event counts as well as RMS energy with hygrothermal aging; losses were attributed to moisture induced attenuation of the AE signal. Komai observed a similar trend in fatigue of aged and unaged CFRP, however, the reduced output was speculated to be a change in damage behavior due to a moisture induced increase in resin ductility [32]. Another investigation of a chopped strand composite speculated that the reduction in energy due to aging could be due to a combination of damage behavior and wave-behavior effects [51]. Collectively, the outcome of the works has shown changes in AE due to hygrothermal aging to be multifaceted, potentially affecting the damage behavior and wave propagation/attenuation behavior simultaneously.

Guided Ultrasonic Waves

Ultrasonic techniques have proven to be a reliable method for interrogating composite materials in determining the damage state. Ultrasound has been widely

adopted as a method to detect flaws such as delamination and cracks in many applications, including inspection of composites for aerospace wind energy application. More recently, composites research has begun to implement another ultrasonic NDT technique, guided ultrasonic waves [3]. Like ultrasound, guided ultrasonic waves involve sending and receiving ultrasonic waves through a material. However, unlike ultrasound, guided ultrasonic waves utilize two or more separate sensors for sending and receiving waves. Ultrasonic waves propagate as lamb waves and travel long distances, even in materials with high attenuation, making them useful for surveying damage in large structures [52]. Since the source is often a user-generated input, unique frequencies and excitation angles can be implemented to excite specific lamb waves in the plate. However, anisotropy and viscoelasticity of composite materials make the study of lamb wave propagation a difficult one.

Despite the complex physical behavior in composite plates, guided ultrasonic waves have been implemented an effective NDE method for composite materials. Most commonly, guided ultrasonic waves are used to detect damage in a composite, which can be identified by distortion in the received wave as it is reflected at damage-induced discontinuities [52]. Aside from monitoring damage, guided ultrasonic waves have shown to be effective in evaluating environmental effects such as moisture uptake to composite laminates [16, 53]. Castaings *et al.* implemented guided ultrasonic for monitoring the attenuation of specific lamb-wave modes in carbon-epoxy pressure vessels for both monitoring moisture and microcracking [53]. In this work, it was discovered that the A_0 antisymmetric lamb wave experienced a 30% increase in attenuation during the aging

while symmetric modes experience no effect. The increase in attenuation correlated to increases in the loss moduli, or viscous response of the material. Further, after drying the aged sample, the attenuation of the A_0 wave was recovered to the original demonstrating the reversibility of moisture uptake in the system. Garg *et al.* observed a similar trend attenuation with moisture exposure, with attenuation increasing due to exposure time in a glass-epoxy system [16]. These findings suggest that moisture uptake affects ultrasonic/lamb wave propagation. Both AE and ultrasonic waves propagate as lamb waves, making ultrasonic waves a valid technique for understanding hygrothermal effects on AE wave behavior. Knowledge of these effects will aid in disseminating changes in AE response from being attenuation-based or damage-behavior based.

Thesis Goals

A shown above, hygrothermal effects on composite materials are complex and varying between material. The goal of this work is to identify the effects of hygrothermal aging on mechanical performance of a fiberglass epoxy system and to characterize the mechanism responsible for subsequent changes in performance.

As laid out in the background, the hygrothermal effects are largely matrix driven. Thus, the first part of this work will characterize the effects of moisture on neat epoxy through both thermal and diffusion analysis. Thermal analysis will determine whether the water is chemically or physically altering the structure of the epoxy, and the diffusion analysis will quantify swelling behavior. These results will aid in understanding the composite response to aging, the primary goal of the study.

Mechanical properties from static tensile tests conducted on several composite layups subjected to hygrothermal aging quantify the effect of hygrothermal effects on mechanical performance. Unidirectional and cross-ply laminates were included to determine whether hygrothermal effects on constituent unidirectional tests translate to cross-ply behavior. Further, the tests were designed to address the temperature effects of the artificial aging process and determine the reversibility of hygrothermal degradation. Additionally, observations from stress-strain behavior and acoustic emission monitoring will be used to help characterize damage behavior and progression.

Finally, a study in the Lamb wave propagation behavior of hygrothermally-aged laminates will be conducted using an ultrasonic guide wave to validate whether changes in AE response are due to moisture-induced changes in wave propagation or damage progression of the material.

MATRIX CHARACTERIZATION

Thermal Analysis: DSC

Differential Scanning Calorimetry (DSC) is one of several methods available for conducting thermal analysis on polymers. DSC compares the heat flow from a known reference sample to the sample of interest during a heating cycle to identify changes in heat capacity of the material; changes in heat capacity correlate to microstructural changes of the material. Quantitatively, DSC results yield the glass transition temperature, T_g. Changes in T_g relate to changes in the microstructure of the polymer and subsequently indicate changes in mechanical behavior. Although this method does not provide measurable changes of the mechanical behavior, it can provide insight into the physical/chemical nature of water in the polymer and aid in interpretation of hygrothermal effects mechanical data of the composite material.

Experimentation

Preliminary tests were conducted to determine an adequate sample manufacturing test method for the epoxy used in this study. The brittle behavior of epoxy makes extraction of small several-milligram size samples from a larger neat resin specimen. Additionally, post-processing operations increase the risk of contamination of the sample. To combat this challenge, samples were cast directly Aluminum DSC pans to prevent any post-processing. A blunt-tip syringe was used to inject a single drop into each pan; this method yielded consistent sample sizes with samples ranging between 18-30 mg.

Preliminary tests revealed that the cast samples produced more consistent results than those fractured from the bulk material.

Development of a test method stemmed from previous research conducted on an epoxy [30, 31]. These tests implemented a temperature control ramp, heating the sample at 20 °C/minute. Often, the first cycle through the glass transition is affected by residual stresses from curing or reaction of previously unreacted monomers remaining in the polymer. These processes, occurring concurrently to the glass transition, could potentially skew the T_g results. Therefore, two ramp cycles were conducted to determine if any of these behaviors existed in this epoxy system. The T_g determined from the second cycle provides a more accurate T_g value if the previous heating cycle does not significantly alter the temperature history of the material. Initial testing showed the 20 °C/ minute heating rate to be too fast, as sample size had significant effects on T_g, likely due to non-isothermal heating during the transient process. The ramp rate was reduced to 10 °C/min to reduce transient heating effects and yielded more consistent results. Specimens showed consistency and reversibility of the transition in the second cycle validating that the test did not significantly alter the temperature history of the epoxy. The final test method for DSC tests is shown in

Table 1: DSC Test method

Step number	Heating/Cooling ramp	End of ramp temperature (°C)
0	Start Test	Room-temperature (20-25 °C)
1	Heat: 10 °C/min	130°C
2	Cool: -10 °C/min	20°
3	Heat: 10 °C/min	130°C
4	Cool: -10 °C/min	20°
5	End Test	Room-temperature (20-25 °C)

To determine the nature of water in the epoxy system three series of tests were conducted. Each series consisted of five samples to determine an accurate T_g value. All samples were cured at 25 °C for 24 hours and 70 °C for 12 hours, meeting the manufacturing specifications (See Appendix B). The first series of tests were conducted on control, as-manufactured, samples that experience no hygrothermal conditioning. The next series was of samples that had been aged in 50 °C distilled water for 300 hours. These tests were conducted to determine the effect of absorbed water on T_g. The final series of samples were subjected to the hygrothermal aging as the second set, but then dried/desorbed until no more moisture was released, determined by equilibrium in the sample mass. The reversibility of this process both in terms of the amount of desorbed moisture and change in T_g may explain the whether the absorbed moisture in this is interacting physically or chemically with the epoxy system. Figure 18 shows an example DSC curve for a hygrothermally aged sample and Table 1 shows the conditioning for DSC samples, moisture contents and measured T_g values. T_g is reported as the center of the transition region determined by the tangent line method.

DSC Results

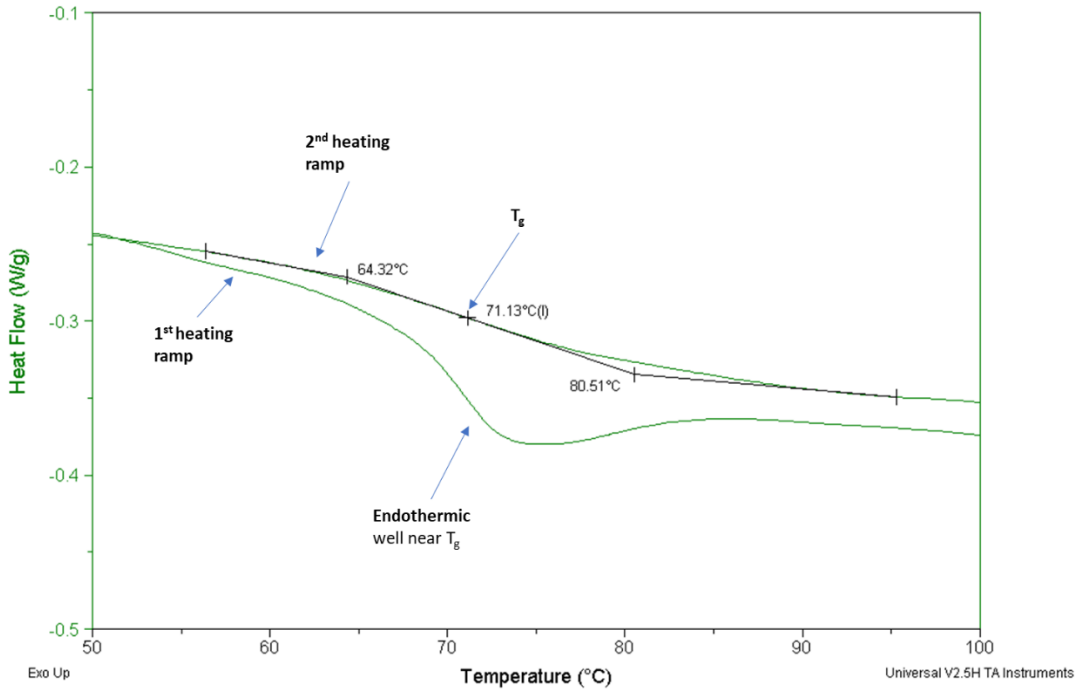

Figure 18: DSC heating curves showing T_g for Hexion 135/1366 with 4% moisture by mass

As shown in Figure 18, the heating curves for the first and second temperature ramps showed different behavior. Most notably, the first ramp cycle experienced an endothermic-well near the glass transition. This correlates to a release of energy from the test sample itself. This could be attributed to primarily two mechanisms; the reaction of monomers that did not react during the curing cycle, or relief of residual stress from the curing cycle, known as enthalpic relaxation. Aside from the endothermic well, both the first and second heating cycles followed one another closely on both the heating and cooling cycles, which would suggest that the source of the endothermic-well did not change the reversibility or structure of the material. This observation supports the

hypothesis that the endothermic-well was, in fact, enthalpic relaxation. Two-cycle DSC methods are recommended to deal with this anomaly [54].

Table 2: DSC sample conditioning and T_g results

Sample Type	Conditioning	Number of Samples	Tested bulk moisture content (%)	T_g measured from the second heating cycle.
Control	none	5	0.0%	86.9
Aged	312 hrs. 50°C distilled water	5	4.0%	69.9
Desorb	1) 312 hrs. 50°C distilled water 2) dried 620 hrs. 50°C	5	0.1%	90.9

The aging time of 312 hours resulted in a bulk uptake of 4% (Eq. 2); however, samples had not reached Fickian equilibrium and therefore m_∞ values of the system could be higher. Desorption returned the samples to a state of nearly 0% moisture content. Due to the small size of the samples, and the resolution 0.1 mg resolution of the mass balance used to weigh samples, the moisture content resolution was ~0.1% . The release of nearly all the moisture in the system at the same temperature as the aging process means most of the water molecules occupied the epoxy physically in free volume. However it is possible that the small amounts of water interacted chemically through hydrolysis or the secondary crosslinking network described by Zhou *et al.* [12]. Figure 19 shows the transition region on the second heating cycle for each test condition; both control and desorbed samples have a similar transition length, while the hygrothermally aged sample

has a premature and prolonged transition region. T_g results at each condition level are depicted below in Figure 20. Error bars represent the standard deviation[§] of the five samples for each test and show consistency in the test method.

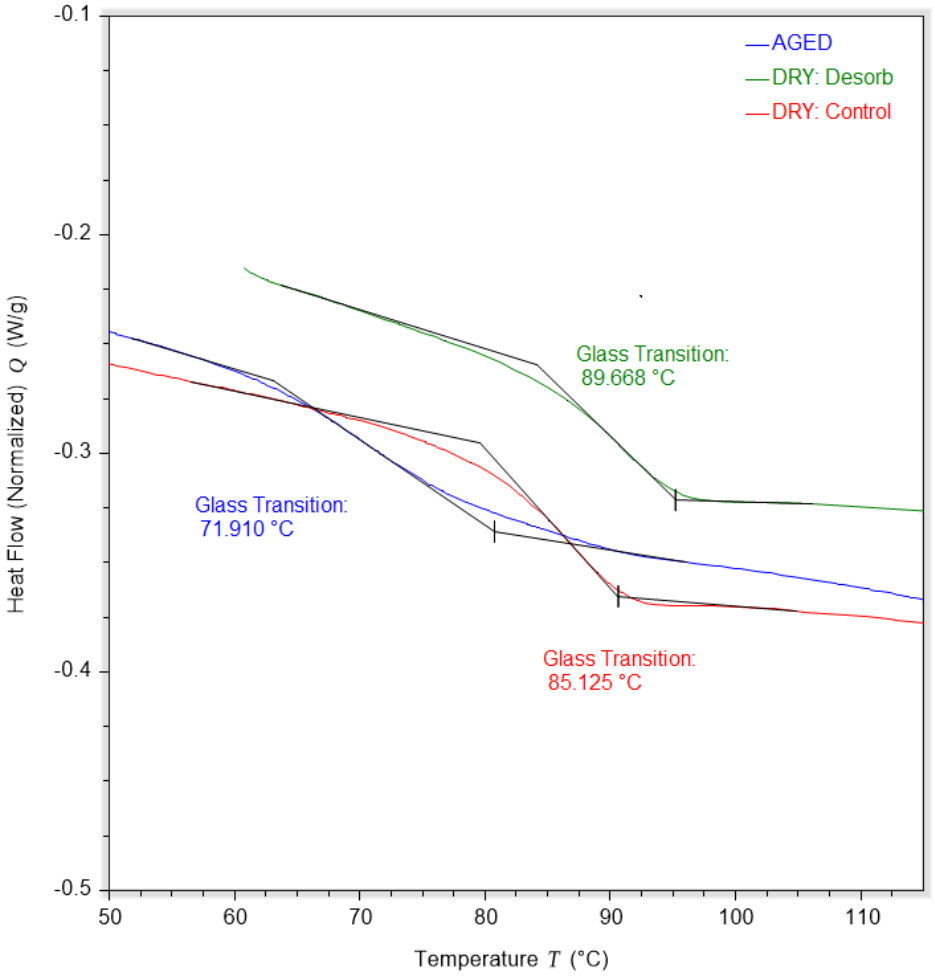

Figure 19: Example second-cycle heating curves for DSC samples of each condition

[§] Unless otherwise stated, error bars presented in throughout this work are standard deviations.

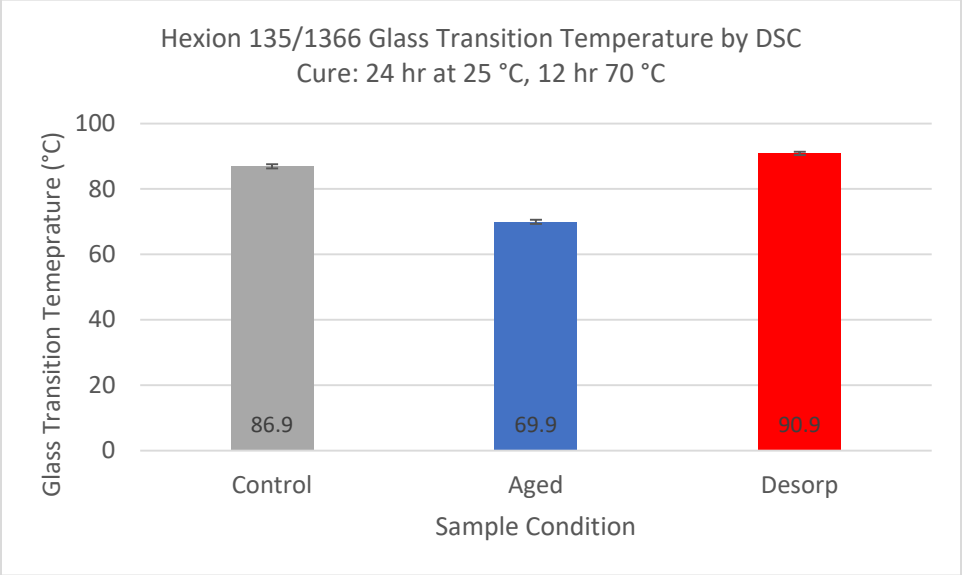

Figure 20: T_g results for hygrothermally aged Hexion 135/1366

T_g depression from the control to aged state confirms that aging-induced matrix plasticization is present in this matrix system. Despite a 17 °C drop after hygrothermal conditioning, T_g was fully recovered and exceeded control T_g of the control samples by 4°C after the desorption process. Full recovery of T_g suggests that plasticization is reversible in conjunction with completing drying of the samples shows that water molecules do not chemically interact with the polymer. The increase of the desorbed samples compared to the controls could be in part to the temperature history due to prolonged exposure to elevated temperature or increased crosslinking from reactions occurring during the conditioning process.

Thermal analysis yielded several findings which will aid in understanding degradation in the composite. First, reversibility of the aging process through desorption shows presence of water in this material system mostly physical. However, small

amounts of residual water could have interacted chemically chemically through hydrolisis and crosslinking. T_g depression confirms that plasticization is present, and T_g recovery with desorption shows this process to be reversible. Literature has shown that plasticization correlates to chagnes in mechanical behavior including reduced strength and modulus of the matrix material [14, 30]

Neat Resin Diffusion and Swelling

Isolation of the diffusion characteristics of just the matrix material helps explain the diffusion and swelling characteristics of the composite. As moisture is diffused in a polymeric material, swelling occurs. Consequently, swelling can alter the internal stress state of the composite, potentially causing damage and alter the mechanical performance.

Experimentation

These moistures induced swelling strains, known as hygro-strains, can be difficult to measure experimentally in a composite and in neat resin with small geometries. To determine hygro-strains, a set of large-geometry neat resin samples manufactured, so that average strains could be measured from larger geometric changes. Neat resin cubes (5 cm x 5 cm x ~4.5 cm") of Hexion 135/1366 were cast in a brass 3-piece mold shown in Figure 21 by hand pouring.

Figure 21: A 3-piece mold for manufacturing neat resin cubes.

After curing the cubes, the samples weighed to get initial masses. A digital caliper was used to measure the size of the cubes to a resolution of 0.05 mm. each face of the cube was measured in width and length from the center of one edge to the center opposite edge. These 12 length measurements could then be used to calculate the volume of the samples. After the initial measurements, the cubes were aged in distilled water at 50°C. The cubes were periodically removed from the water and dried so that mass and volume could be measured and monitored throughout the diffusion process. The bulk moisture uptake was calculated by Equation 2 and the average swelling strain was calculated from the measured change in cube dimensions at each measurement interval. Since the diffusion is a transient process, it is important to note, strain levels will vary spatially with moisture content. Three cubes were aged, and 3 cubes were kept in their control-dry state for later comparison.

Neat Resin Diffusion and Swelling Results

Figure 22 shows the bulk mass diffusion for the three neat resin cubes plotted versus the square root of time. The diffusion behavior of the pure matrix material appears linear in the square root of time domain, as anticipated for Fickian behavior. However, due to the size of the samples, the diffusion process takes an exceedingly long time to reach equilibrium, and as seen in Figure 22, the neat resin cubes have not yet begun to approach the asymptotic equilibrium value. The final data point published in this work was for an aging time of 5000 hours. After 5000 hours of aging, samples absorbed 5.72% moisture by mass and could increase with continued aging. This value is more than observed in the DSC test (not soaked to equilibrium) and is on the upper end of the 2-7% expected for an epoxy system [12]. These values will be compared to the *in situ* matrix-uptake values of composite specimens in the subsequent section.

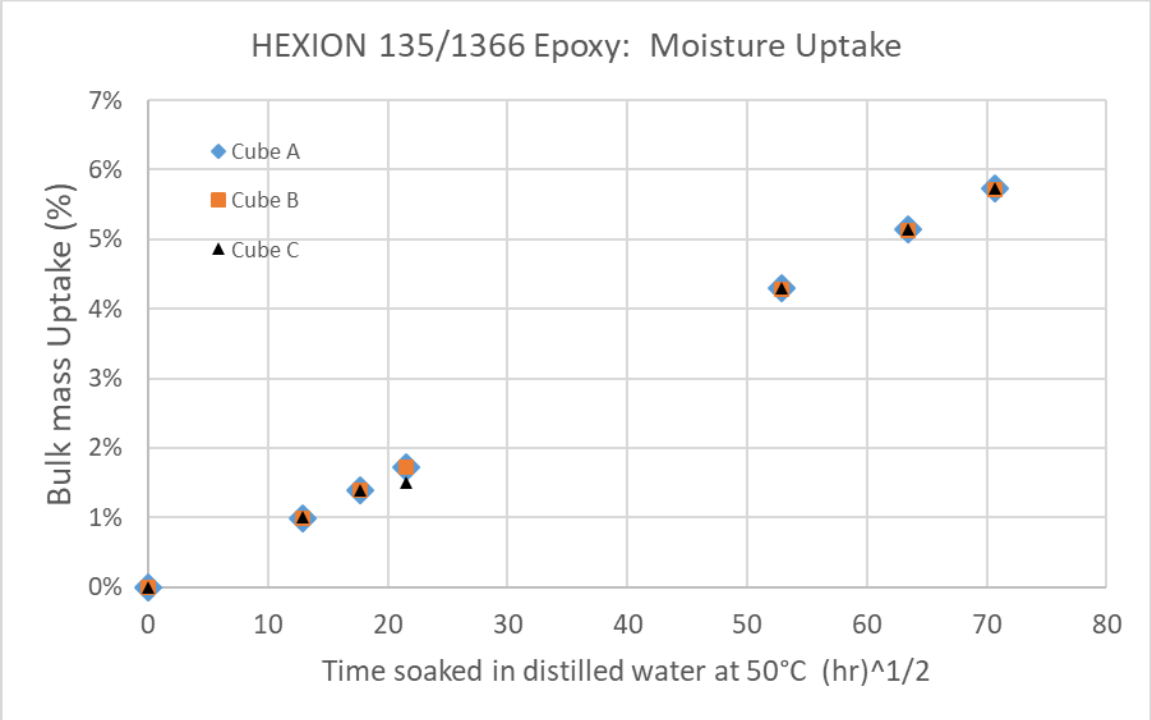

Figure 22: Neat resin cube bulk diffusion

A significant amount of moisture uptake resulted in a significant swelling strain, shown in Figure 23. After 5000 hours, strains reached an average of 1.94% strain. The increase in swelling strain correlates well with the increase in moisture content.

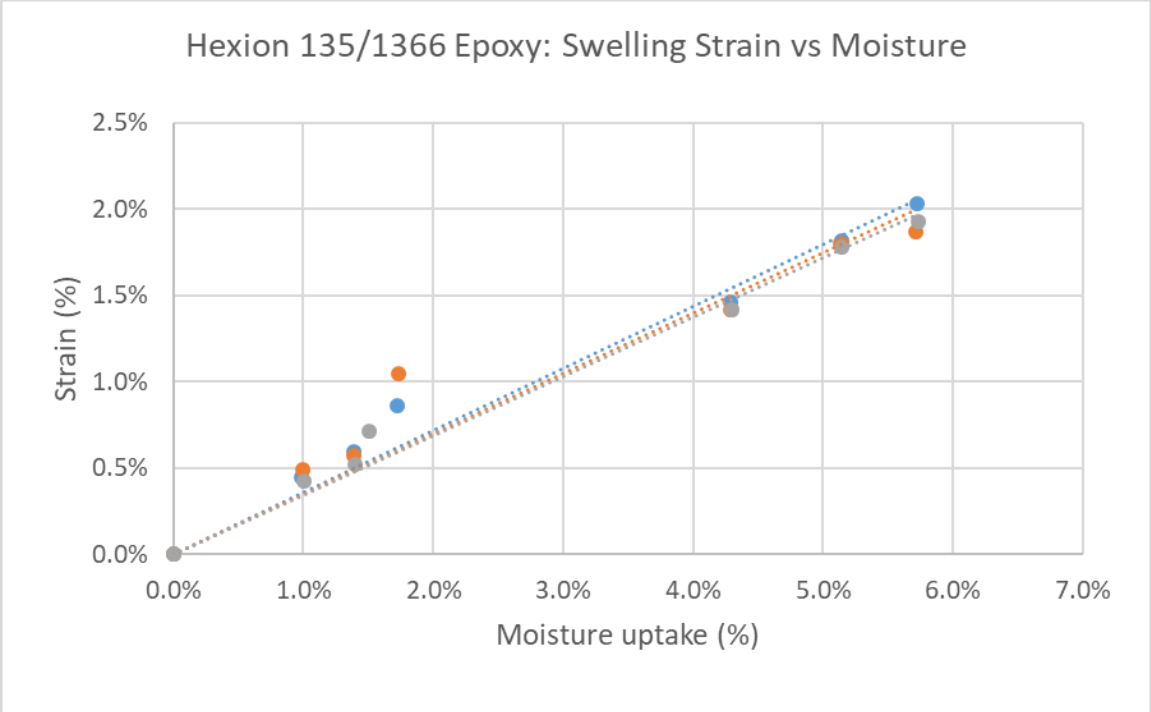

Figure 23: Swelling strains during transient diffusion of neat resin cubes.

Moisture uptake and swelling of this magnitude possess the ability to cause large internal stresses which could damage the composite or alter the damage progression upon loading. Using the bulk strain and moisture uptake, a hygrothermal swelling coefficient for the matrix material β_m can be determined for this epoxy system as shown in Equation 7.

$$\beta_m = \frac{C}{\varepsilon} \tag{7}$$

C is the bulk moisture uptake of the isotropic material and ε is the strain. The slope of the strain plots shown in Figure 23 gives this value. For the Hexion 135/1366, β_m is 0. 35 (%ε / %m). Theoretical hygro-stresses in composite laminates will be evaluated using laminate theory in the subsequent static test section.

Comparison of hygrothermally aged neat resin cubes control samples revealed significant changes in the appearance due to aging. Changes in appearance from a control to aged state include both changes in color and opacity as well as visible damage within aged samples. Figure 24 shows this obvious change in color from the aging process and notes areas where the damage occurred. Figure 25 shows the cross-section of the cubes, where the internal damage can be observed.

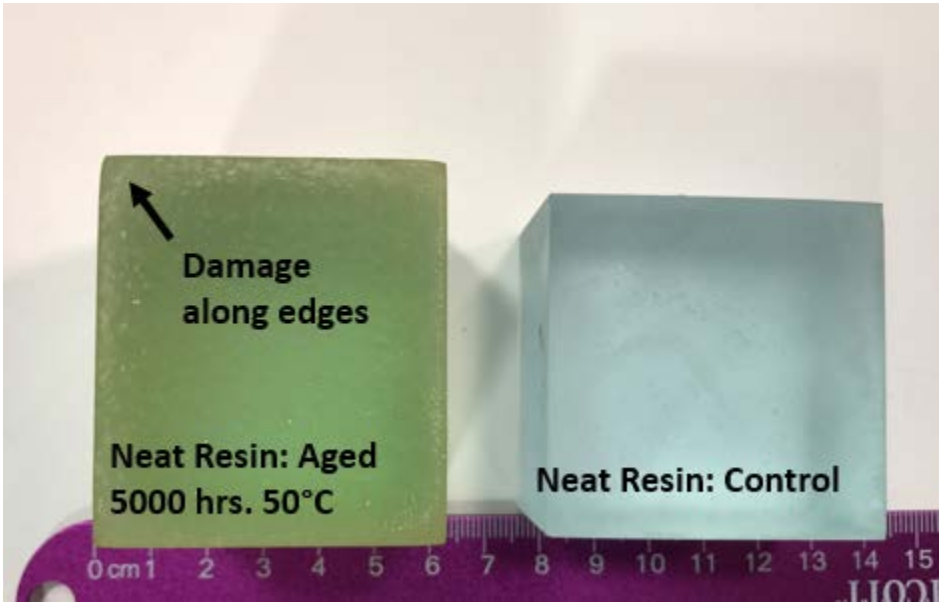

Figure 24: Neat resin cubes aged 5000 hours (left) and control (right)

As seen in by the cross-sections in Figure 25, many cracks formed along the edges of the cube and ranged in size from 0.4mm to 2mm. High moisture contents along the boundaries of the cube caused large amounts of localized swelling which ultimately lead to damage.

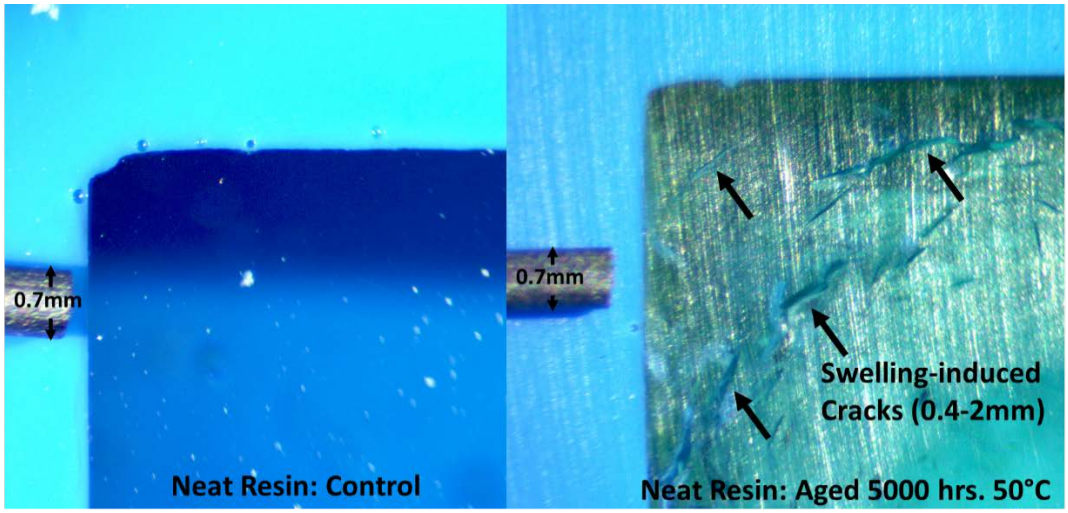

Figure 25: Cross section of selling damage of neat resin (Hexion 135/1366) under an optical microscope (5X).

STATIC TESTS

Test Design

Characterization of composite materials for marine environments relies on the characterization of mechanical properties through mechanical testing. This work focusses on exploring the effects of a marine environment on one material system to classify changes in mechanical properties as well as the underlying changes in damage behavior. The results of this study will aid engineers in the application of this material system in the design of MHK devices and off-shore wind turbines, as well as provide further insight into mechanisms of hygrothermal degradation and methods to identify these mechanisms in future studies involving diverse material systems.

This work stems as a continuation of the work of Jake Nunemaker, which explored the effects of partial saturation on strength of fiberglass-epoxy, cross-ply laminates by confirming that moisture reduced the strength of lead-bearing plies [22]. Significant strength degradation occurred with aging, particularly in the fully saturated state, the mechanisms of which were not fully understood. To aid in the evaluation of the changes in the static strength of cross-ply laminates, this works adds tensile tests of unidirectional laminates in both the longitudinal and transverse directions. Little work has been done to classify aging effects from constituent unidirectional laminates to multi-directional laminates. With damage mechanisms and damage progressions of unidirectional and cross-ply laminates being well understood, comparison of laminates in aged and unaged states should give insight into the hygrothermal degradation mechanisms at large in this material system. Additionally, this work includes test samples

that have been soaked and dried or desorbed to determine the reversibility of the degradation mechanisms. To verify that changes in performance are not an artifact of elevated aging temperatures altering the temperature history of the FRP, samples with just temperature exposure were also tested. Five tensile were tested for each laminate in each condition. Table 3 shows the mechanical tests conducted in this study.

Table 3: E-LT3800 Mechanical Test Matrix

Layup	Condition	Test Method	Number of Samples	Acoustic Emission
$[0]_2$	Dry: control	Static-Tensile	5	Yes
$[0]_2$	Saturated	Static-Tensile	5	Yes
$[0]_2$	Dry: desorb	Static-Tensile	5	Yes
$[90]_2$	Dry: control	Static-Tensile	5	Yes
$[90]_2$	Saturated	Static-Tensile	5	Yes
$[90]_2$	Dry: desorb	Static-Tensile	5	Yes
$[0/90]_s$	Dry: control	Static-Tensile	5	Yes
$[0/90]_s$	Saturated	Static-Tensile	5	Yes
$[0/90]_s$	Dry: desorb	Static-Tensile	5	Yes
$[0/90]_s$	Temperature only	Static-Tensile	5	No
$[90/0]_s$	Dry: control	Static-Tensile	5	Yes
$[90/0]_s$	Saturated	Static-Tensile	5	Yes
$[90/0]_s$	Dry: desorb	Static-Tensile	5	Yes
$[90/0]_s$	Temperature only	Static-Tensile	5	No

The conditions of the test coupons, Dry-control, Saturated, Dry-desorb, Saturated, and Temperature-only (no moisture) will be explained in detail in “Experimental Methods” section. In addition to the results of the mechanical testing, AE data was collected to aid in described the changes experienced by hygrothermal aging. Further, this work will include both macro and microscopic evaluation of damage occurring laminates

due to hygrothermal aging as well as evaluation of failure types observed during static testing

Experimental Methods

Materials and Manufacturing

Infused, textile-type, E-glass FRP's have been the material of choice in the wind industry, with static and fatigue properties for these types of materials being well characterized and readily available. Consequently, with the emerging MHK designs sharing many of the same design parameters, these materials present a viable choice for selection in these new energy harvesting devices. The laminates of this work were manufactured with Vectorply E-LT3800 fabric and a Hexion 135/1366 two-part epoxy. The manufacturer's specification sheet for these materials can be found in Appendix A. The E-LT 3800 is a stitched, predominantly unidirectional consisting of 1138 g/m^2 (91%) of longitudinal tows and 114 g/m^2 of transverse backing strands, stitched together with polyester thread. Although this fabric is truly a biaxial fabric, it will be considered a unidirectional lamina due to a large number of fibers in the longitudinal direction. In the stacking sequence, backing strands are oriented towards the centerline of the laminate so a $[0/90]_s$ is equivalent to a $[0_b\backslash 90_b]$s laminate, where "b" indicates the location of the fabric backing[**]. Presence of backing strands but be considered when interpreting static test results.

Laminates were manufactured using the VARTM process depicted in Figure 5. An aluminum plate was used as a mold, featuring an inlet and an outlet port at either end of

[**] "s" indicates a symmetric laminate; $[0/90]_s$ is equivalent to [0/90/90/0].

the infusion process. The mold was treated with a mold release agent to prevent the laminate from bonding to the mold surface. A layer of peel ply was placed above and below the fabric stacking sequence aid in the demolding process. Flow media, a plastic mesh was placed on top of the upper peel ply to allow the resin to flow across the top of the laminate and diffuse downward through the thickness. Synthetic rubber sealing tape was placed along the perimeter of the mold, and the layup was sandwiched beneath a plastic bagging film to seal the one-side mold. A vacuum pump attached to the outlet port via a plastic was used to infuse resin into the fabrics.

The resin was mixed per the manufactures specification (100g RIMR 135 to 30g RIMR 1366). Mixing was achieved using a motorized spindle at a speed that was fast enough to agitate the resin but slow enough to prevent porosity from turbulent flow. Mixing was conducted for 4 minutes to thoroughly mix the two-part resin. After mixing the resin, the tube connected to the inlet port was placed in the container of mixed resin, and the infusion process was started. Depending on the laminate, diffusion times could vary, ranging between 10 and 15 minutes.

The laminates were cured using the two-step cure cycle recommended by the manufacturer. The first step was a 24 hour room temperature cure (25 °C) on the mold after which the laminate could be removed from the mold and placed in the post-cure oven. The post-cure was maintained at a temperature of 70 °C with a temperature controller and lasted 12 hours. Matrix burn-off tests were completed for each laminate with the fiber volume fractions ranging between 55 and 58%.

After curing, laminates cut into tensile test coupons using a water-lubricated diamond abrasion saw. The coupon geometries were a nominal 30 mm by 300 mm, but actual sample dimensions, including thickness, were measured using digital calipers and recorded. These sample dimensions were chosen to provide enough area to capture an adequate amount AE data. After the conditioning process, but before the tensile testing, tabs made of G10 fiberglass plates were adhered to the test samples using adhesive. Tabs measured 64 x 32 millimeters and alleviate some of the damage from the grips of the testing machine during the static tests. This sample layout is depicted in Figure 27.

Sample Conditioning

To simulate a marine environment, samples were subjected to hygrothermal aging. Samples receiving no conditioning after manufacturing are referred to as “dry-control”. Dry-control samples may still contain moisture absorbed through the manufacturing process or humidity, but this intrinsic moisture should be minimal. Samples hygrothermally-aged samples were soaking in 50°C distilled water. Distilled water was chosen over synthetic seawater because previous work at MSU has found that salt build up on the coupon surfaces can alter moisture content measurements; further, distilled water usually results in more moisture uptake into the composite and would represent more conservative case. Further, EDX/EDS have shown that salt does not diffuse into the composite as a compound or an ion [19, 20]. Prior to hydrothermal aging, the initial mass of the sample was obtained using a digital scale to the resolution of 0.001 grams. After subsequent periods of hygrothermal exposure this mass could be remeasured to give the bulk moisture content of the sample by the Equation 3. Samples were aged

until the bulk moisture content plateaued to equilibrium as shown in Figure 10. After reaching equilibrium, samples were removed from the water, and tabs were applied with an epoxy adhesive and allowed to cure at ambient conditions for 12-16 hours. Specimens were tested within 24 hours of removal from the water to prevent significant loss of moisture. These samples reached the maximum moisture content and will be referred to as “Saturated” and the moisture content reported is the moisture content before tabs were applied. An additional set of saturated samples were then placed in a 50 °C environment and dried to remove moisture. The process of drying is known as desorption; thus, aged-then-dried samples are referred to as ‘Dry-desorbed”. Like the saturated samples, the desorbed samples were tabbed and tested after an equilibrium was reached. Another set of control samples referred to as “Temperature-only” were aged in a dry 50 °C environment for the same duration as the saturated samples to isolated temperature history effects of the accelerated-aging process.

Mechanical Testing Procedures

Samples were tested monotonically in quasi-static tension until ultimate failure in accordance with ASTM D3039 [55]. Testing took place in an Instron 8562 servo-electric load frame in position control with a cross-head displacement rate of 15.2 mm/minute for all samples. The hydraulic grip pressure of 21 MPa was applied for laminates containing 0° plies and 7 MPa for transverse ($[90]_2$) samples. Strain was measured with an Instron 12.7 mm gage section extensometer; Figure 26 shows the experimental setup. Both load data and strain data were collected using the Mistras AE system. To prevent damage to the extensometer at final failure, the gage was removed between 1% and 1.5% strain. The

strain rate of the last 0.2% of collected strain was linearly extrapolated to ultimate failure so that stress-strain curves could be generated for these tests. For unknown reasons, parametric outputs shorted-out during some tests and thus strain data is not available for all samples; however, ultimate loads were collected for all samples.

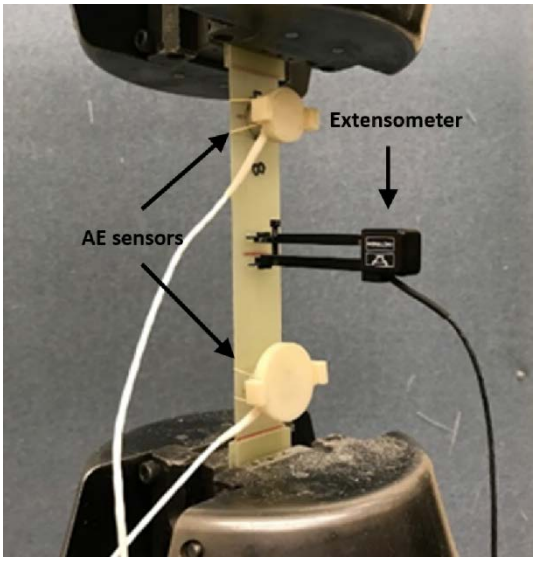

Figure 26: Tensile test experimental setup.

Acoustic Emission Setup and Data Collection

All tensile tests except the temperature-only tests were monitored with a Mistras PCI- Micro-II system. This AE setup parameters utilized in this work were developed by Michael Schuster; a more detailed explanation of the system operation and setup can be found in his thesis [38]. To use the linear-locating functionality of the system, two Physical Acoustics wideband sensors were attached to the test specimens in a linear array as shown in Figure 27. Sensors were spaced 128 mm apart and centered across the width

of the sample. 40 dB external amplifiers magnified the AE signals. A thin layer of vacuum grease ensured good contact with the test specimen.

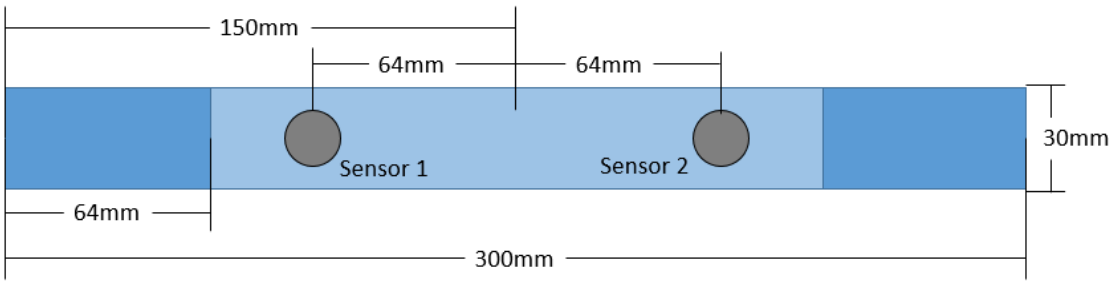

Figure 27: Tensile test sensor layout[††]

The Mistras system featured an AE sampling rate of 3 MHz and a bandpass filter for the range of 50-400 kHz. A threshold of 40 dB was sensitive enough to pick up damage-induced AE activity without collecting ambient noise. Events were collected with 128k of pretrigger and a total waveform length of 1024k. The timing parameters peak definition time (PDT), hit definition time (HDT), hit lockout time (HLT), and max duration was set to 50, 100, 300, and 99 microseconds. A time of flight-based filter used to limit recorded events to those occurring between the sensors.

In preparation for the mechanical test, two system tests were conducted. The first system test was the sensor test using the Acoustic Property Matrix Generator (APMG). The sensor test uses the AE sensors as actuators to pulse the system. Time of flight between sent and received pulses determine the wave speed and compare the response of the sensors. If energy and amplitude response between sensor varied by more than 10%,

[††] Jake Nunemaker

the sensors were reapplied and tested again. The second system test simulated an acoustic emission event by conducting a pencil lead break (PLB) test to generate an elastic wave. Breaking pencil lead on the sample in various locations verifies that linear locating is working correctly and that no extraneous noise events are picked up. Upon completion of these tests, a collection of AE is initiated followed by the start of the static test. AE data were collected through the ultimate failure of the test specimens and truncated at the ultimate load in the post-processing.

Results

Moisture Absorption and Desorption

The moisture absorption curves and desorption results are shown below in Figure 28 and Figure 30 for both unidirectional and cross-ply laminates. The absorption diffusion curve, plotted against the square root of time, matches Fickian behavior shown in Figure 10. The behavior is linear for the first portion and then asymptotically approaches equilibrium. Two-ply samples soaked for 1150 hours to reach equilibrium while 4-ply specimens required 5100 hours to achieve equilibrium. A thickness normalized diffusion curve (Figure 29) was used to compare the diffusion rates of both 2-ply and 4-ply laminates to incorporate the effect of thickness in Eqn. 4. Diffusivity values were calculated for the linear portion and ranged between 1.03e-3 mm^2/hour and 1.09e-3 mm^2/hour for both 2-ply and 4-ply laminates using Eqn. 4. These results, combined with the consistent diffusion trends between $[0]_2$ and $[90]_2$ suggests that edge diffusion was minimal. Bulk moisture content at saturation ranged between 0.89% and

0.94%. Rule of mixtures was applied to determine the *in situ* M_∞ of the epoxy (Equation 8).

$$M_\infty = \frac{M_{bulk}}{\rho_{matrix}} * (v_f \rho_{fiber} + (1 - v_f)\rho_{matrix}) \quad (8)$$

For the range of bulk moisture contents, the measured volume fraction, and a measured matrix and glass density of 1.128 g/cm^3 and 2.55 g/cm^3, respectively, the in-situ M_∞ for the epoxy was 2.64 -2.84 % by mass. As shown in the matrix characterization section, neat resin samples for the Hexion 135/1366 absorbed 6 % moisture and had not yet reached equilibrium. The variance between the in-situ matrix absorption and neat resin absorption implies there is a stress equilibrium associated with aging, with reinforcement fibers acting as a limiter to swelling strains and preventing moisture uptake.

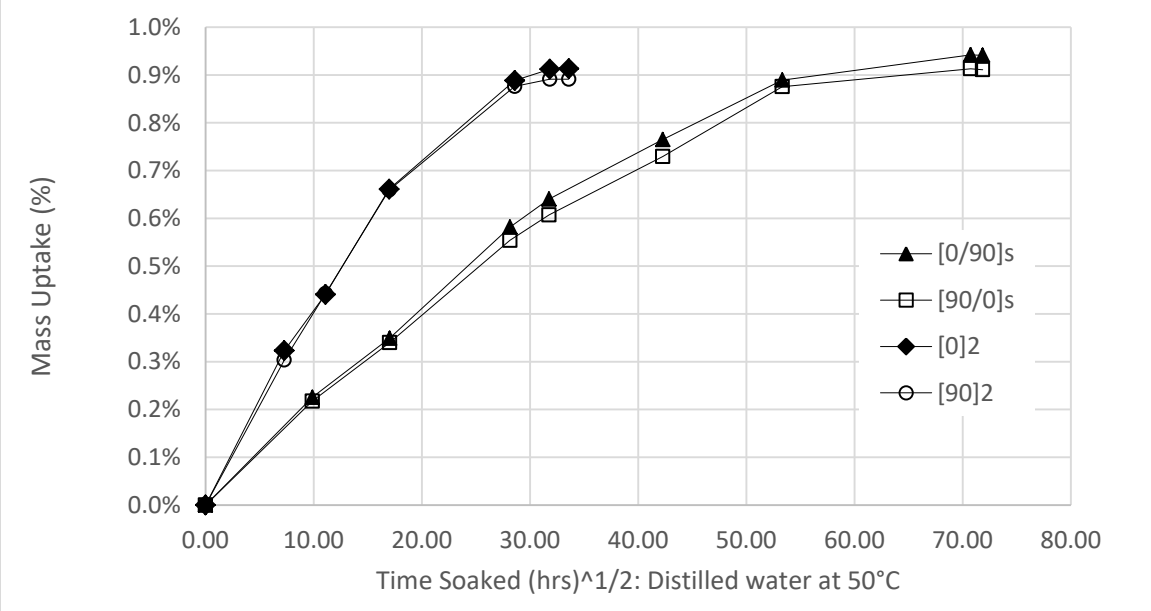

Figure 28: Bulk moisture absorption curves

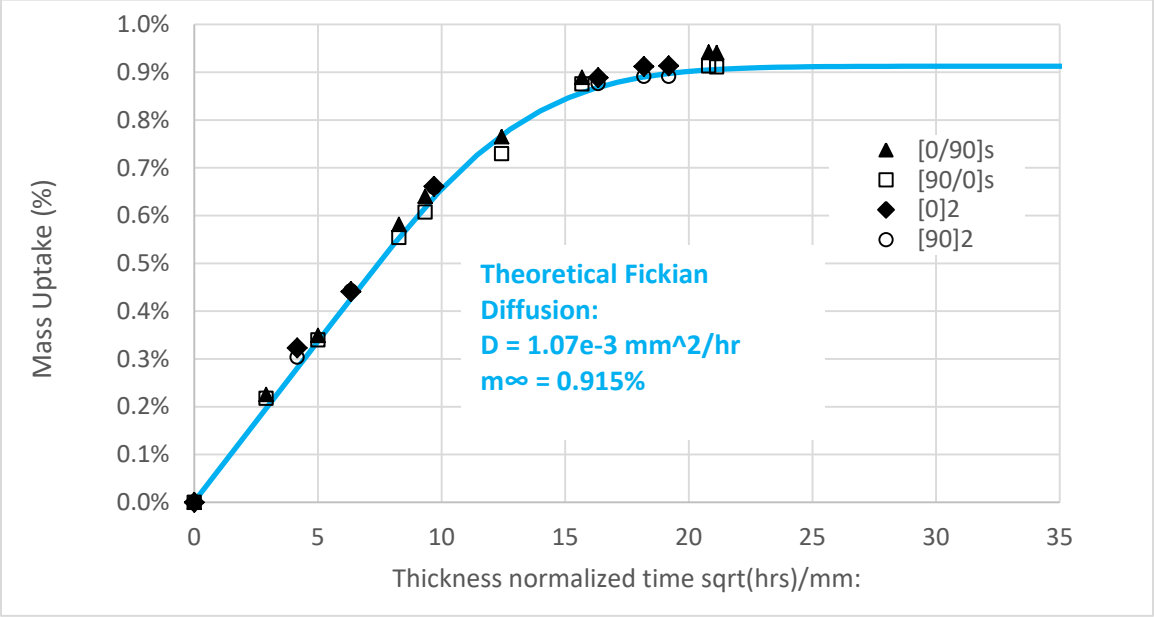

Figure 29: Thickness-normalized absorption curves with theoretical fickian diffusion.

Desorption samples also showed a consistent Fickian trend. Four-ply laminates asymptotically approached a zero-moisture state, with less than 0.02% moisture by mass remaining. Two-ply laminates showed a similar trend but showed a net loss in mass ranging from -0.21% to -0.06%. A loss in mass could indicate leaching of the matrix material into the water; however, 2-ply desorption samples were conditioned several months after the months after manufacturing and could have absorbed ambient moisture prior to conditioning, skewing the initial mass reading. The total drop in the mass of about 0.9% correlates the M_∞ value and would indicate that all mass losses were due to loss of water. However, chemical interaction of water molecules could have degraded the epoxy causing leeching of the polymer into the water resulting in mass loss.

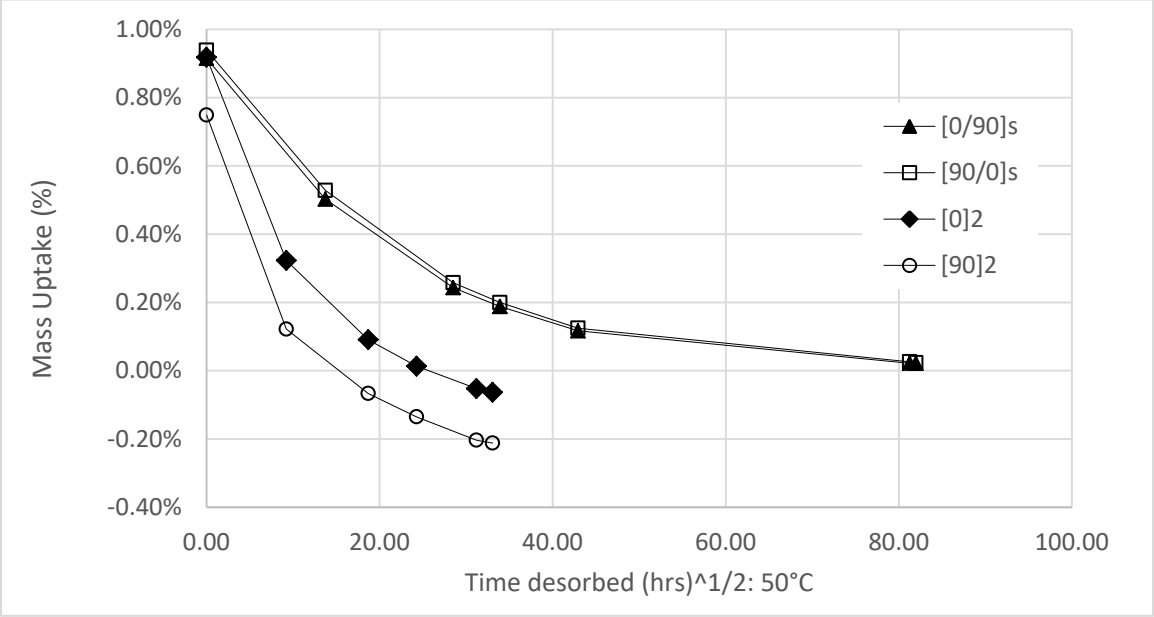

Figure 30: Bulk moisture desorption curves.

The Fickian absorption suggests that the occupation of moisture in the polymer is physical in nature, occupying free volume rather than chemical interaction through secondary bonding or hydrolysis. Further, nearly all the moisture was desorbed at the same temperature as the absorption temperature. This coincides with the findings from the matrix characterization section and provides evidence that most of the water occupied the composite physically. If chemical interactions such as a secondary bond network or hydrolysis occurred, interacting water molecules would not be able to be expelled at without elevating the drying temperature above the original conditioning temperature [12].

Theoretical Swelling Stresses in FRP laminates

A lamina-based model was implemented to determine the theoretical stresses induced by hygrothermal swelling. Since non-organic fibers are considered impermeable,

expansion coefficients for a transversely isotropic lamina can be calculated from just the expansion value for the neat resin determined in the matrix characterization section. Equations 9a and 9b show the formulations for the hygro-expansion coefficient in the longitudinal β_L, and transverse direction, β_T. [29]

$$\beta_L = 0 \tag{9a}$$

$$\beta_T = \frac{\rho_c}{\rho_m}(1 + \nu_m)\beta_m \tag{9b}$$

Expansion in the fiber direction is considered negligible due to high fiber stiffness in comparison to the matrix. In the transverse direction, the expansion coefficient is related to the matrix mass fraction, Poisson ratio of the matrix, ν_m and the swelling coefficient of the matrix. Using previously mentioned densities for glass and the Hexion 135/1366 epoxy, an average fiber volume fraction of 56% and assuming an epoxy Poisson ratio of 0.33, the β_L can be calculated as 0.8 (%ε /%m). These expansion coefficients, implemented with classical plate theory, can give the lamina stresses induced by swelling alone. To do this, the swelling coefficients must be transposed to the global coordinate system using the transformation matrix [T], as shown in Equation 10 [5].

$$\begin{Bmatrix} \beta_x \\ \beta_y \\ \frac{1}{2}\beta_{xy} \end{Bmatrix} = [T]^{-1} \begin{Bmatrix} \beta_L \\ \beta_T \\ 0 \end{Bmatrix} \tag{10}$$

Stress can be solved by using the global stiffness matrix for the material. Strain can be induced by mechanical loads of extension and bending, thermal, and hygro-

strains. For analysis of hygro-swelling, only the hygro-strains are considered (Equation 11)

$$\{\sigma\} = [\bar{Q}](\{\varepsilon_0\} + \{k\}z - \{\alpha\}\Delta T0 - \{\beta\}\Delta C) \tag{11}$$

If hygrothermal loads are the only loads applied, they must equilibrate and therefore satisfy the force- stress balance in Equation 12.

$$\{N\} = \int_{-h/2}^{h/2} \{\sigma\} dz = 0 \tag{12}$$

These stresses were calculated for the laminates tested in this study. Although truly a biaxial fabric, the E-LT 3800 will be considered as a purely unidirectional lamina for this analysis. The analysis was conducted with CADEC analysis software using classical plate theory. The input data for the E-LT 3800 Hexion/135/1366 lamina is shown below in Table 4.

Table 4: Lamina-swelling stress model inputs for Hexion/ Vectorply E-LT3800[⌗⌗]

Input	Symbol	Value	Units
Longitudinal Modulus	E_1	40.2	GPa
Transverse Modulus	E_2	15.9	GPa
In-plane Poisson Ration	ν_{12}	0.27	n/a
Out-of-plane Poisson Ratio	ν_{23}	0.35	n/a
In-plane Shear Modulus	G_{12}	3.54	GPa
Out-of-plane Shear Modulus	G_{23}	5.889	GPa
Longitudinal coefficient of Moisture Expansion	β_1	0.0	%ε/%m
Transverse coefficient of Moisture Expansion	β_2	0.8	%ε/%m
Moisture content	C	0.92%	%m

[⌗⌗] Dan Samborsky: Summary of Vectorply E-LT 3800 Fabric Properties

Lamina-Swelling Results: Application of the swelling model induced strain in the unidirectional layups of $[90]_2$ and $[0]_2$, but with no transverse plies to limit swelling, no stress was induced. The model did not account for backing strands in the fabric architecture which could allow stresses to develop. Cross-ply laminates, however, saw a change in internal stress from hygro-swelling, causing the 90° plies to undergo a compressive stress, and 0° plies to undergo a tensile stress. This axial stress distribution is shown below in Figure 31.

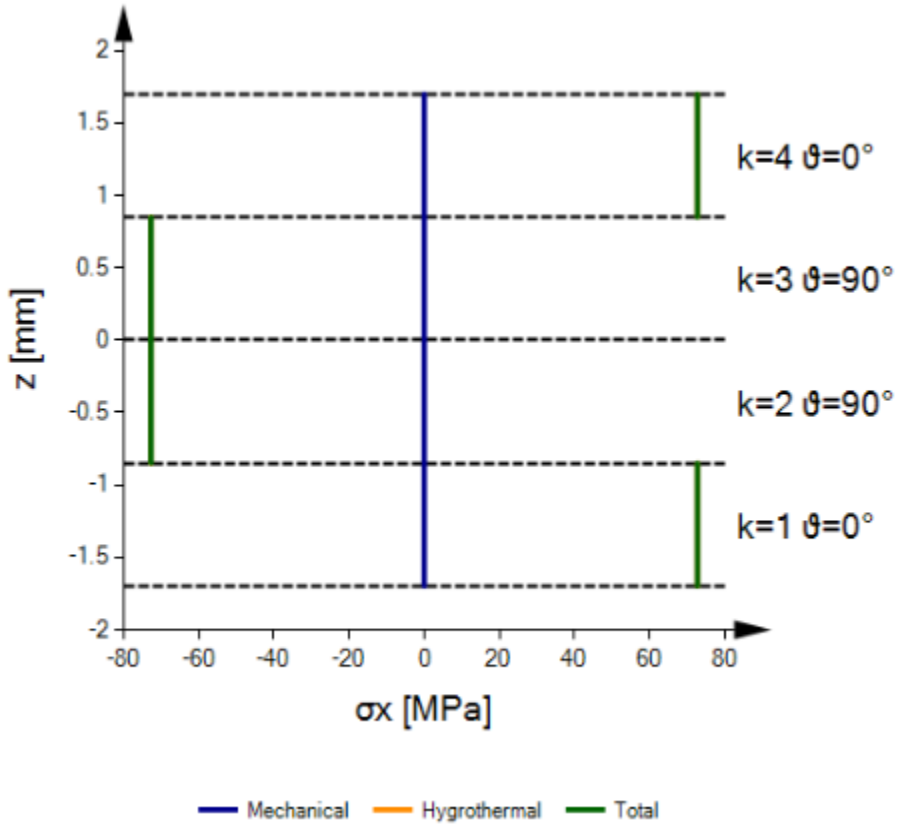

Figure 31: Cross-ply hygrothermal stress distribution (k = lamina number; ϑ = ply angle)

The stress levels in the cross-ply laminates reached a magnitude of 72 MPa. This swelling stress is significant and could certainly influence the mechanical loading of the

composite, as well as induce damage. The lack of recoverability of laminate strengths with desorption (“Mechanical Properties” section) would indicate that the swelling stress state alone does not account for the degradation of the material system. However, the stresses are high enough that damage could occur on a micromechanical level. Figure 33 in the next section shows the spatial variability of the volume fraction in textile laminates which would be the means for variability in expansion coefficients and ultimately large stress gradient which could cause damage. Interestingly, the stress gradient between 0° and 90° lamina in the cross-ply laminates could cause large shear stress between plies and thus be a source of interply damage and attribute to the larger strength drops in the cross-ply laminates in the “Mechanical Properties” section.

Hygrothermal-aging Damage

Physical damage to the aged composite laminates apparent upon inspection of conditioned laminates. Visual inspection of coupons after aging showed streaking in tows of all layups. An example of the damage is shown below in Figure 32.

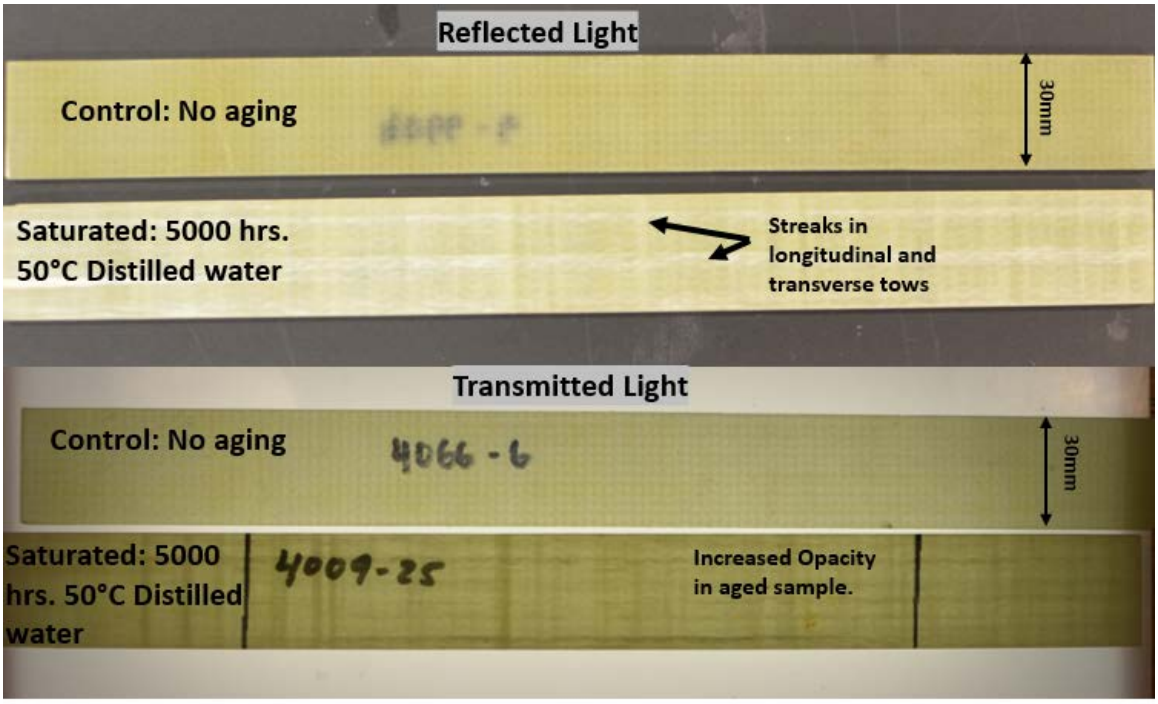

Figure 32: Visible damage from hygrothermal aging in the cross-ply laminate.

In reflected light, the damage streaks reflect light, lightening the color of the composite. In transmitted light, the damage streaks increase the opacity, darkening the composite. Damage in a transparent material creates surfaces which scatter and reflect light, ultimately altering the optical properties. Further, the damaged remained after the desorption process which would indicate the change in opacity was physical and not a result of entrapped water altering the optical properties. Interestingly, streaks correlated with fiber tows which would suggest physical damage of fiber-matrix interface

To explore the nature of this aging damage, SEM microscopy was performed on both control samples and hygrothermally aged samples in their untested states. Both 2-ply and 4-ply coupons were examined. Samples were cut with a tile saw and then cast into a puck using quick-set acrylic. Preparation involved sanding with 1000, 2400, and

4000 grit sandpaper, polishing with 0.3 μm alumina compound, and ultrasonically cleaned in distilled water. Dry-control samples of all layups showed no visible damage under the SEM in all layups. Macro-damage in fiber tows was visible in hygrothermally laminates but was not wide-spread as the optically visible damage.

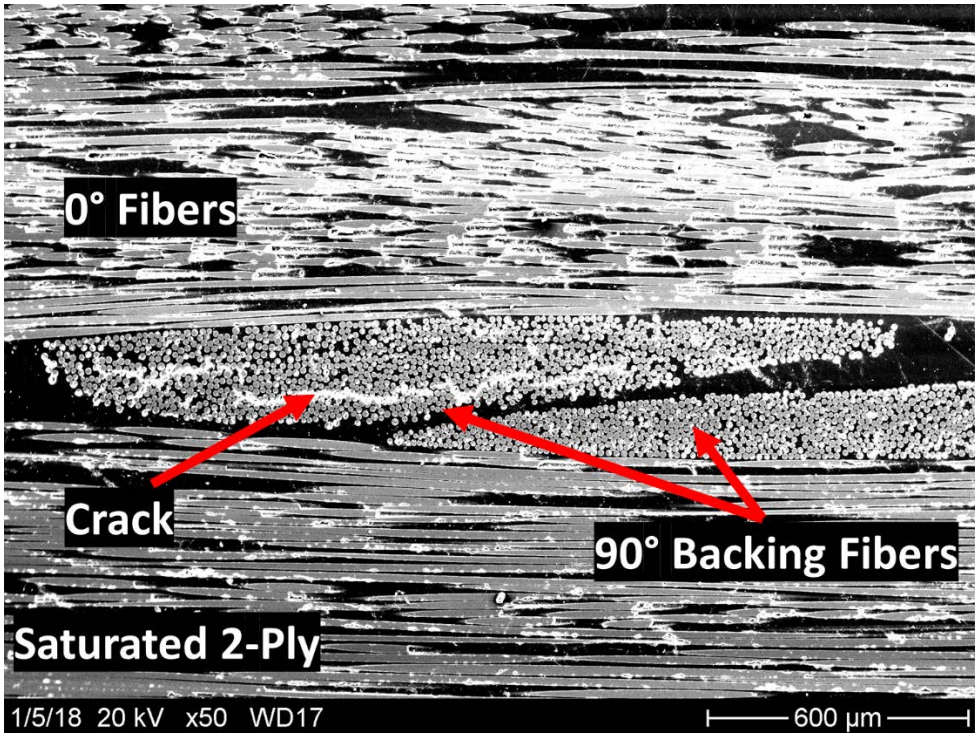

Figure 33: SEM: Crack in a backing strand in un-tested, saturated, 2-ply laminate.

2-ply laminates experienced cracking in the backing strands of plies which are shown above in Figure 33. This damage feature was present in some but not all of the backing strands. Inspection of micro-level damage was not possible at this level of polishing (Figure 34), thus higher magnification was inconclusive in determining whether these cracks propagated in the matrix or along fiber-matrix interfaces. Cracks in the backing strands propagated from areas resin-rich areas; spatially varying volume

fractions of this architecture could cause large differentials and concentration from swelling stresses.

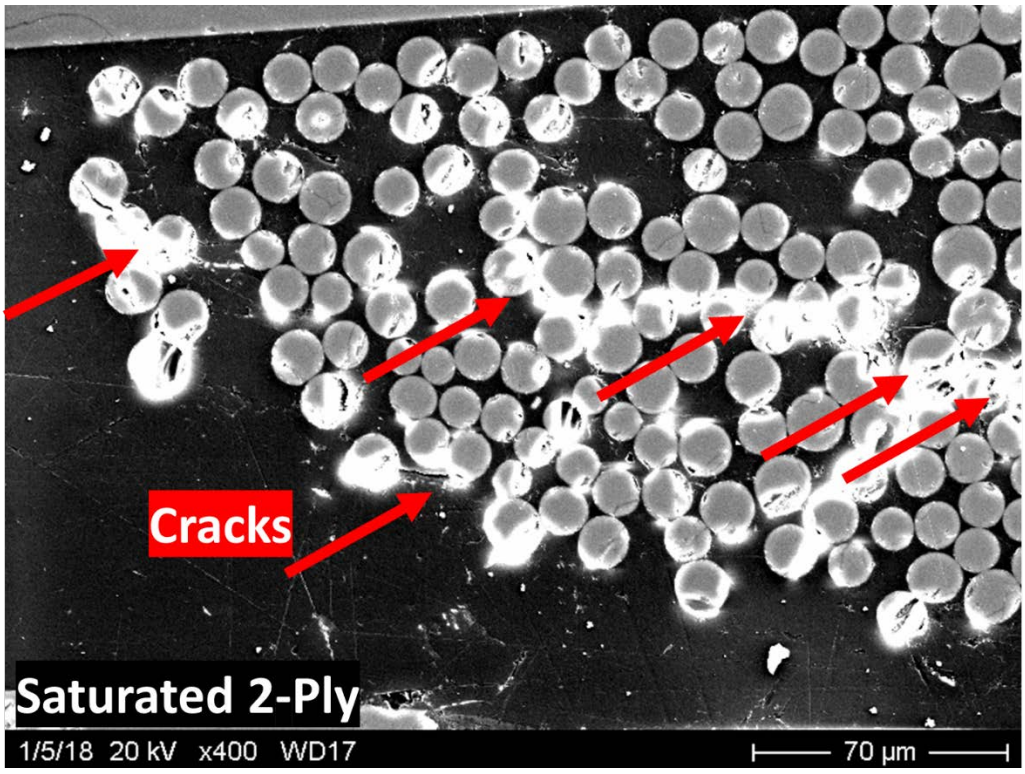

Figure 34: SEM: High magnification of crack in saturated 2-ply coupon.

Cracks were observed in the SEM inspection of saturated-untested 4-ply laminates but were less prevalent and less consistent than those found in the 2-ply laminates. Figure 35 shows one of the cracks in the outer 90° ply of a 4-ply (cross-ply).

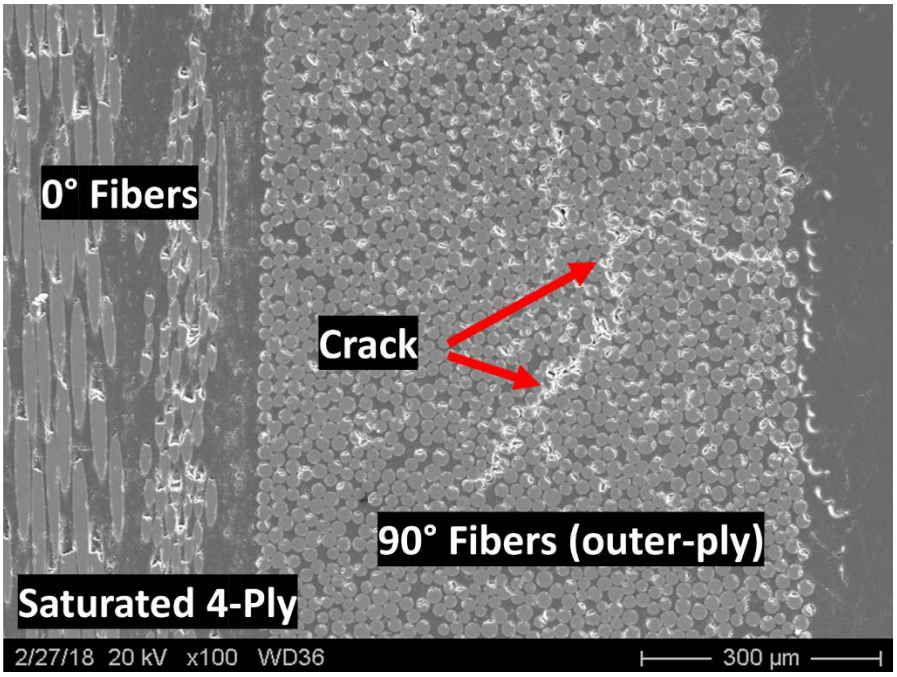

Figure 35: SEM: crack in outer 90° ply of saturated, untested, 4-ply laminate.

The damage from hygrothermal aging was quite apparent through visual inspection of samples but was less apparent in an inspection by SEM. However, the cracks observed under SEM were large, spanning whole tows; with damage of this magnitude, it is possible that swelling-induced micro-damage has also occurred. More extensive sample polishing would be necessary to observe micro-damage. Regardless, the presence of hygrothermal damage could alter the damage progression of the laminates, as the damage has already been initiated prior to any load being applied. The damage observed from swelling was confined to the fibrous-tow regions of the laminates which would suggest that damage occurring to both the interface and matrix material.

Mechanical Properties

Summary: The average mechanical properties of static tensile tests are below in Table 5.

Table 5: Static test results

Layup	Condition	Ultimate Stress (MPa)	Ultimate Load (N/mm)	Modulus (GPa)
$[0]_2$	Dry: control	971	1754	40.1
$[0]_2$	Saturated	591	1062	40.3
$[0]_2$	Dry: desorb	653	1162	38.9
$[90]_2$	Dry: control	90	165	13.6
$[90]_2$	Saturated	53	98	12.8
$[90]_2$	Dry: desorb	55	98	13.8
$[0/90]_s$	Dry: control	564	1955	27.9
$[0/90]_s$	Saturated	258	892	27.3
$[0/90]_s$	Dry: desorb	282	974	28.1
$[0/90]_s$	Dry: temp. only	586	2045	27.9
$[90/0]_s$	Dry: control	585	1986	28.1
$[90/0]_s$	Saturated	266	907	26.9
$[90/0]_s$	Dry: desorb	263	891	28.1
$[90/0]_s$	Dry: temp. only	621	2110	28.7

Hygrothermal aging-induced strength reductions were widespread across all layups tested. Figure 36: Ultimate strengths for E-LT 3800/Epoxy system. graphically shows these reductions in strength. From dry-control to the saturated condition $[0]_2$ and $[90]_2$ laminates experienced strength drops of 39% and 41%, respectively; $[0/90]_s$ and $[90/0]_s$ laminates each experienced a reduction of 54%. These strength reductions indicate a reduced damage tolerance due to aging, especially in cross-ply laminates.

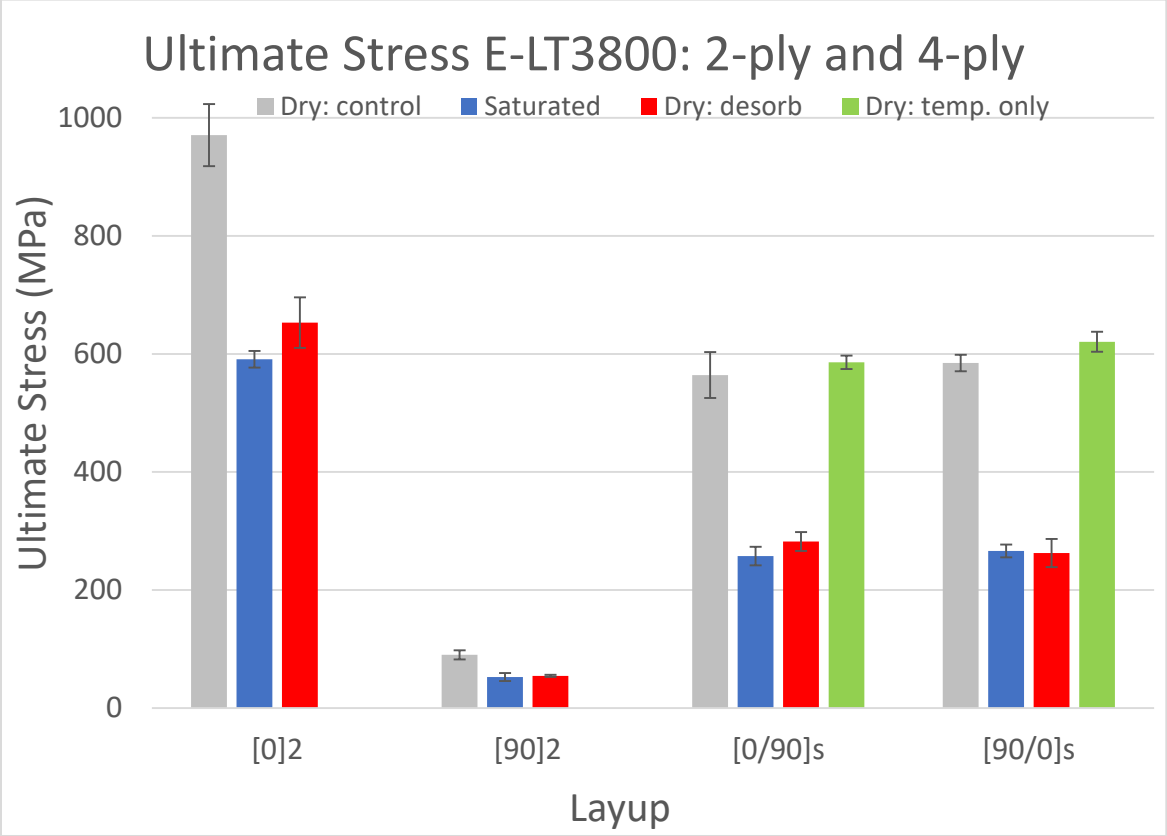

Figure 36: Ultimate strengths for E-LT 3800/Epoxy system.

Cross-ply laminates exposed to temperature-only conditioning retained the strength properties of the dry-control specimens. This finding validates the conditioning temperature history was not responsible changes in performance, and that all changes in properties can be attributed to solely to moisture-related mechanisms. This also validates that the aging temperature of 50°C was adequate for this material.

The dry-desorbed test samples, although containing no moisture, did not recover strengths to those of unconditioned samples. Slight recoveries of the strength of the $[0]_2$ and $[0/90]_s$ were observed but were minimal. In general, the dry-desorbed strengths matched those of the saturated samples. Plasticization of the matrix

material was shown to be reversible with moisture desorption; therefore, it is evident that constituent mechanical behavior due to plasticization of the matrix was not the hygrothermal mechanism responsible changes in mechanical performance in this material. Further, this suggests that mechanical performance was reduced due to physical damage occurring due to swelling during the hygrothermal aging process, which was irreversible.

The difference in strength reductions between unidirectional laminates and cross-ply laminates indicates hygrothermal aging affects unidirectional and multiangle laminates differently. To convey this change, ultimate loads were compared in addition to ultimate strengths. Stress normalizes load across the thickness of the sample, describing a uniform average stress, but in the case of multiangle laminates, this stress state is not uniform. In cross-plie laminates, transverse plies offer negligible load carrying capacity in comparison to longitudinally-oriented plies. Thus, cross-ply laminates contained two 0° plies, making their ultimate loads relatable to those of the $[0]_2$ laminates.

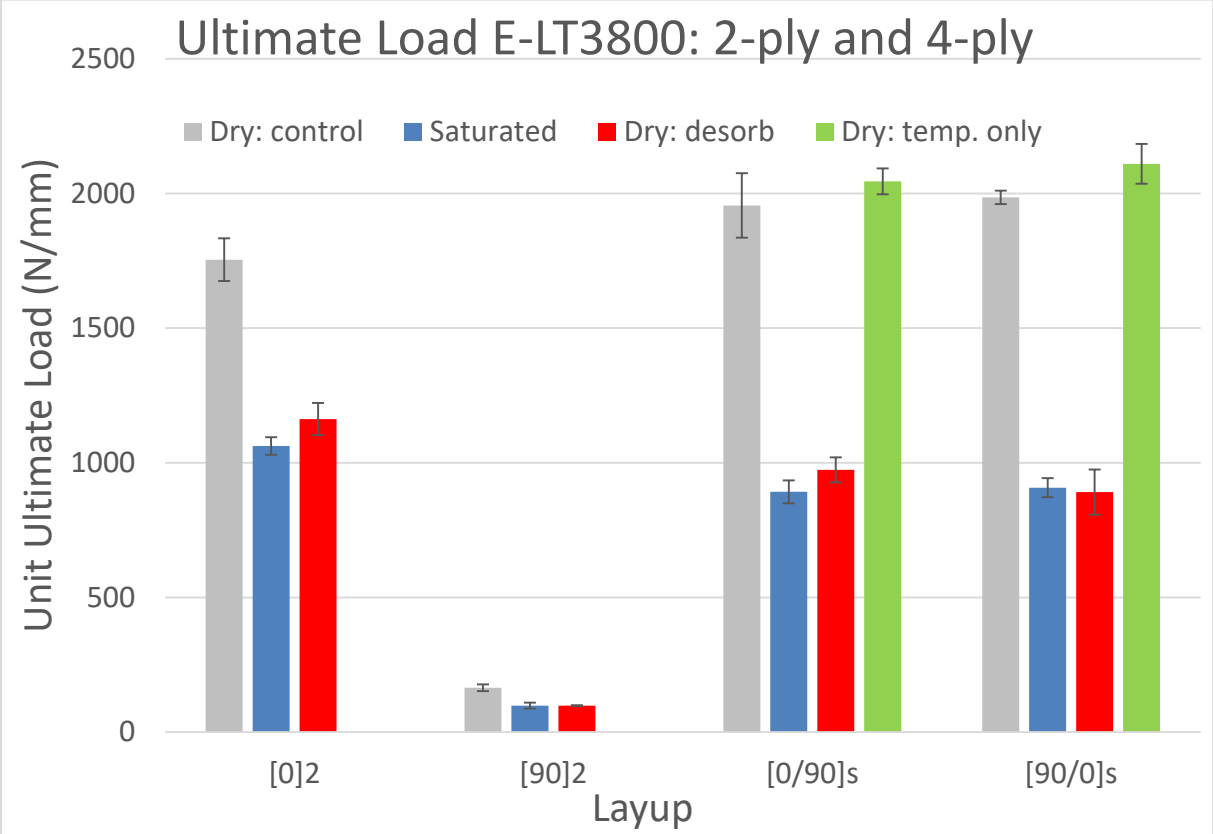

Figure 37: Ultimate loads for E-LT 3800/Epoxy System.

In the dry-control condition, cross-ply laminates withstand more load than $[0]_2$ samples. This suggests that in the control state, transverse plies add strength to cross-ply laminates. However, in the saturated and desorbed conditions, cross-ply laminates are significantly weaker than $[0]_2$ laminates. This result suggests that ply interactions are affected by aging, causing even greater reductions in damage tolerance in laminates containing multi-angle plies. Consequently, material properties from testing of hygrothermally-aged unidirectional laminates may not be adequate when designing structures with multiangle laminates using lamina-based models.

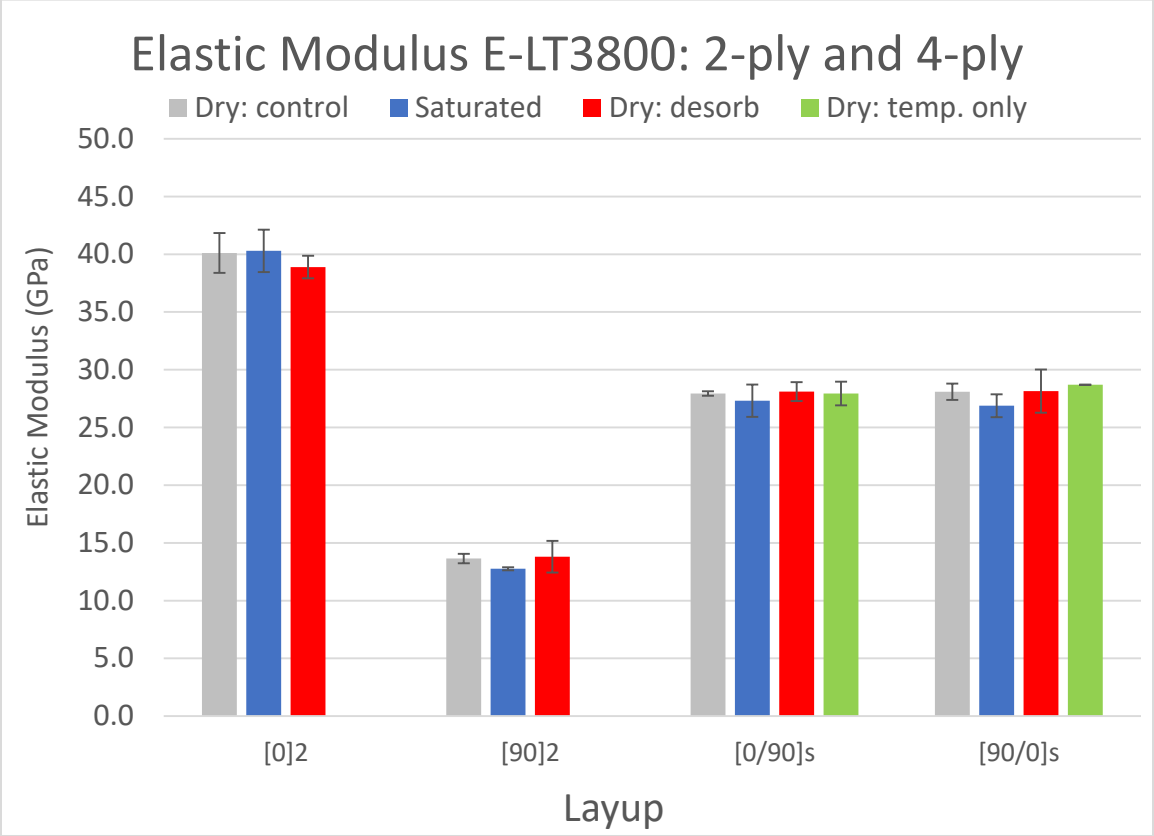

Figure 38: Elastic moduli for E-LT 3800/Epoxy system.

Figure 38 shows the elastic moduli all laminates to be unaffected by hygrothermal aging. Two observations can be made regarding the hygrothermal degradation mechanisms. First, it shows matrix plasticization and the anticipated reduction in modulus was not apparent in the composite. Unidirectional-dominated laminates should not see significant reductions in modulus, but the matrix dominated $[90]_2$ should be sensitive to these changes. Negligible reductions in the modulus of the matrix imply that the matrix can still efficiently transfer load between fibers. Second, damage in composite materials may affect the residual modulus. Hygrothermally-induced damage, although

apparent, did not affect the modulus, indicating that the damage occurred on the micromechanical level or did not affect the global stiffness along the loading axis.

Stress-Strain Curves: Inspection of stress-strain curves can often provide insight into the damage mechanics and damage progression of the material. Transverse plies, lacking reinforcement in the loading direction, making these plies susceptible to damage at low strain levels. Figure 39 shows the stress-strain response of transverse, $[90]_2$ samples.

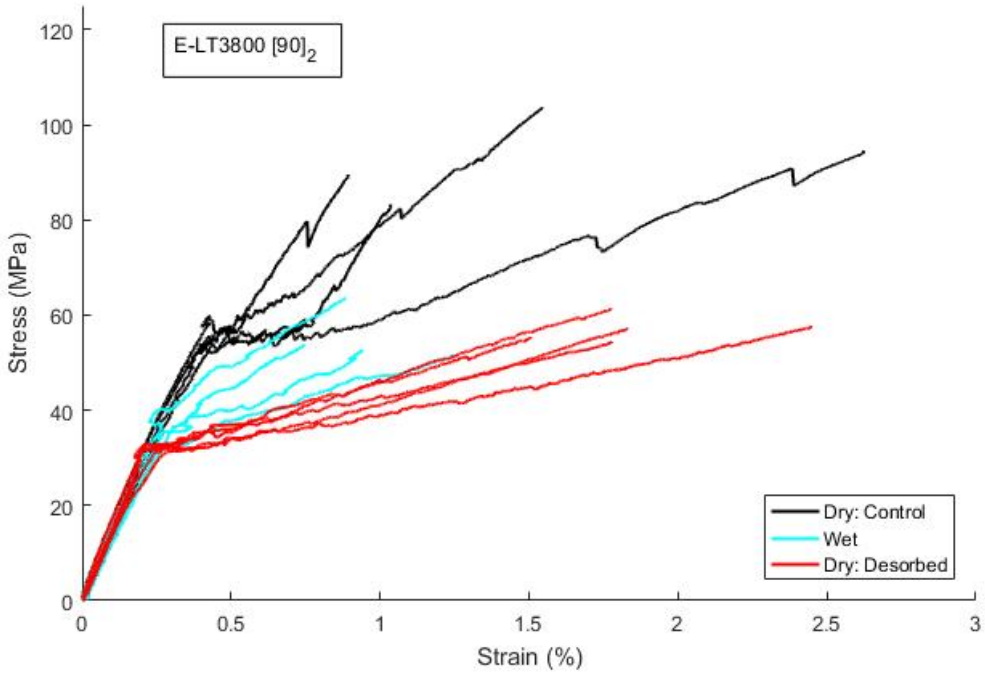

Figure 39: Stress-strain response of $[90]_2$ samples.

It must be noted that longitudinally-oriented backing strands are still present in these samples. Typically, in a purely transverse laminate, the first crack would propagate across the cross-section and cause ultimate failure. With the addition of a few

longitudinally orient strands, global failure does not occur after the first crack, resulting in the bilinear behavior in Figure 39. The knee following the linear-elastic portion, therefore, correlates to the onset of transverse failures and reduces the material stiffness. Stress-strain beyond this point can be variable due to variation in the backing strands both in terms of number, spacing and alignment/waviness, as well as variation in strain collection due, do localized damage within the small-gage section of the extensometer. The nature of these failures are attributed to matrix cracking and debonding of the fiber-matrix interface. These are competing for mechanisms; thus, the nature of transverse failures is difficult to discern. Interestingly, for this material system, the hygrothermal conditioning affects strain levels at which transverse failures occur. In the dry-control samples, damage begins at 0.43% strain, while in saturated samples, damage begins at 0.28% strain. Desorbed samples follow closely the behavior of the saturated samples with damage beginning at 0.3% strain. The lower initiation strains of saturated and dry-desorbed samples would reflect damage growth of existing damage induced by the aging process.

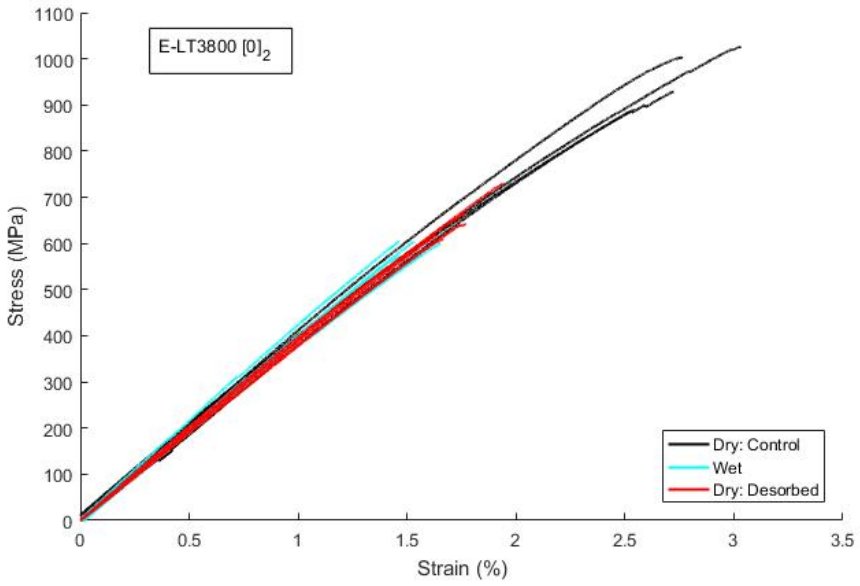

Figure 40: Stress-strain response of $[0]_2$ samples.

Figure 40 shows the stress-strain curves for $[0]_2$ samples. Since the predominant damage mechanism in longitudinal plies is fiber breakage, minimal strain energy is released until final failure. $[0]_2$ laminates of all conditions follow the stress-strain response, with condition samples being truncated due to premature failure; there is no energy release to foreshadow this behavior.

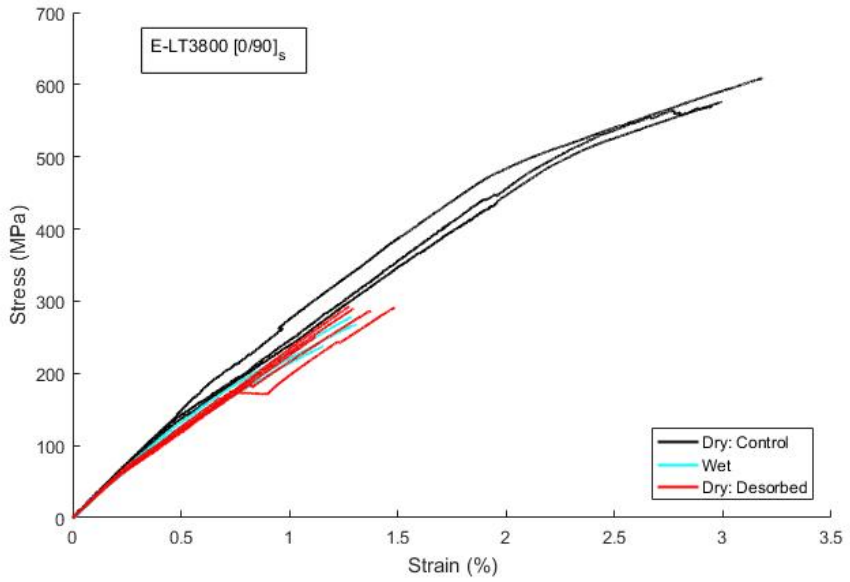

Figure 41: Stress-strain response of $[0/90]_s$ samples.

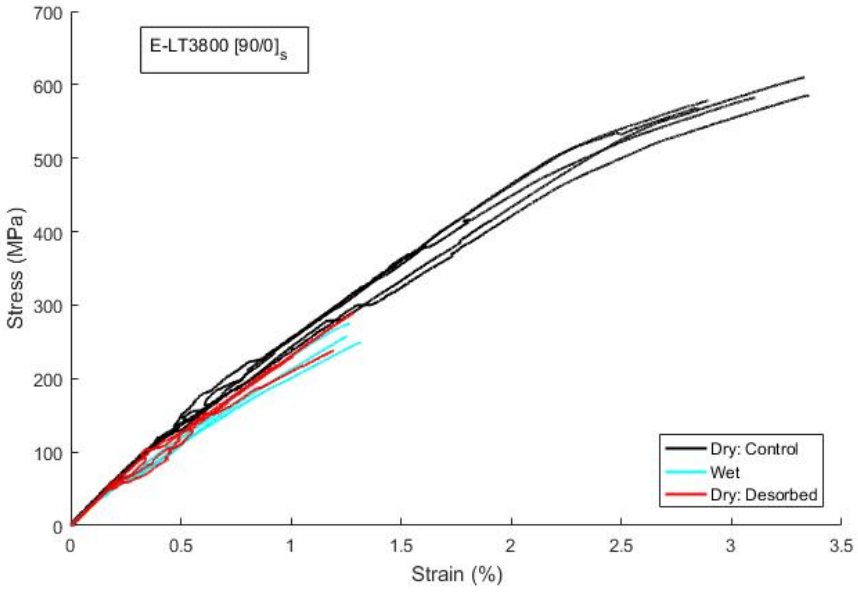

Figure 42: Stress-strain response of $[90/0]_s$ samples.

The stress-strain curves for the cross-ply laminates are shown in Figure 41 and Figure 42. Both layups displayed similar behavior between at each level of conditioning; however, the results for to $[90/0]_s$ tend to be noisier than the $[0/90]_s$. Damage to 90° plies of the $[90/0]_s$ layup induced noise in the strain measurement, as the strain measured beneath the extensometer did not reflect the global strain level. Interestingly, the cross-ply laminates show a bilinear behavior as see in the $[90]_2$ samples, with modulus being reduced after failures in the traverse plies. Again, samples that subjected to hygrothermal aging experienced this knee at lower strains than the control samples, causing separation between the control and conditioned curves around 0.3% strain The premature growth of damage could be in part due to the increased stress state from swelling, but the knee does not recover after desorption which would suggest that damage onset was from the growth of damage accrued during the aging process.

Sample Failure Inspection

Inspection of failed test specimens provides qualitative information about the damage progression in composite laminates, specifically damage progression at final failure. Figure 43 shows failed $[90]_2$ samples for dry-control, saturated and desorbed samples. The longitudinally oriented backing strands of this laminate allowed the laminates to develop transverse cracks. Crack saturation resulted in the ultimate failure of the $[90]_2$ laminates. Red ink was used as a penetrant to make crack more visible during inspection; ink was only applied to one side of the coupon. The control sample experienced uniform crack distribution and a crack density of 4 cracks/cm. Saturated and desorbed samples featured a more random crack pattern with a lower crack spacing of 2.7

and 3.0 cracks/cm, respectively. Without exact failure strains, it is difficult to compare these numbers as crack density is related strain level. Regardless, the crack behavior still offers an interesting point of discussion. Matrix plasticization could cause stress redistribution and reduce stress concentrations resulting in lower crack densities of saturated samples. However, desorbed samples, with no moisture and theoretically no plasticization, failed in a similar form. Another possibility would be internal damage in both the matrix and the interface [23] which could also reduce stress concentrations and lower crack density.

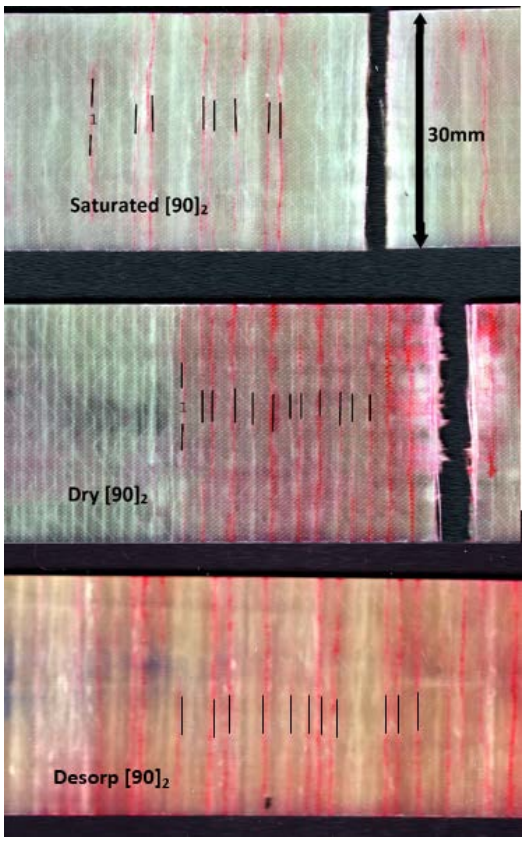

Figure 43: Failed $[90]_2$ coupons: Saturated (top), Dry (middle) desorbed (bottom).

[0]2, [0/90]s, and [90/0]s are shown in Figures 42, 43 and 44, repectively. Due to the large strain energy release during the failure of 0° plies, these coupon failures are often explosive and result in widespread damage to the coupon. This behavior was present in dry control samples which experience significant splitting (Figure 44), brooming (Figure 45), and widespread delamination (Figure 46). In the saturated and the desorbed cases, the damage was less explosive with failures confined to localized areas. This observation would suggest that damage coalesces and grows at much lower global strain energies than in dry samples. However, high local strain energies are still necessary to propagate damage. Stress concentrations from aging-induced damage could serve as nucleation points for damage. This premature damage initiation would result in earlier onset of cascading damage in hygrothermally- exposed samples.

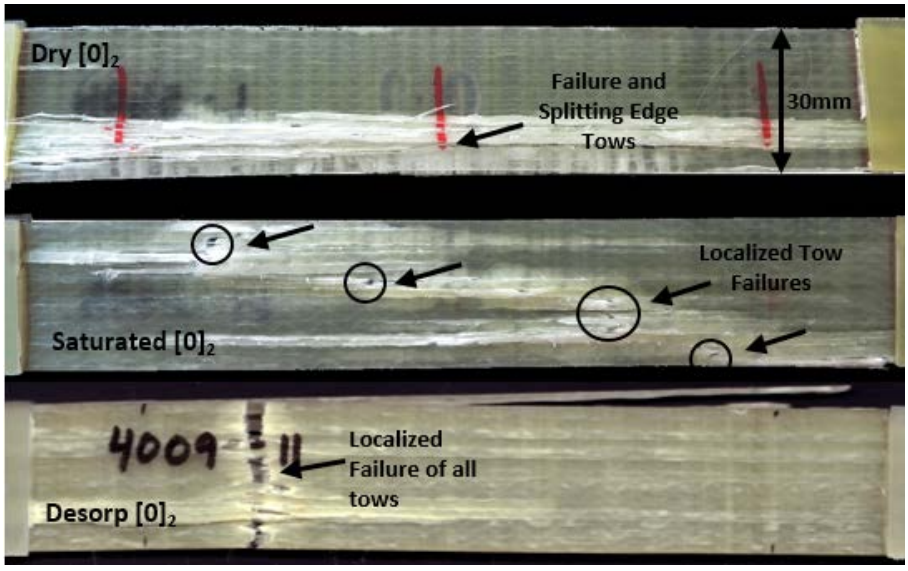

Figure 44: Failed $[0]_2$ coupons

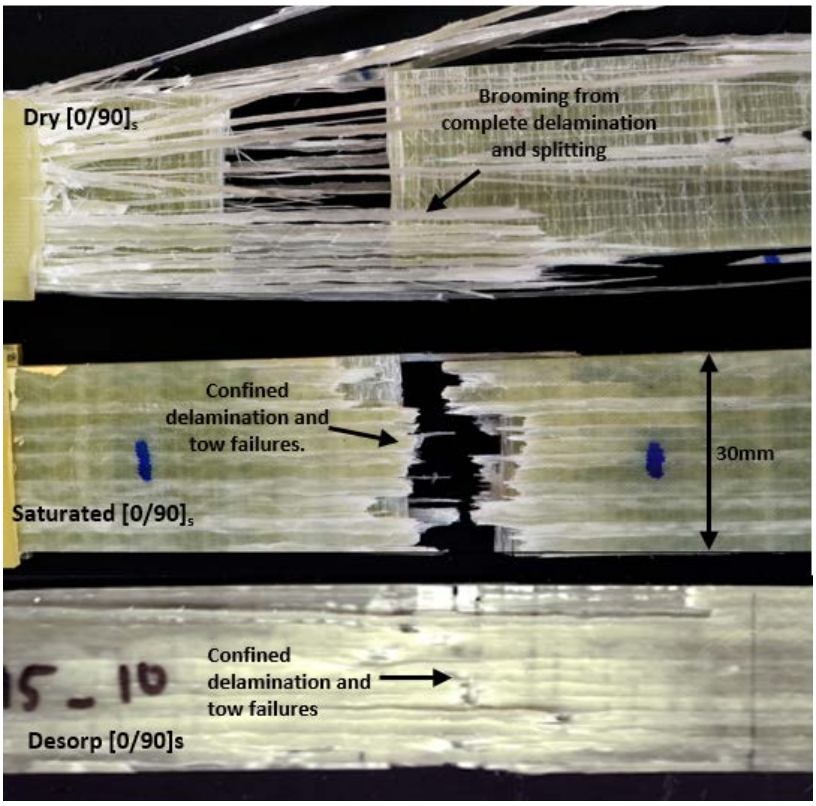

Figure 45: Failed $[0/90]_s$ coupons

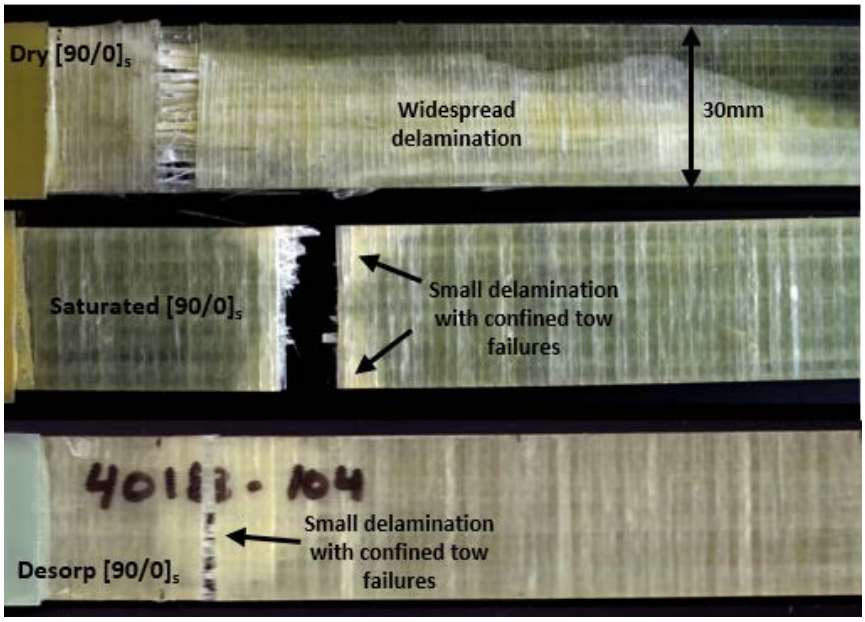

Figure 46: Failed $[90/0]_s$ coupons

Acoustic Emission

AE monitoring acquired during these tests aids in interpreting the hygrothermal mechanisms responsible for changes in the damage progressions. As discussed in the background section, many analysis techniques exist to correlate AE data to damage in FRP's, and validation of these techniques resides as an ongoing focus of study in composite material research. The analysis for this dataset will be two-fold: First, general trends in the level of activity will be analyzed; then frequency analysis technique will be applied to describe the nature of specific damage mechanisms in the material and their response to hygrothermal aging. All analyses were conducted on data collected up to ultimate failure; events occurring after ultimate failure were truncated. AE data is stored in a MATLAB structure and scripts were written for data processing.

General Trends: Several AE parameters are of interest for describing the overall AE behavior, these include number of events, accumulated energy, and detected damage initiation. Table 6 outlines the general AE average results for each laminate and condition tested.

Table 6: AE general trends (averages)

Layup	Condition	Number of events	Total Accumulated Energy[§§] (aJ)	Average Energy per Event (aJ)	Initiation Strain by AE (%)
[0]2	Dry: control	9463	9.8E+08	1.0E+05	0.31
[0]2	Saturated	611	9.3E+07	1.5E+05	0.34
[0]2	Dry: desorb	1546	2.3E+07	1.5E+04	0.19
[90]2	Dry: control	984	4.1E+09	4.1E+06	0.55
[90]2	Saturated	586	3.4E+08	5.8E+05	0.25
[90]2	Dry: desorb	914	6.5E+08	7.1E+05	0.22
[0/90]s	Dry: control	13157	3.1E+09	2.3E+05	0.20
[0/90]s	Saturated	789	1.3E+07	1.7E+04	0.08
[0/90]s	Dry: desorb	2144	4.4E+08	2.0E+05	0.14
[90/0]s	Dry: control	7113	1.2E+10	1.7E+06	0.13
[90/0]s	Saturated	1769	1.3E+08	7.2E+04	0.08
[90/0]s	Dry: desorb	2584	1.8E+09	6.8E+05	0.08

The number of AE events corresponds to the number of damage events that occurred in the gage section of the sample during the loading cycle. Although events can vary in size, the number events can serve as a metric for measuring the amount of damage sustained by the material and thus correlated to damage tolerance. Figure 47 graphically shows the number of events collected for each laminate under each condition.

[§§] aJ = 10^{-18} J

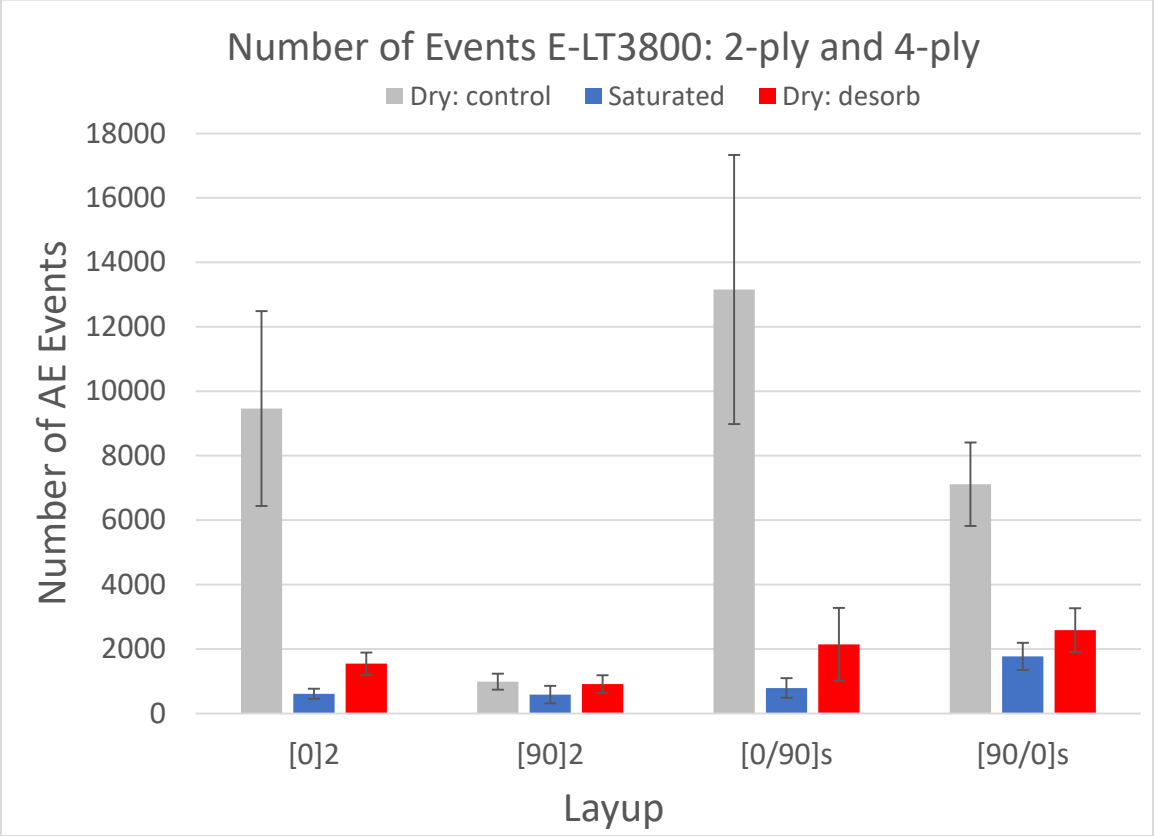

Figure 47: Average number of AE events.

From Figure 47, it is apparent that hygrothermal aging significantly reduced the number of detected damage events. $[0]_2$ samples in the saturated condition were reduced by over 90% from control samples. Similar reductions were present in the cross-ply laminates. Damage accrued during the aging process would be unaccounted for in the AE monitoring and would result in fewer recorded events. Correlation between the number of events and damage would indicate that hygrothermal aging reduces the damage tolerance of the material.

AE activity was not recovered by drying/desorbing the samples which would imply that the change in AE activity was not due to damping induced by plasticization

which was shown to be recovered in the matrix characterization section. Attenuation of AE elastic waves due to damage or material damping is more thoroughly explored in the subsequent chapter and showed that aging did not affect the materials propagation or attenuation behavior.

Accumulated energy also serves as another metric for interpreting the amount of damage sustained in the material, accounting for the magnitude of damage event. AE energy can be considered representative of the energy dissipated of the composite. Dissipated energy is a measure of global-elastic strain energy that has been released due to damage to the material and can no longer be recovered during subsequent unloading cycles. AE energy is also a measure of strain energy released, but rather than measuring this release as a change in the global stress/strain energy state, it is a measure of the intensity of transient stress waves propagating through the material. In general, dissipated energy and AE energy have shown correlation [38], but since AE is an indirect measure of strain energy release, there are variations. For example, in a 0° plie, a matrix crack could occur, emitting a sizable stress wave. Locally, this would change the strain energy state, increasing the stored energy in neighboring fibers, however, this would not result in a significant change in the global strain energy state, thus minimal dissipated energy. Despite this disconnect, accumulated energy can still provide insight into the amount of damage accumulated in the material.

The accumulated energy curves for all the layups are shown below in Figure 48 - Figure 51 (note: logarithmic scale). In all layups and conditions, the largest change in energy occurred between 0.1 and 0.6% strain, which correlates to the strain levels at

which matrix cracking is expected. The $[90]_2$ laminates, shown in Figure 48 feature a large step in accumulate energy below 0.5% strain with little energy growth during the later portion of the loading cycle. This trend held true for all conditions, but the step does appear to occur at lower strain levels in laminates exposed to hygrothermal conditioning.

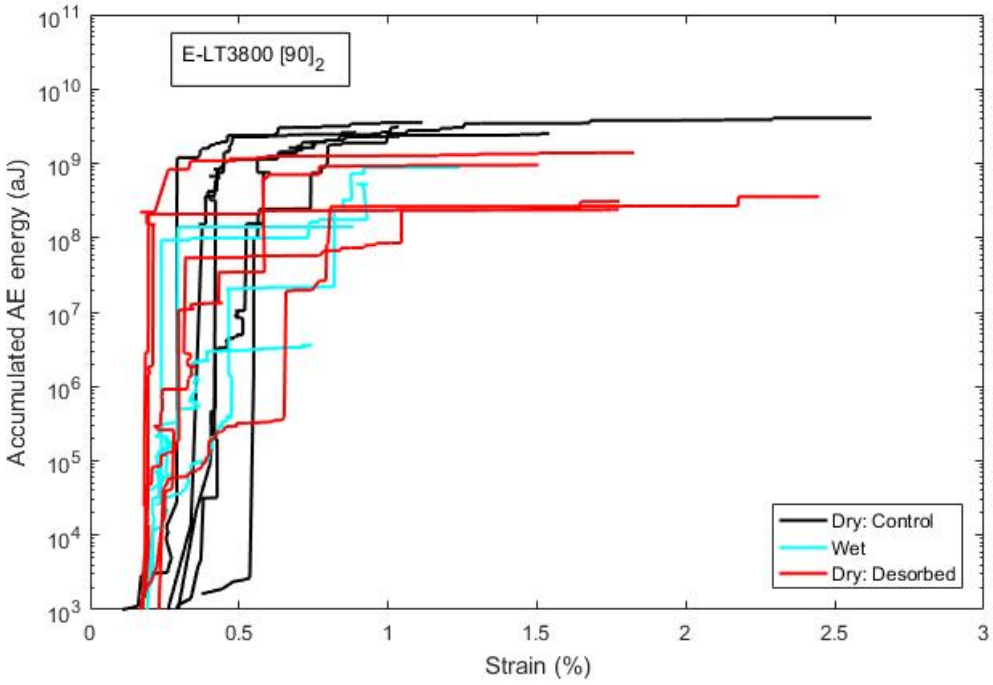

Figure 48: Accumulated AE energy for $[90]_2$ samples

$[0]_2$ laminates, also show the initial step in energy, followed by a plateau in energy accumulation. $[0]_2$ laminates also experienced a sizeable increase in energy directely proceeding failure. In terms of conditioning, laminates that have been hygrothermally aged begin to accumulate energy at lower strain levels, but plateau at lower total energy values. Cross-ply laminate energies, shown in Figure 50 and Figure 51, have a similar step in energy around 0.5% strain, but minimal growth in energy immediately preceding failure. In conditioned cross-plies, this step occurs at a lower strain level but plateaus at a

lower total energy value. Total accumulated energies are compared directly in Figure 52 for all conditions and layups.

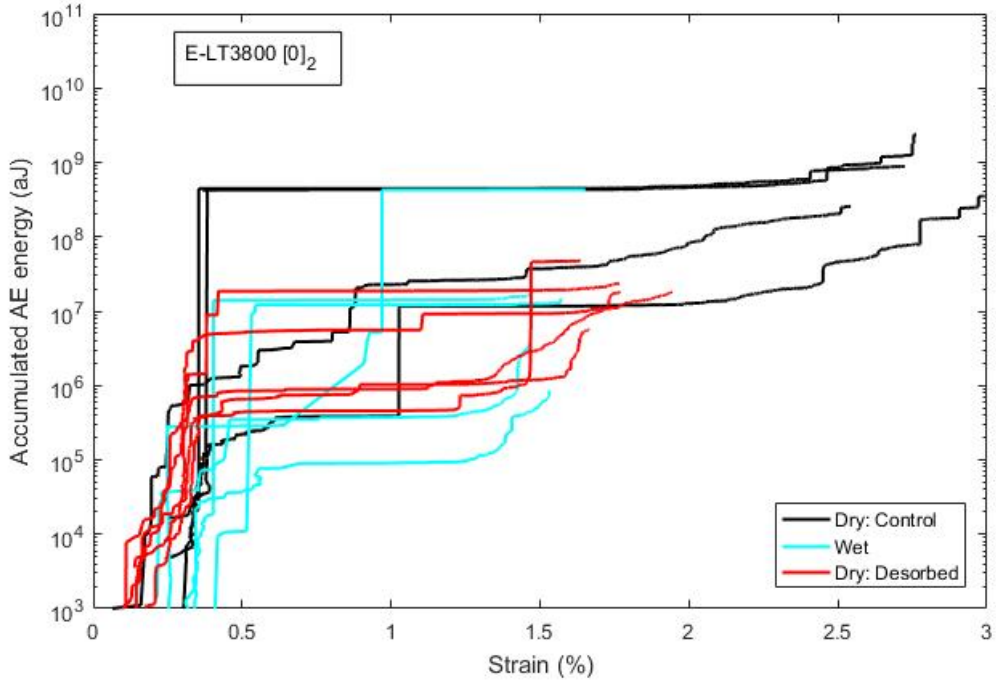

Figure 49: Accumulated AE energy for $[0]_2$ samples

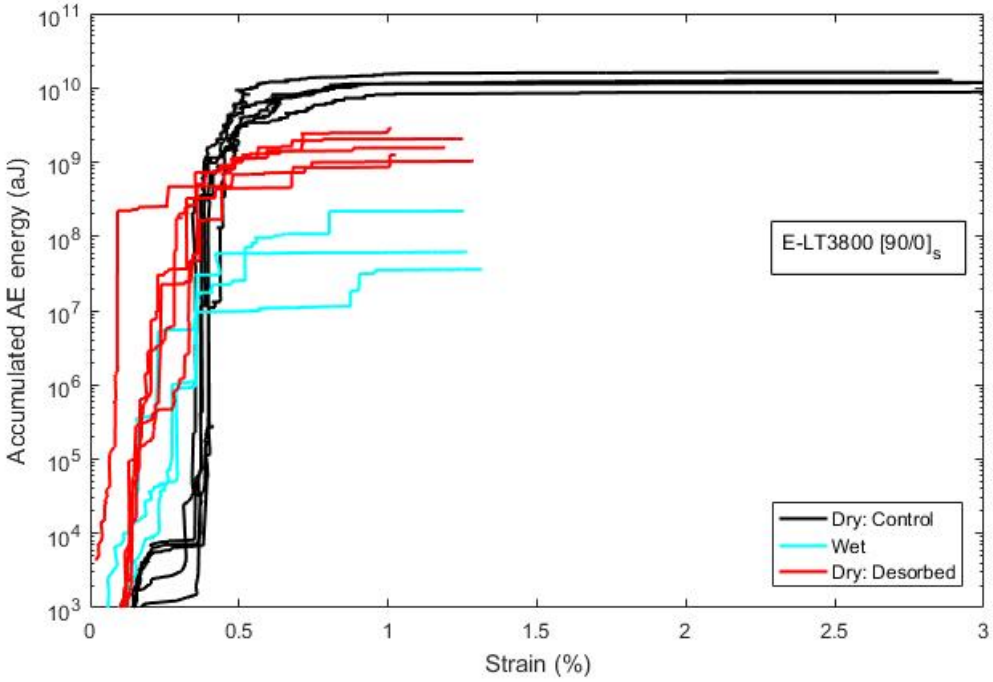

Figure 50: Accumulated AE energy for [90/0]s samples

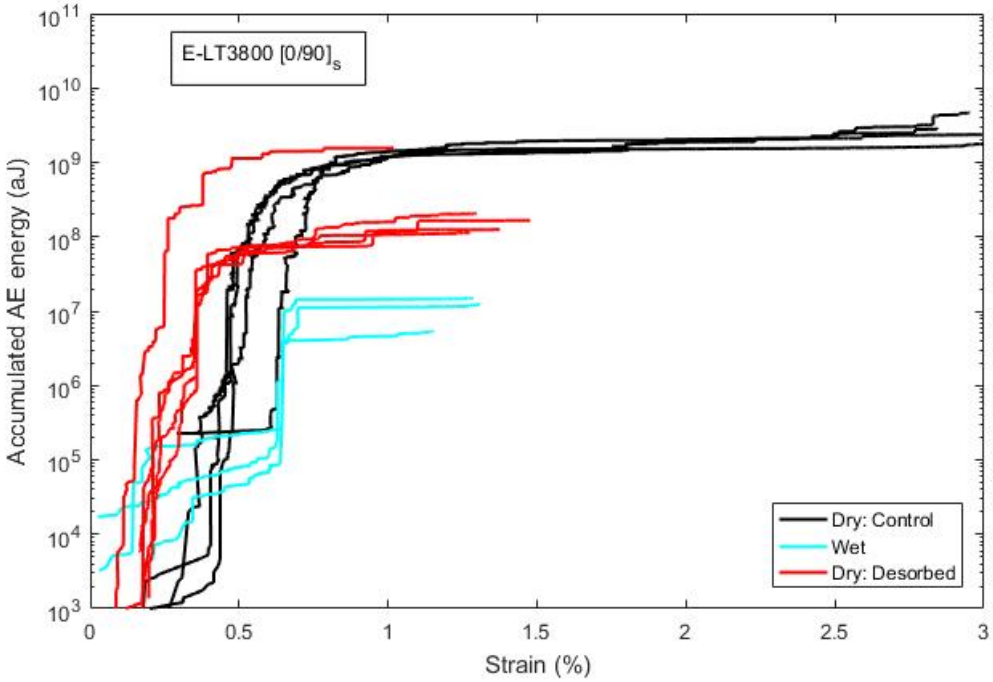

Figure 51: Accumulated AE energy for $[0/90]_s$ samples

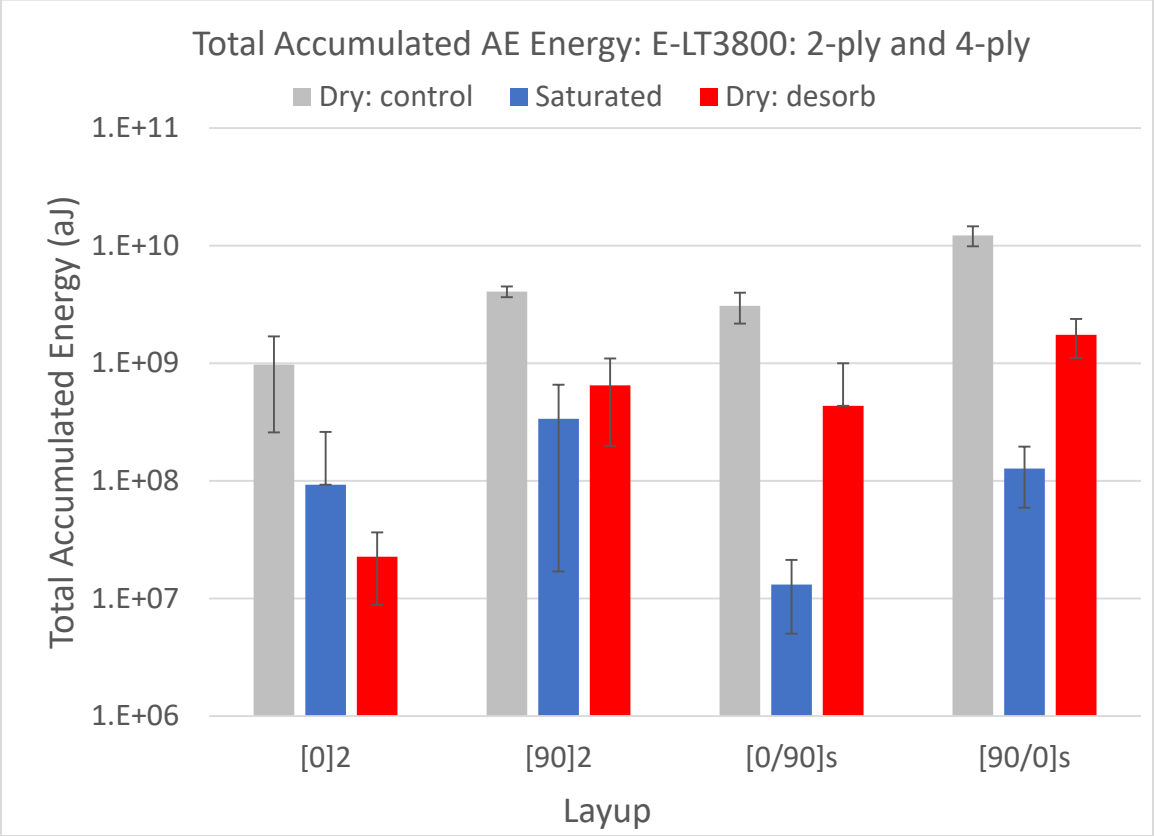

Figure 52: Total accumulated AE energies.

It should be noted that in Figure 52, the energy scale is logarithmic, thus reductions in AE accumulated energy from hygrothermal aging are quite significant. From control to saturated, energies were reduced one order of magnitude in, and two orders of magnitude in cross-ply laminates. Again, this larger change in the cross-ply laminates suggests that inter-ply effects influence damage tolerance of multi-angle laminates. Following desorption, energies were recovered partially in cross-ply laminates but were still far from those of the control specimens. From these results, it can be interpreted that the amount of damage sustained during the loading cycle was reduced by hygrothermal aging.

Aside from quantifying damage, AE is an excellent tool for detecting when a failure occurs in composites. In this study, the onset of damage was correlated to the onset of AE activity. Damage onset was prescribed as the strain level at the occurrence of the 10th event. If 10 events occurred, this would be deemed enough activity to be attributed to damage rather than anomaly or noise. Results of the damage initiation strains detected by AE are depicted in Figure 53.

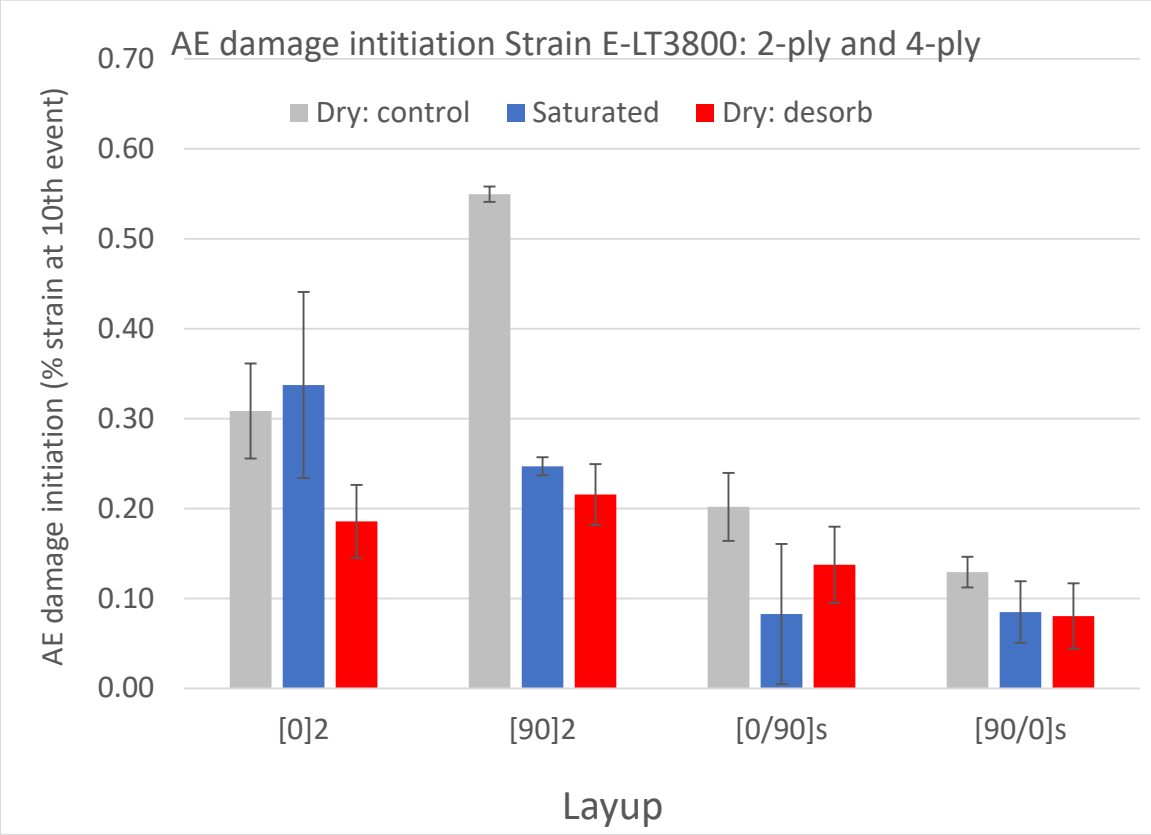

Figure 53: AE damage initiation strains.

In all laminates, except $[0]_2$, the damage was detected much earlier in the loading cycle for saturated samples than the control samples. This correlates to observed behavior

in the stress-strain curves, where damage initiated at lower strains in saturated laminates. However, the actual strain values do not match perfectly. For example, $[90]_2$ control samples detect damage at 0.55% strain, whereas stress-strain data shows 0.43%. Perhaps changing the criteria for what is deemed relevant AE activity would yield more consistent results. Despite this slight inconsistency between methods, it is confirmed that AE is effective for detecting damage onset in materials. Stress-strain data did not show clear damage onset for $[0]_2$ laminates, but AE data fills this void. Interestingly, control and saturated $[0]_2$ samples experience damage at similar strain levels, while desorbed samples initiated at much lower strain levels.

Together, these parameters support the mechanical data, indicating that hygrothermal aging reduces damage tolerance of the material and reduces the energy required to initiate/grow damage. However, it is important to verify these results are in fact due to changes in damage behavior and not a function of absorbed moisture affecting the nature of AE waves. This subject is explored in more detail in the subsequent wave propagation chapter.

Frequency Analysis: Frequency analysis of AE waveforms provides a method to inspect the damage progression of a composite material in terms of types of damage mechanisms present. Changes in the damage mechanisms present during the loading of composite material with aging may provide insight on hygrothermal degradation mechanisms. For this work, the three damage mechanisms of interest were matrix failure, interphase failure, and fiber failure. The respective frequency bins for these damage mechanisms are shown below in Table 7. These bins are derived from literature review

and previous work conducted at MSU [38]. Experimental validation and first-principal understanding of the relationship between the frequency and damage mechanisms is a subject of interest in on-going AE research.

Table 7: Frequency analysis bin ranges.

Bin	Damage Mechanism	FFT-Peak-Frequency Range (kHz)
Bin 1	Matrix	<120
Bin 2	Fiber/matrix interphase	120-300
Bin 3	Fiber	>300

Note: for this work, fiber-debond and pullout are combined into a singular fiber/matrix interphase bin. Normalizing the number of damage events in each frequency bin by the total number evens gives the bin percentages, compared below in Figure 54-Figure 57. Examples of the progression of these events during the loading cycle are provided in Appendix B.

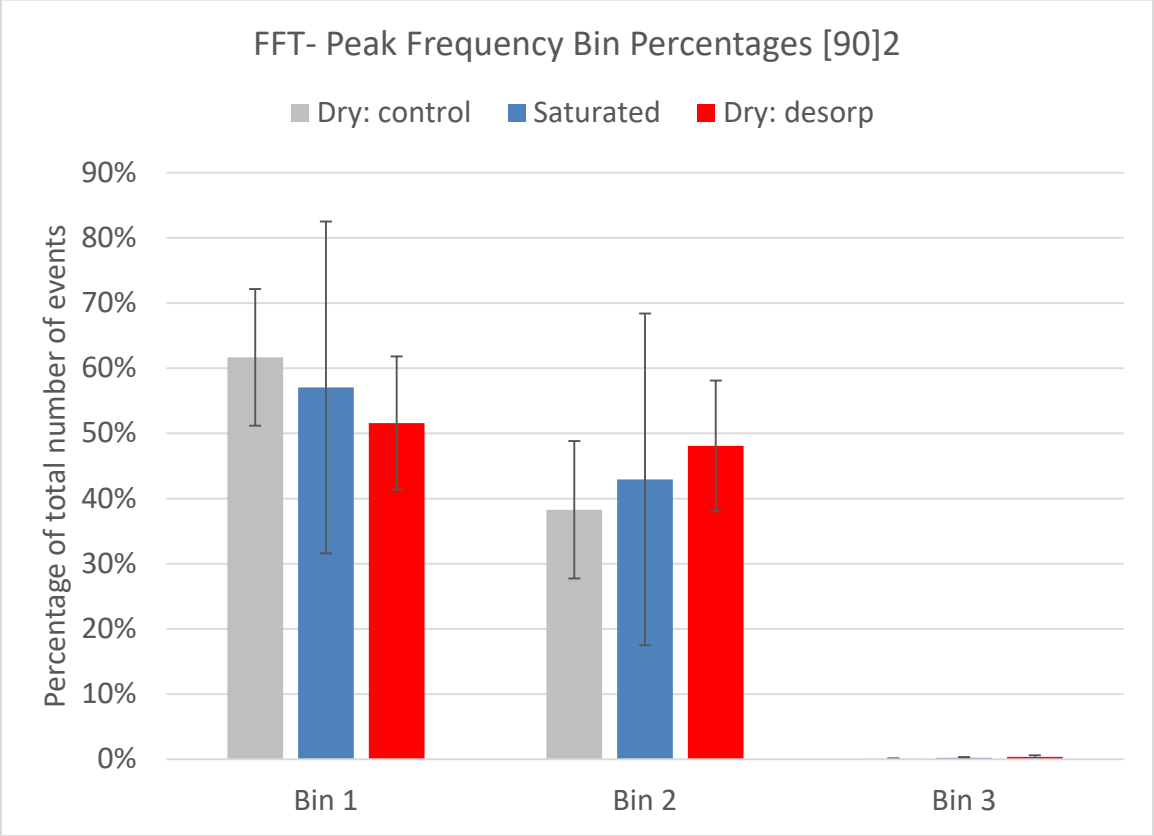

Figure 54: Frequency bin percentages $[90]_2$

As shown in Figure 54, damage in transverse tension is a consist of competing damage mechanisms of matrix crack and interphase failures. Slight increases in the contribution of interface failures were observed but were not statistically significant to be attributed to change in interface integrity. $[0]_2$ layups were dominated may interphase failures rather than matrix failures. Typically, 0° plies would also experience fiber failure as a damage mechanism, however, this mechanism occurs near ultimate failure of the composite and is therefore difficult to capture with AE monitoring.

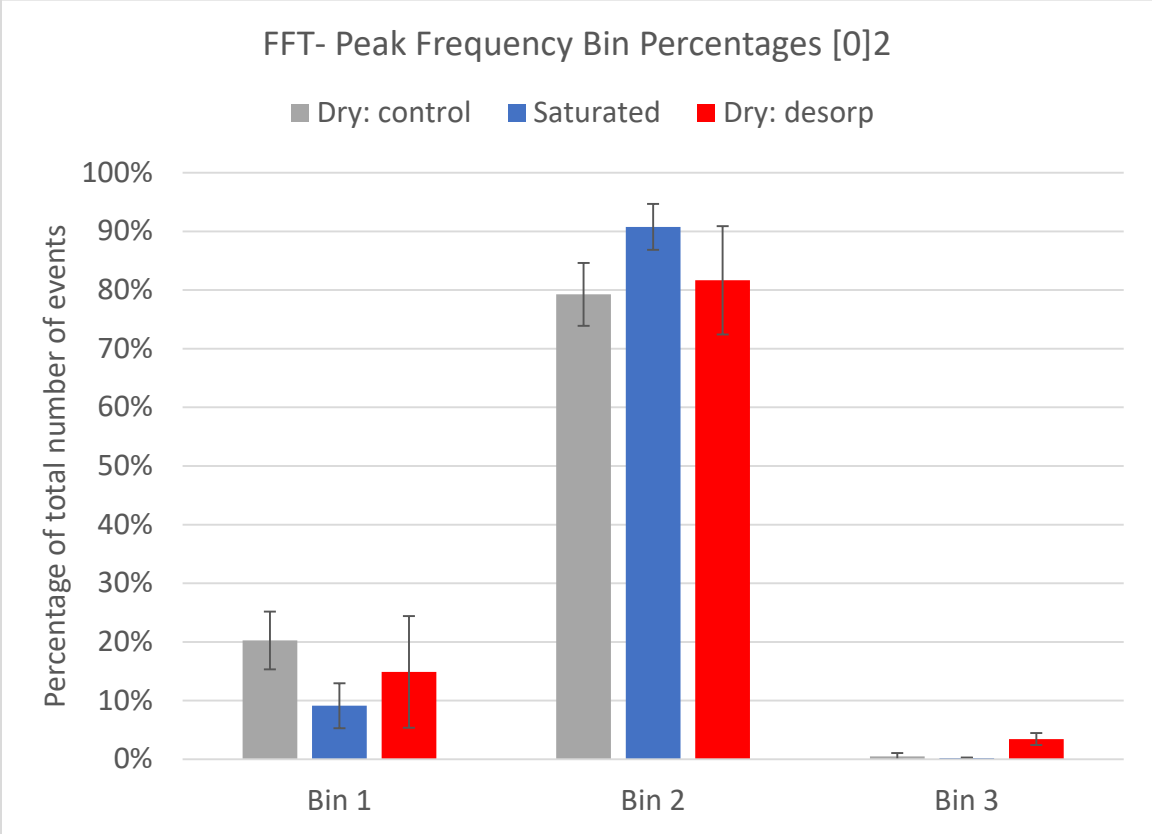

Figure 55: Frequency bin percentages $[0]_2$

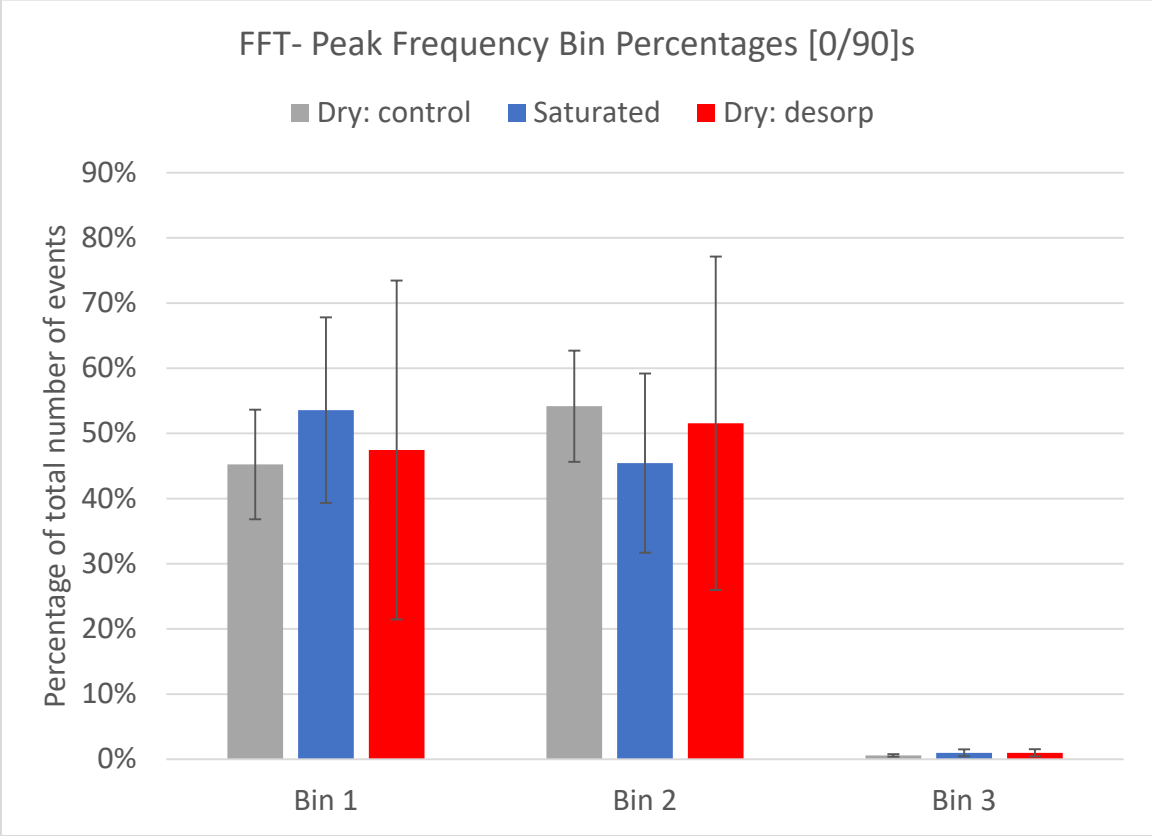

Figure 56: Frequency bin percentages $[0/90]_s$

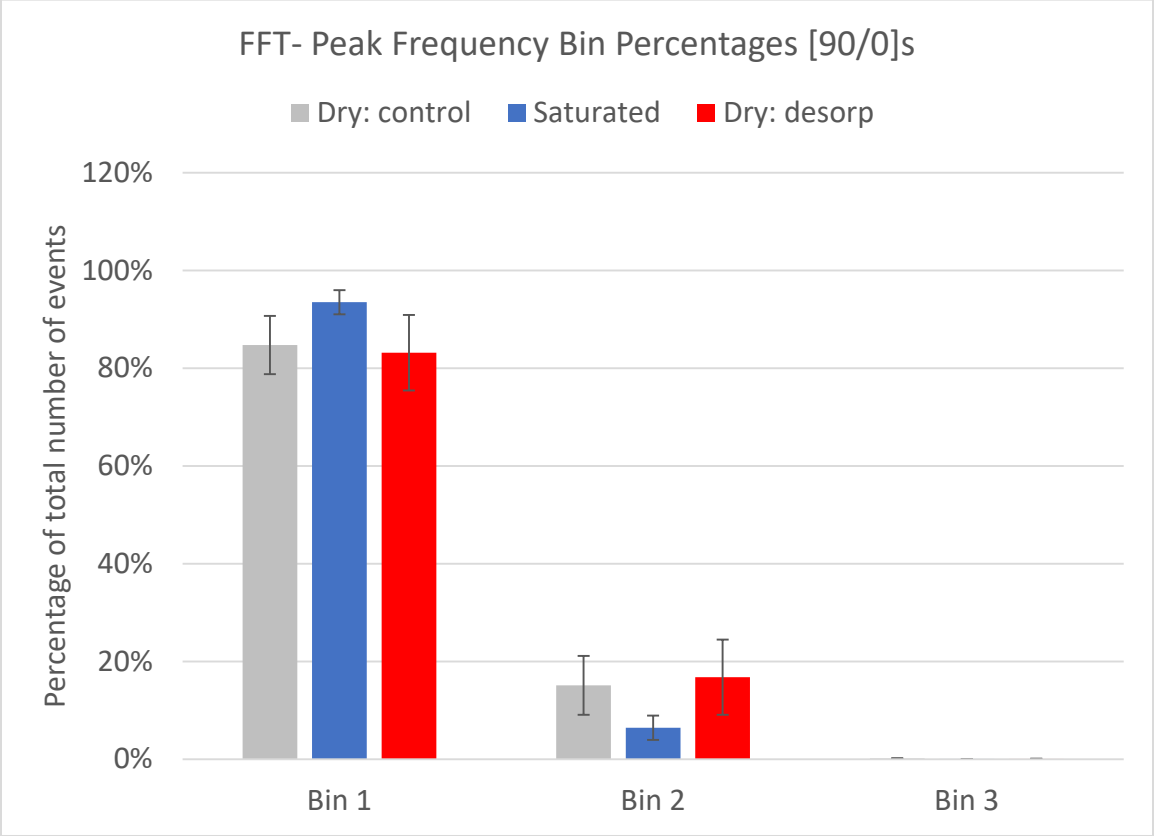

Figure 57: Frequency bin percentages $[90/0]_s$

$[0/90]_s$ and $[90/0]_s$, shown above in Figure 56 Figure 57, did not appear to be significantly affected by hygrothermal aging. Interestingly, the damage response of the two laminates is significantly different with $[0/90]_s$ experiencing near-equal amounts of matrix failures and interface failures, while $[90/0]_s$ are dominated by just matrix failure. It would be anticipated that both configurations of cross-ply would experience similar damage progressions. It could be hypothesized that the variation of the AE response is due to both attenuation and source behavior of damage mechanisms being dependent on ply location in the laminate. For example, cracking in the outer ply of the $[90/0]_s$ laminate could attenuate waves propagating from the internal 0° plies of the and thus alter the

received AE response between laminates. Also, the location of the transverse plies in the stacking sequence could alter the transmitted shear stress and result in varying transverse crack densities between the two cross-ply layups. Further investigation in AE analysis is necessary to understand this behavior. However, assuming the correlation between frequency of AE events and damage mechanisms exists, the consistency in frequency results between control, aged and desorbed samples suggest that the contribution of damage mechanisms themselves independent of hygrothermal-aging. Appendix B shows the typical events frequencies versus strain for each layup and condition. The damage bins appear to accumulate in the same order throughout the loading cycle which implies that the sequence of damage evolution did not change with conditioning.

WAVE PROPAGATION AND ATTENUATION

The changes in the AE response described in the previous chapter show significant changes in the damage behavior of hygrothermally-aged composite materials. However, further investigation into wave propagation and attenuation is necessary to verify the reason for these substantial changes in AE response. The ingress of moisture into the composite may affect the AE activity in several ways. This effect can be divided into two main categories: effects on wave propagation and effects on source behavior.

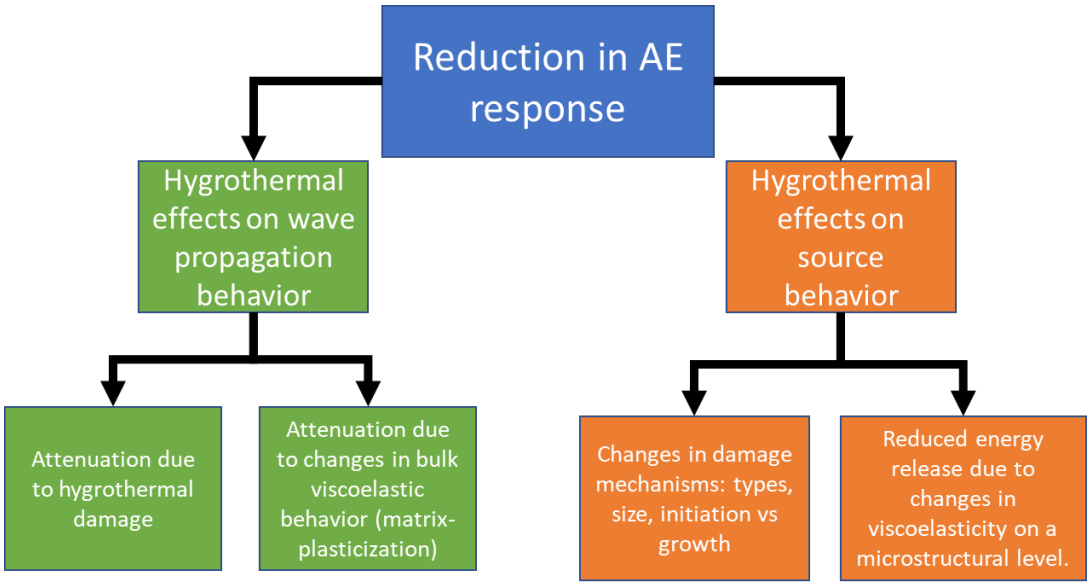

Figure 58: Root cause of the reduction in AE response.

Both the source behavior and wave propagation behavior can be affected by changes in the viscoelastic behavior of the matrix material. Plasticization typically increases the vicious response of the polymer resulting in energy absorption and

dissipation of AE signals, both on a bulk composite level and a microstructural level. Additionally, damage accrued from loading or swelling may attenuate signals.

Sensor Test: Guided Ultrasonic

Experimentation A sensor test was executed to simulate the propagation of an AE elastic wave. The sensor test, a built-in function of an AE acquisition system, may be implemented as a quasi-guided ultrasonic system [56]. Since both AE wave and ultrasonic waves are both lamb waves, attenuation of guided waves is representative of the attenuation of AE waves. The sensor test uses two AE senses to pitch and receive ultrasonic pulses as shown in Figure 59.

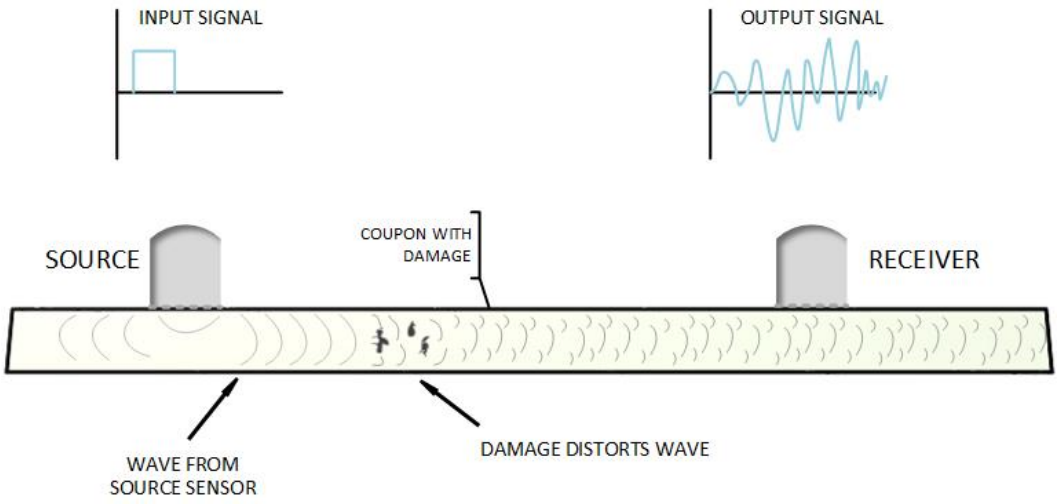

Figure 59: Sensor test schematic.

Sensor tests were conducted on untested 2-ply samples in both control and saturated conditions; Table 8 outlines these tests. Two combinations of sensors were implemented per each specimen to eliminate the deviations to variation in sensor

response. Each test yields a pulse for each sensor in the array; with six tests for five coupons, this results in 60 send-receive pulses for each laminate in each condition.

Table 8: Sensor-test test matrix

Layup	Condition	Number of coupons	Number of sensor combinations	Number of tests (per coupon)
$[0]_2$	Control - untested	5	2	6
$[0]_2$	Saturated - untested	5	2	6
$[90]_2$	Control - untested	5	2	6
$[90]_2$	Saturated - untested	5	2	6

The samples were tested without tabs in the unloaded configuration. Simply supported boundary conditions were implemented by placing the samples on pin supports spaced 220mm apart. Sensor spacing followed that of the AE setup outlined in the Static Test Chapter, incorporating vacuum grease and retainer clamps. The source generated a 5μs pulse. The recorded output metrics of the sensor tests were those corresponding to the receive-sensor including, time of flight, wave speed, amplitude, and energy (MARSE, not absolute).

Results: The averaged results from the sensor-tests are shown below in Table 9.

Table 9: Sensor-test results (averaged)

Layup	Condition	Wave speed (m/s)	Received Amplitude (dB)	Received MARSE energy
$[0]_2$	Control - untested	4.33E+03	78.1	78
$[0]_2$	Saturated - untested	4.34E+03	77.3	68
$[90]_2$	Control - untested	2.74E+03	64.7	17
$[90]_2$	Saturated - untested	2.69E+03	65.2	15

The wave speed collected show minimal change with aging. Based on Equations 6a and 6b, this would be the anticipated as aging caused minimal changes in both the bulk elastic properties of the material (Figure 38). The amplitude and MARSE energy also showed minimal changes with aging, differing by less than 1 dB and 10 E, respectively. However, significant variability existed with these parameters from test to test, especially energy. Figure 60 graphically shows the received amplitudes as well as the standard deviations.

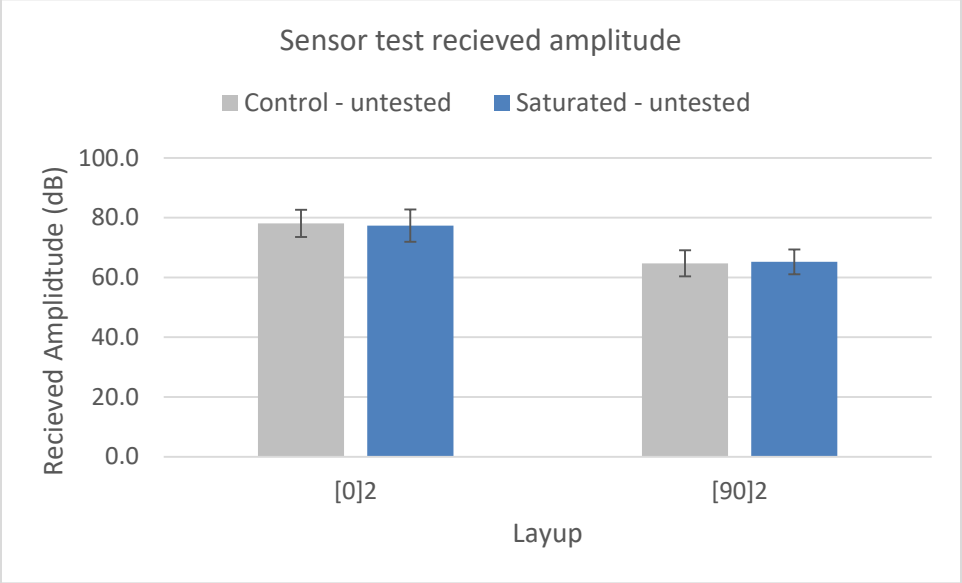

Figure 60: Sensor test received amplitude for untested two-ply laminates.

The standard deviation was significant, approximately 5 dB for both layups and conditions. Large deviations suggest variability in this test method; presence in all laminates shows the deviation to be symptomatic the test method rather than the material. In this case, however, a sufficient number of tests were conducted to show that the pulse from the sensor test did not change with aging. This would support that for this material

system the propagation behavior of AE waves was not inhibited by moisture uptake, either from moisture-induced damping or damage-based attenuation. This result that a using this ultrasonic method to determine the presence of moisture or hygro-damage would not be effective of this scale; however, large propagation distances expected in the ultrasonic analysis of large structures may show more significant attenuation.

CONCLUSIONS

Design and development of MHK devices and off-shore wind turbine requires classification of the effects of moisture on the durability and mechanical performance of the selected fiberglass-epoxy system. In this work mechanical was performance characterized by static strength with the goal of comparing a cross-ply performance to constituent unidirectional lamina performance. The fiberglass-epoxy system studied in this work experienced significant static strength reductions due to hygrothermal aging across all laminates with unidirectional laminate strengths were reduced by 40% and cross-ply laminates experienced strength reductions of 54%. Variation between the strength reductions of unidirectional laminates and cross-ply laminates implies that performance of unidirectional laminates may not reflect the performance of cross-ply laminates and that interacting ply behavior increases the severity of hygrothermal effects.

This work also applied techniques to address the potential degradation mechanisms for the substantial reductions in static strength. It can be concluded that presence of water in the matrix was predominantly physical in nature since desorption revealed that little water was entrapped in the neat resin or the composite. T_g depression showed that plasticization was present, but not reflected in the elastic properties of the composite. Further, Tg-recovery did not correlate to the recovery of composite strength in desorbed. Additionally, control samples exposed to temperature condition without moisture verify that the degradation of the composite was not an artifact of the accelerated aging temperature.

Physical damage from the hygrothermal aging process was observed in both neat resin and composite samples. Large swelling strains caused cracking in neat resin samples, and through laminate theory, translated to large internal stresses within the composite, especially in the interply regions. Physical damage was prevalent in the composites after hygrothermal exposure and was visible both optically and through SEM. Mechanical properties were not recoverable with desorption which again supports the hypothesis of physical damage was induced during the aging process.

The physical damage induced by the aging process altered the damage progression of the composite and reduced the damage tolerance. Both stress-strain response and AE data showed damage occurred at lower strains in laminates that received hygrothermal exposure. Physical damage induced during swelling permitted damage to grow at lower strain energies rather than those needed to initiate damage in an unconditioned laminate. Premature damage growth accelerated that damage progression causing damage coalescence much lower in the loading cycle, which was evidenced by coupon failures as well as the reduced amount of AE response in terms of number of events and energy. This finding corresponds to a reduced damage tolerance from hygrothermal aging. AE frequency analysis revealed that the normalized contribution and sequence of damage mechanisms was unaffected by hygrothermal aging and supports the idea that aging-induced physical damage rather than altering the nature of damage mechanisms themselves. A guided ultrasonic test showed no change in lamb wave attenuation with hygrothermal aging, confirming that the changes in AE response did, in

fact, correlate to changes in the damage behavior rather than changes in material damping.

Broader Impacts

This results in impact selection and application materials for MHK devices in several ways. First and foremost, the material investigated in this study experienced a substantial reduction in strength that should be accounted for should this material be used in a marine structure. Further, the varied degradation in properties of unidirectional laminated did not reflect degradation experienced in cross-ply. This result presents an interesting challenge to MHK design, as a conventional characterization of a material through unidirectional tests may not account for the hygrothermal effects of interacting ply behavior encountered in multi-angle laminates, necessitating the need for tests representative of the design layups.

The result of this work also offers insight into material development for MHK materials. With swelling-induced damage being the main driver for degradation of material performance, better performance could be achieved by minimizing the free volume in the polymer consequently, the bulk moisture uptake of the FRP.

The results from AE and guided-ultrasonic methods also have impacts on the application of SHM techniques. Reduced AE response suggests a marine structure equipped with an AE system for health monitoring may need different criteria for evaluation of health compared to land-based structures. Implementation of a guided ultrasonic test using the AE sensor test function did not show changes hygrothermally

induced changes attenuation behavior on a coupon level, but more in-depth exploration would be necessary to determine its validity in evaluating health of marine structures.

Future Work

This study was confined to characterizing the hygrothermal effects of one material system. Logically, characterization of hygrothermal effects on mechanical performance of more diverse FRP's would be useful in material selection for MHK design. This will be the subject of future work at MSU known as the Diverse Material Systems (DMS) which will evaluate hygrothermal effects on a plethora of FRP systems.

Mechanical testing conducted in this work was limited to static tensile tests. Expanding this work to include hygrothermal effects on fatigue performance would be more insightful to the dynamic, oscillatory, loading regime anticipated in MHK structures.

This work subjected virgin sample to hygrothermal aging and then tested the material properties to understand the effects of hygrothermal aging on a constitutive level. However, the separation environmental exposure from the loading does not reflect the real-world problem as MHK devices will be subjected to mechanical loads and environmental exposure simultaneously. Specifically, damage from loading could allow more rapid diffusion of moisture into areas already near their critical loads. Previous work at MSU has investigated the effect of static stress on diffusion but did not characterize these effects in terms of mechanical performance [9]. Siriruk *et al* demonstrated that for fatigue, immersion of a carbon vinyl-ester sample during testing had a larger effect on the fatigue life than the hygrothermal condition imposed on

samples prior testing, [24]. Other literature regarding this phenomenon is sparse, making it a relevant path of future development.

Work could also be conducted to further explore the acoustic emission. The variation between $[0/90]_s$ and $[90/0]_s$ laminates in this work show dramatic differences in AE response for laminates that typically follow similar damage behavior. These differences were hypothesized to be variations in the attenuation of AE waves due to damage in the outer plies, or variation in the damage behavior of the two layups. These hypotheses could be tested by conducting load-unload-reload tests and comparing the attenuation after each load step using a guided wave. Other methods of damage evaluation such as Digital Image Correlation (DIC) or microscopy could be employed to identify the damage prese4nt after each subsequent load step and correlate the results to the AE data.

REFERENCES CITED

1. *U.S. Energy Information Administration*. Electric Power Monthly 2016; Available from: https://www.eia.gov.

2. *Marine and Hydrokinetic Resource Assesment and Characterization*. 2017.

3. Mishnaevsky, L., et al., *Materials for Wind Turbine Blades: An Overview.* Materials, 2017. **10**(11): p. 1285.

4. Samborsky, D., J. Mandell, and D. Miller, *The SNL/MSU/DOE Fatigue of Composite Materials Database: Recent Trends*, in *53rd AIAA/ASME/ASCE/AHS/ASC Structures, Structural Dynamics and Materials Conference*. 2012, American Institute of Aeronautics and Astronautics.

5. Barbero, E.J., *Introduction to Composite Materials Design, Second Edition*. 2010: Taylor & Francis.

6. Bergan, A., et al., *A Mode I cohesive law characterization procedure for through-the-thickness crack propagation in composite laminates.* Composites Part B: Engineering, 2016. **94**(Supplement C): p. 338-349.

7. Cantwell, W.J. and J. Morton, *The significance of damage and defects and their detection in composite materials: A review.* The Journal of Strain Analysis for Engineering Design, 1992. **27**(1): p. 29-42.

8. Reifsnider, K., *FATIGUE BEHAVIOR OF COMPOSITE-MATERIALS.* International Journal of Fracture, 1980. **16**(6): p. 563-583.

9. Stoffels, M., *Effects of externally applied tensile stresses on the moisture diffusion characteristics of epoxy glass composites*, in *Mechanical Engineering*. 2013, Montana State UNiversity.

10. Shen, C.H. and G.S. Springer, *Moisture Absorption and Desorption of Composite-Materials.* Journal of Composite Materials, 1976. **10**(Jan): p. 2-20.

11. Tsai, Y., et al., *Influence of hygrothermal environment on thermal and mechanical properties of carbon fiber/fiberglass hybrid composites.* Composites Science and Technology, 2009. **69**(3): p. 432-437.

12. Zhou, J.M. and J.P. Lucas, *Hygrothermal effects of epoxy resin. Part I: the nature of water in epoxy.* Polymer, 1999. **40**(20): p. 5505-5512.

13. Zhou, J.M. and J.P. Lucas, *Hygrothermal effects of epoxy resin. Part II: variations of glass transition temperature.* Polymer, 1999. **40**(20): p. 5513-5522.

14. Nogueira, P., et al., *Effect of water sorption on the structure and mechanical properties of an epoxy resin system.* Journal of Applied Polymer Science, 2001. **80**(1): p. 71-80.

15. Grammatikos, S.A., et al., *On the response to hygrothermal aging of pultruded FRPs used in the civil engineering sector.* Materials & Design, 2016. **96**(Supplement C): p. 283-295.

16. Garg, M., et al., *Effect of hygrothermal aging on GFRP composites in marine environment.* Steel and Composite Structures, 2017. **25**(1): p. 93-104.

17. Tsenoglou, C.J., S. Pavlidou, and C.D. Papaspyrides, *Evaluation of interfacial relaxation due to water absorption in fiber-polymer composites.* Composites Science and Technology, 2006. **66**(15): p. 2855-2864.

18. Perreux, D. and C. Suri, *A study of the coupling between the phenomena of water absorption and damage in glass/epoxy composite pipes.* Composites Science and Technology, 1997. **57**(9): p. 1403-1413.

19. Mourad, A.-H.I., et al., *Effect of Seawater and Warm Environment on Glass/Epoxy and Glass/Polyurethane Composites.* Applied Composite Materials, 2010. **17**(5): p. 557-573.

20. Miller, D., et al., *Performance of composite materials subjected to salt water environments.* 2012 AIAA SDM Wind Energy Session, 2012.

21. Nunemaker, J.D., *Effects of saltwater saturation on the static strength and acoustic emission signatures of epoxy glass composites* in *SAMPE Conference Proceedings*. 2016, Society for the Advancement of Material and Process Engineering. : Long Beach, CA.

22. Nunemaker, J.D., *Static strength reduction and acoustic emission analysis of fiberglass-epoxy samples subjected to various levels of moisture absorption* in *SAMPE Conference Proceedings*. 2017, Society for the Advancement of Material and Process Engineering – North America: Seattle, WA.

23. Liao, K., C.R. Schultheisz, and D.L. Hunston, *Effects of environmental aging on the properties of pultruded GFRP.* Composites Part B-Engineering, 1999. **30**(5): p. 485-493.

24. Siriruk, A. and D. Penumadu, *Degradation in fatigue behavior of carbon fiber-vinyl ester based composites due to sea environment.* Composites Part B-Engineering, 2014. **61**: p. 94-98.

25. Xin, H., et al., *Hygrothermal aging effects on flexural behavior of pultruded glass fiber reinforced polymer laminates in bridge applications*. Vol. 127. 2016. 237-247.

26. Garg, A. and O. Ishai, *Characterization of Damage Initiation and Propagation in Graphite/Epoxy Laminates by Acoustic-Emission.* Engineering Fracture Mechanics, 1985. **22**(4): p. 595-608.

27. Garg, A. and O. Ishai, *Hygrothermal influence on delamination behavior of graphite/epoxy laminates.* Engineering Fracture Mechanics, 1985. **22**(3): p. 413-427.

28. Liu, P.F., J. Yang, and X.Q. Peng, *Delamination analysis of carbon fiber composites under hygrothermal environment using acoustic emission.* Journal of Composite Materials, 2017. **51**(11): p. 1557-1571.

29. Hahn, H. and R. Kim, *Swelling of Composite Laminates*, in *Swelling of Composite Laminates*. 1978.

30. Papanicolaou, G.C., et al., *Water absorption mechanism and some anomalous effects on the mechanical and viscoelastic behavior of an epoxy system.* Journal of Applied Polymer Science, 2006. **99**(4): p. 1328-1339.

31. Netravali, A.N., et al., *Effects of water sorption at different temperatures on permanent changes in an epoxy.* Journal of Applied Polymer Science, 1985. **30**(4): p. 1573-1578.

32. Komai, K., K. Minoshima, and S. Shiroshita, *Hygrothermal degradation and fracture process of advanced fibre-reinforced plastics.* Materials Science and Engineering: A, 1991. **143**(1): p. 155-166.

33. Assarar, M., et al., *Influence of water ageing on mechanical properties and damage events of two reinforced composite materials: Flax-fibres and glass-fibres.* Materials & Design, 2011. **32**(2): p. 788-795.

34. Ray, B.C., *Temperature effect during humid ageing on interfaces of glass and carbon fibers reinforced epoxy composites.* Journal of Colloid and Interface Science, 2006. **298**(1): p. 111-117.

35. Gaur, U., C.T. Chou, and B. Miller, *Effect of hydrothermal ageing on bond strength.* Composites, 1994. **25**(7): p. 609-612.

36. Bradley, W.L. and T.S. Grant, *The effect of the moisture absorption on the interfacial strength of polymeric matrix composites.* Journal of Materials Science, 1995. **30**(21): p. 5537-5542.

37. Gorman, M.R., *Plate wave acoustic emission.* The Journal of the Acoustical Society of America, 1991. **90**(1): p. 358-364.

38. Schuster, M., *Characterization and Energy Analysis of Fiber Reinforced Polymer Composites by Acoustic Emission Analysis*, in *Mechanical Engineering*. 2014, Montana State University.

39. deGroot, P.J., P.A.M. Wijnen, and R.B.F. Janssen, *Real-time frequency determination of acoustic emission for different fracture mechanisms in carbon epoxy composites.* Composites Science and Technology, 1995. **55**(4): p. 405-412.

40. Ramirez-Jimenez, C.R., et al., *Identification of failure modes in glass/polypropylene composites by means of the primary frequency content of the acoustic emission event.* Composites Science and Technology, 2004. **64**(12): p. 1819-1827.

41. Suzuki, M., et al., *Fatigue Fracture Mechanism of Class A-SMC by Acoustic Emission Method.* Journal of the Society of Materials Science, Japan, 1987. **36**(411): p. 1402-1408.

42. Bohse, J., *Acoustic emission characteristics of micro-failure processes in polymer blends and composites.* Composites Science and Technology, 2000. **60**(8): p. 1213-1226.

43. Ni, Q.-Q. and M. Iwamoto, *Wavelet transform of acoustic emission signals in failure of model composites.* Engineering Fracture Mechanics, 2002. **69**(6): p. 717-728.

44. Bourchak, M., et al., *Acoustic emission energy as a fatigue damage parameter for CFRP composites.* International Journal of Fatigue, 2007. **29**(3): p. 457-470.

45. Kumar, C.S., V. Arumugam, and C. Santulli, *Characterization of indentation damage resistance of hybrid composite laminates using acoustic emission monitoring.* Composites Part B-Engineering, 2017. **111**: p. 165-178.

46. Gutkin, R., et al., *On acoustic emission for failure investigation in CFRP: Pattern recognition and peak frequency analyses.* Mechanical Systems and Signal Processing, 2011. **25**(4): p. 1393-1407.

47. Pashmforoush, F., M. Fotouhi, and M. Ahmadi, *Acoustic emission-based damage classification of glass/polyester composites using harmony search k-means algorithm.* Journal of Reinforced Plastics and Composites, 2012. **31**(10): p. 671-680.

48. Surgeon, M. and M. Wevers, *Modal analysis of acoustic emission signals from CFRP laminates.* Ndt & E International, 1999. **32**(6): p. 311-322.

49. Voth, M.M., *Exploring frequency based analysis methods for damage identification in fiberglass-epoxy composite systems*, in *SAMPE Conference Proceedings*. 2017, Society for the Advancement of Material and Process Engineering – North America: Seattle, WA.

50. Hamstad, M., *Local characterization of fiber composites by acoustic emission.* The Journal of the Acoustical Society of America, 1983. **73**(6): p. 2230-2230.

51. Czigány, T., Z.A. Mohd Ishak, and J. Karger-Kocsis, *On the failure mode in dry and hygrothermally aged short fiber-reinforced injection-molded polyarylamide composites by acoustic emission.* Applied Composite Materials, 1995. **2**(5): p. 313-326.

52. Su, Z., L. Ye, and Y. Lu, *Guided Lamb waves for identification of damage in composite structures: A review*. Journal of Sound and Vibration, 2006. **295**(3): p. 753-780.

53. Castaings, M. and B. Hosten, *Ultrasonic guided waves for health monitoring of high-pressure composite tanks.* NDT & E International, 2008. **41**(8): p. 648-655.

54. Instruments, T., *Interpreting Unexpected Events and Transitions in DSC Results*.

55. *Standard Test Method for Tensile Properties of Polymer Matrix Composite Materials*. 2014, ASTM International.

56. Murdy, P., *Detecting damage progression in gfrps through use of ultrasonic impulses and acoustic emission for structural health monitoring*, in *SAMPE 2016*. 2016: Long Beach, CA. p. 1916-1928.

APPENDICES

APPENDIX A

APPENDIX A: MATERIALS

HEXION

Technical Data Sheet

Issued: August 2006

EPIKOTE™ Resin MGS™ RIMR 135 and EPIKURE™ Curing Agent MGS™ RIMH 134–RIMH 137

CHARACTERISTICS

Approval	German Lloyd
Application	Specially designed for infusion processes (RMT, SCRIMP/VARI); rotor blades for wind turbines, boat and shipbuilding, sports equipment
Operational Temperature	-60 °C up to +50 °C (-76 °F up to 122 °F) without heat treatment -60 °C bis +80 °C (-76 °F up to 176 °F) after heat treatment
Processing	At temperatures between 10 °C and 50 °C (50-122 °F) due to the very low mixing viscosity especially suited for infusion, injection and pultrusion
Features	Very low viscosity, excellent initial curing properties at room temperature, pot life from approx. 0,5 hours to approx. 4 hours, short curing times at high temperatures
Storage	Shelf life of 24 months in originally sealed containers

APPLICATION

Very low viscosity laminating resin system with different pot lives for processing of glass, carbon and aramide fibers. Due to its good mechanical properties, this system is suitable for the production of components featuring high static and dynamic loadability.

The range of pot lives is between approx. 0,5 hour and 3-4 hours. The parts can be worked and demoulded after curing at room temperature. Curing at higher temperatures (up to approx. 80-100 °C, 176-212 °F) is possible, depending on layer thickness and geometry of the parts to be manufactured. The curing times can be reduced to a few minutes by this.

Adding internal parting agents, such as zinc stearate, etc., has proven useful for pultrusion processes. Profiles with good surface qualities are obtained. Depending on profile geometry, mould temperatures in the range of 180-230 °C (356-446 °F) are possible, thus permitting high drawing speeds.

The mixing viscosity is very low, which is especially advantageous for infusion and injection processes. It may be lowered to approx. 150 mPas by heating the resin mass (see diagram). This means that even complicated molded parts with long flow paths can be easily infused. The temperature rise with hardener RIMH 137 remains very low up to a mold temperature of approx. 30 °C, so that even parts of greater thickness can be produced at elevated temperatures.

The infusion resin system does not contain any unreactive components. The raw materials used feature a

very low vapor pressure. This permits processing of the material under vacuum even at elevated temperatures (VARIM process). Compatibility problems are not to be expected in combination with UP gelcoats, various paints (e.g. PUR-based), etc. However, comprehensive tests are indispensable.

The relevant industrial safety regulations for the handling of epoxy resins and hardeners and our instructions for safe processing are to be observed.

The resin and hardeners can be stored for at least 24 months in their carefully sealed original containers. The resin and hardeners may crystallise at temperatures below +15 °C (59 °F). The crystallisation is visible as a clouding or solidification of the contents of the container. Before processing, the crystallisation must be removed by warming up. Slow warming up to approx. 50-60 °C (122-140 °F) in a water bath or oven and stirring or shaking will clarify the contents of the container without any loss of quality. Use only completely transparent products. Before warming up, open containers slightly to permit equalization of pressure. Caution during warm-up! Do not warm up over an open flame! While stirring up, use safety equipment (gloves, eyeglasses, respirator).

SPECIFICATIONS

		Infusion Resin RIM 135
Density	[g/cm³]	1,13 - 1,17
Viscosity	[mPas]	700 - 1.100
Epoxy equivalent	[g/equivalent]	166 - 185
Epoxy value	[equivalent/100g]	0,54 - 0,60
Refractory index		1,548- 1,552

		Hardener RIMH 134	Hardener RIMH 137
Density	[g/cm³]	0,93 - 1,00	0,93 - 0,98
Viscosity	[mPas]	10 - 80	10 - 50
Amine Value	[mg KOH/g]	550 - 700	400 - 600
Refractory index		1,4900 - 1,5000	1,460 - 1,463

Measuring conditions: measured at 25 °C / 77 °F

PROCESSING DETAILS

	Infusion Resin RIMR 135	Hardeners RIMH 134-137
Average EP - Value	0,56	-
Average amine equivalent	-	52

MIXING RATIOS

	Infusion Resin RIMR 135 : Hardener RIMH 134 – RIMH 137
Parts by weight	100 : 30 ± 2
Parts by volume	100 : 36 ± 2

The specified mixing ratios must be observed as exactly as possible. Adding more or less hardener will not effect a faster or slower reaction - but in incomplete curing which cannot be corrected in any way. Resin and hardener must be mixed very thoroughly. Mix until no clouding is visible in the mixing container. Pay special attention to the walls and the bottom of the mixing container.

TEMPERATURE DEVELOPMENT

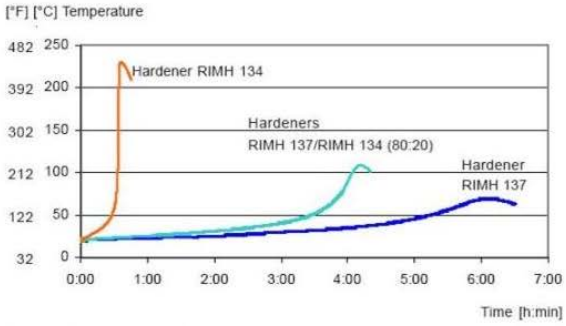

Quantity: 100 g / 20 °C (77 °F)

The optimum processing temperature is in the range between 20 °C and 25 °C (68-77 °F). Higher processing temperatures are possible, but will shorten pot life. A rise in temperature of 10 °C (50 °F) will halve the pot life. Water (for example very high humidity or contained in fillers) causes an acceleration of the resin/hardener reaction. Different temperatures and humidities during processing have no significant effect on the strength of the hardened product.

Do not mix large quantities - particularly of highly reactive systems - at elevated processing temperatures. The heat flow from the mixing container is very low, so the contents will heat up fast because of the dissipating reaction heat (exothermic resin-hardener reaction). This can result in temperatures of more than 200 °C (392 °F) in the mixing container, which may cause smoke-intensive burning of the resin mass.

VISCOSITY

Viscosity of mixture at different temperatures

Infusion resin RIM 135 with mixture of Hardeners RIMH 137 (80 %) /RIMH 134 (20 %)

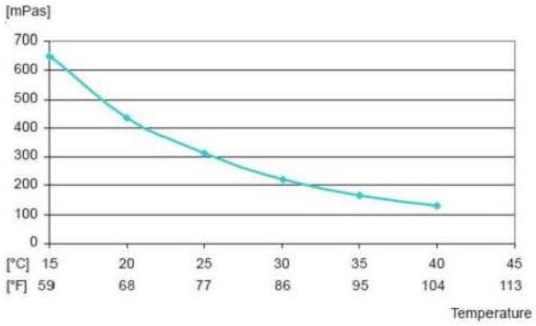

Viscosity development

Infusion resin RIM 135 with mixture of Hardeners RIMH 137 (80 %) /RIMH 134 (20 %) and Hardener RIMH 137

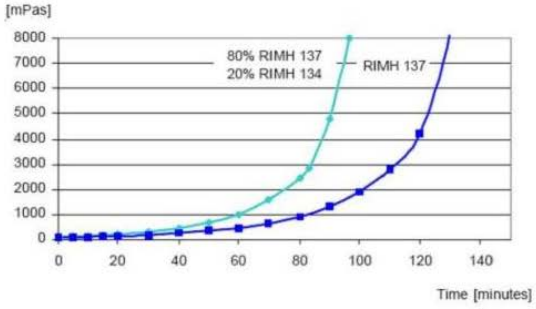

Measuring conditions:
Temperature: 40°C (104 °F); measuring gap 0,2 mm

MECHANICAL DATA

Mechanical Data of Neat Resin		
Density	[g/cm³]	1,18 - 1,20
Flexural strength	[N/mm²]	90 - 120
Modulus of elasticity	[kN/mm²]	2,7 - 3,2
Tensile strength	[N/mm²]	60 - 75
Compressive strength	[N/mm²]	80 - 90
Elongation of break	[%]	8 - 16
Impact strength	[KJ/m²]	70 - 80
Water absorption at 23 °C	24 h [%] 7 d [%]	0,10 - 0,20 0,20 - 0,50
Fatigue strength under reversed bending stresses acc. to DLR Brunsw.	10% 90%	exp. > 1 x 10^6 exp. > 2 x 10^6
Curing: 24 h at 23° C (74° F) + 15 h at 60° C (140° F), partly cured/full cure Typical data according to WL 5.3203 Parts 1 and 2 of the GERMAN AVIATION MATERIALS MANUAL		

Advice: Mechanical data are typical for the combination of laminating resin RIMR 135 with hardener RIMH 137. Data can differ in other applications.

T_G DEVELOPMENT

Development of glass transition temperature (T_G) at 60 °C

Infusion resin RIM 135 with mixture of Hardeners RIMH 137 (80 %) /RIMH 134 (20 %)

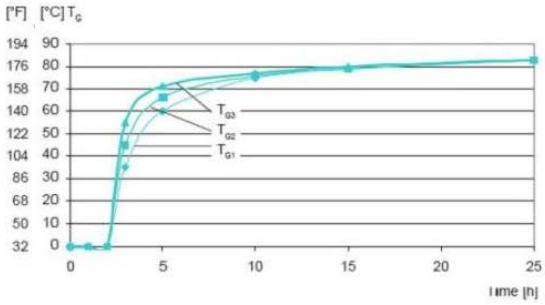

DMA

DMA Measuring after heat treatment

DMA-T_G (peak) tan delta
Infusion resin RIM 135 with mixture of Hardeners RIMH 137 (80 %) /RIMH 134 (20 %)

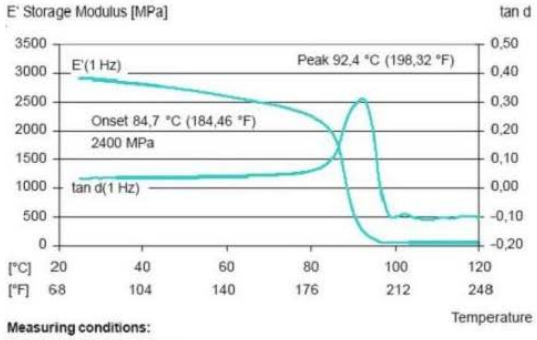

Measuring conditions:
Sample thickness: 2 mm
Heat rate: 2 K/min

VECTORPLY
Performance Composite Reinforcements

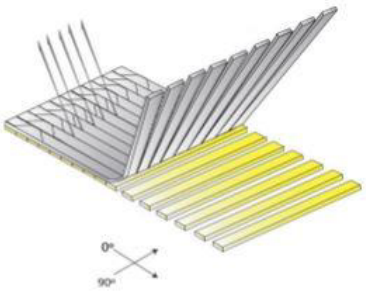

E-LT 3800-10

Fiber Type: E-Glass
Architecture: 0º/90º Biaxial

Total Weight: 37.26 oz/sq.yd / 1263 g/sq.m

Roll Specifications			Fiber Architecture Data	
Roll Width:	Roll Weight:	Roll Length:	0 º :	33.55 oz/sq.yd / 1138 g/sq.m
50 in. / 1270 mm	220 lbs / 100 kg	68 yd / 62 m	90 º :	3.36 oz/sq.yd / 114 g/sq.m
			Chopped Mat:	N/A
			Polyester Stitching:	0.35 oz/sq.yd / 12 g/sq.m

* Packaging: Bag

Vectorply Corporation
3500 Lakewood Drive Phenix City, AL 36867
tel. 334-291-7704 fax. 334-291-7743

REV: 3/13/2015

APPENDIX B

APPENDIX B: AE FREQUENCY-SCATTER PLOTS

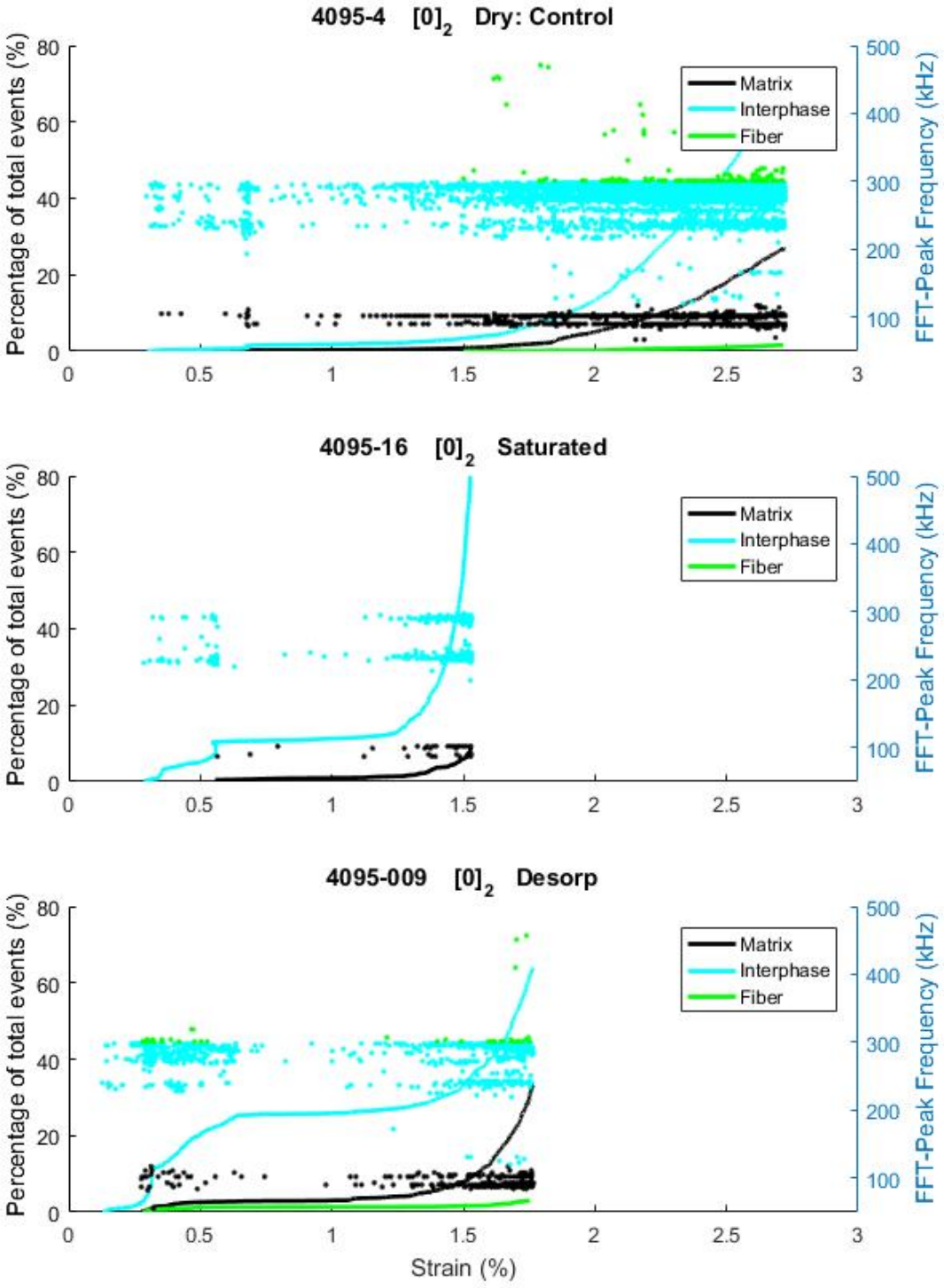
4095-4 [0]2 Dry: Control
4095-16 [0]2 Saturated
4095-009 [0]2 Desorp
Percentage of total events (%)
FFT-Peak Frequency (kHz)
Strain (%)
Matrix
Interphase
Fiber
0
20
40
60
80
100
200
300
400
500
0.5
1
1.5
2
2.5
3

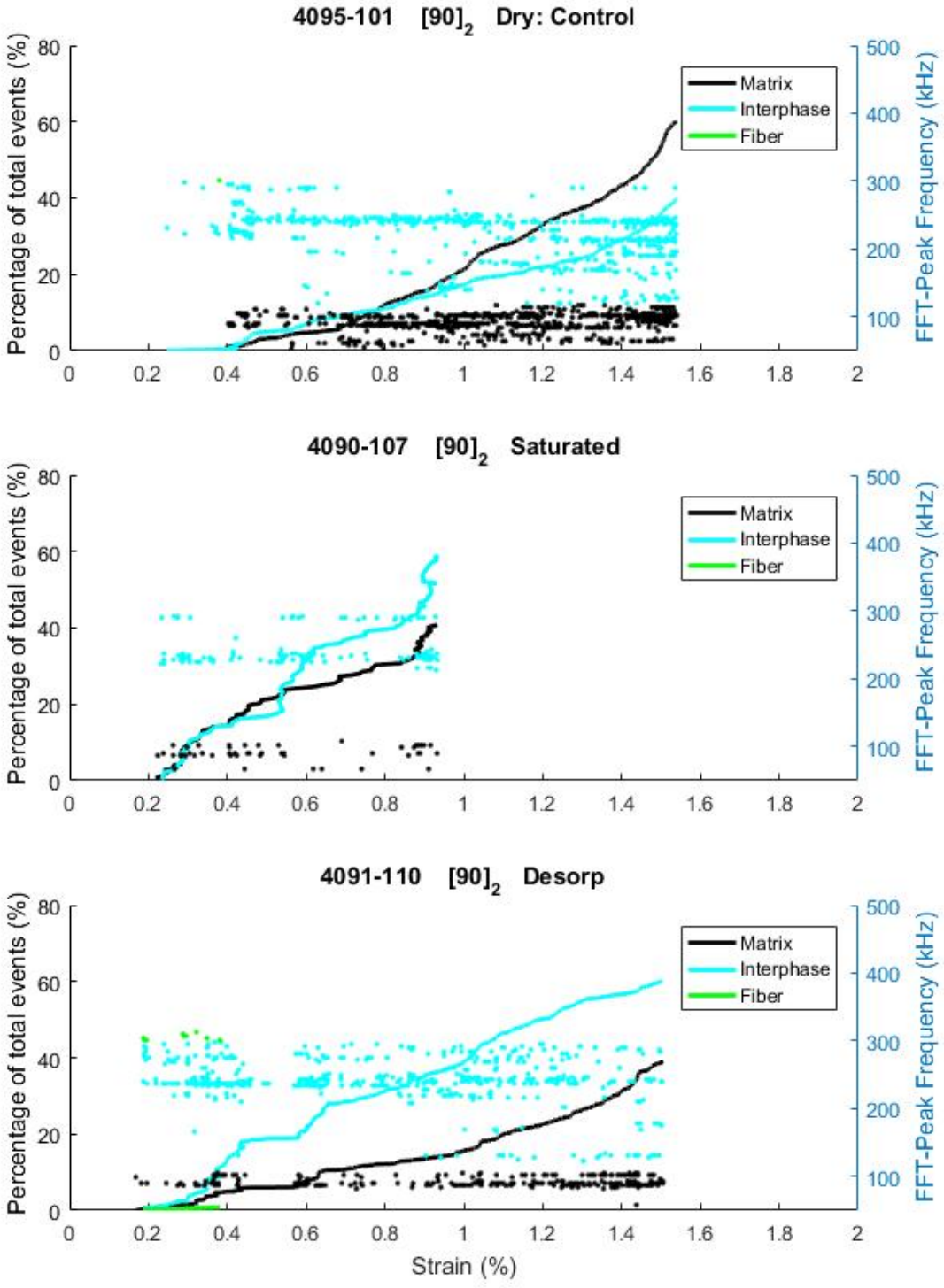
4095-101 [90]2 Dry: Control
4090-107 [90]2 Saturated
4091-110 [90]2 Desorp
Matrix
Interphase
Fiber
Percentage of total events (%)
FFT-Peak Frequency (kHz)
Strain (%)

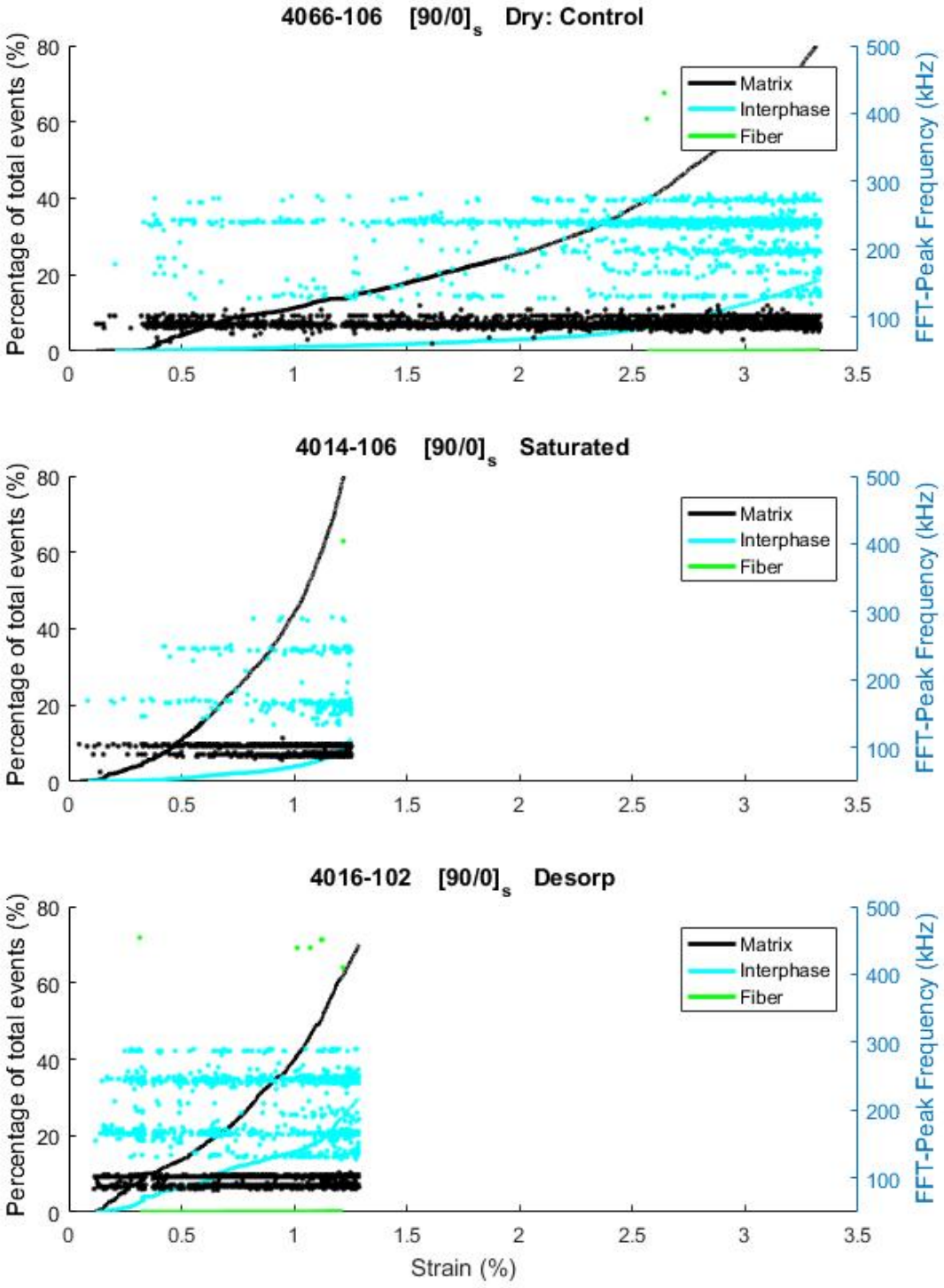
4066-106 [90/0]s Dry: Control
4014-106 [90/0]s Saturated
4016-102 [90/0]s Desorp
Percentage of total events (%)
FFT-Peak Frequency (kHz)
Strain (%)
Matrix
Interphase
Fiber
0
20
40
60
80
100
200
300
400
500
0.5
1
1.5
2
2.5
3
3.5

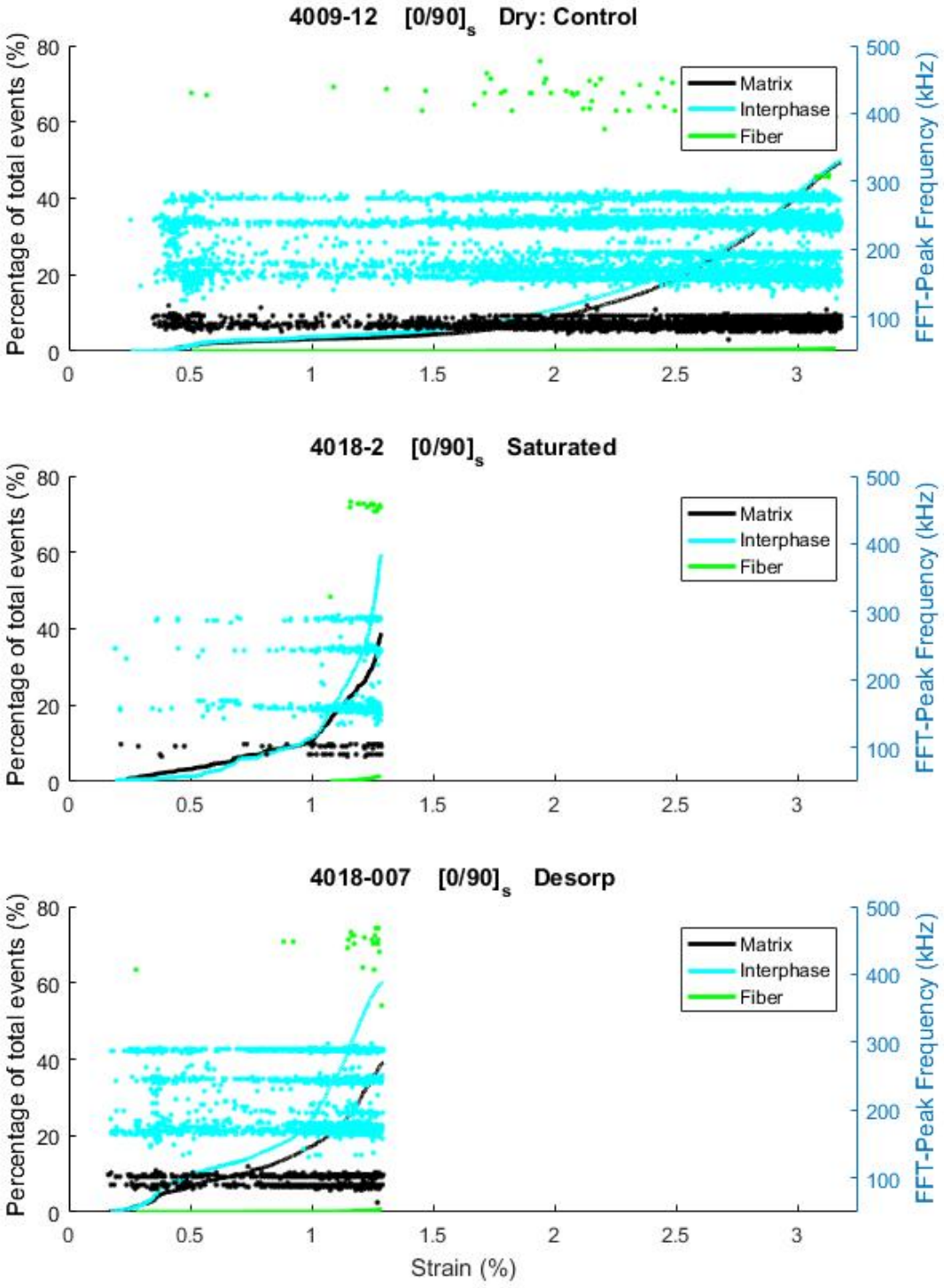
4009-12 [0/90]s Dry: Control
4018-2 [0/90]s Saturated
4018-007 [0/90]s Desorp
Matrix
Interphase
Fiber
Percentage of total events (%)
FFT-Peak Frequency (kHz)
Strain (%)
0
20
40
60
80
100
200
300
400
500
0.5
1
1.5
2
2.5
3